INVESTIGATION OF FLAME CHARACTERISTICS IN A TURBULENT PREMIXED COMBUSTION

A Dissertation

By
Mohammed Khudhair Abbas Alhumairi

Submitted to the
Graduate School of Sciences and Engineering
In Partial Fulfillment of the Requirements for
the Degree of

Doctor of Philosophy

in the
Department of Mechanical Engineering

Özyeğin University
October 2018

INVESTIGATION OF FLAME CHARACTERISTICS IN A TURBULENT PREMIXED COMBUSTION

Approved by:

Asst. Prof. Dr. Dr. Ing. Özgür Ertunç
Supervisor
Department of Mechanical Engineering
Özyeğin University

Prof. Dr. M. Pinar Mengüç
Department of Mechanical Engineering
Özyeğin University

Asst. Prof. Dr. Altug Başol
Department of Mechanical Engineering
Özyeğin University

Prof. Dr. I. Bedii Özdemir
Department of Mechanical Engineering
Istanbul Technical University

Prof. Dr. Ali Koşar
Department of Mechatronics Engineering
Sabancı University

Date of approved: 3 October 2018

To our families and mentors

ABSTRACT

In this thesis, the turbulent flame closure (TFC) model and coherent flame model (CFM) of turbulent premixed flames as steady state flow are used. In addition, large eddy simulation (LES) model as unsteady state flow is used. The effects of different turbulent parameters such as Reynolds number based in a Taylor micro scale Re_λ, turbulence length scale l_t turbulence intensity T_i and the constant of the TFC model A on the combustion are modelled for steady reacting flow. In addition, the characteristics of sinusoidal wave, such as amplitude of pulsation A_o and the frequency f are used for unsteady reacting flow to show the behavior of the flame topology and flame location of jet flow combustor of lean propane-air combustion. The simulations are achieved with 3, 5 and 9 kW thermal loads at constant inlet velocity and equivalence ratio. Transport equations for progress variable (c) are shown in terms of Reynolds and Favre averages, and the reaction rate terms are used to calculate heat release at different turbulent flow conditions. The results are compared with existing experimental data from the combustor performance studies.

The lean premixed combustion under the influence of active grid turbulence was computationally investigated, and results were compared with the experiments. In the experiments, the transverse and longitudinal active grids generated turbulence. The experiments were conducted to generate a premixed gas flame at a given inlet power 3, 5 and 9 kW. Turbulent burning modelling such as CFM, TFC and LES models were implemented to conduct simulations under different turbulent flow conditions as steady and unsteady state flows, respectively. The turbulent flow conditions obtained in the simulations were specified by the dissipation rate of turbulence (ϵ) and a turbulent

kinetic energy (k) at the inlet region for steady reacting flow. All simulations were used to simulate the turbulent reacting flows at the equivalence ratios of 0.606 and 0.588 to estimate the combustion conditions of the propane. The heat release field was used for comparison with experimental cases. Acceptable agreement is found between the simulations and the experimental results. The flame topology is more sensitive to turbulence in CFM model than that simulated by the TFC model, and the flame location moved toward to inlet region by increasing Re_λ. CFM and TFC models were used Re_λ as a fundamental parameter. In addition, in the LES model, the turbulence was attained by setting the characteristics of a sinusoidal wave such as A_o and f. Three numerical models were used to prediction the flame topology and flame location at different turbulent flow conditions, and three different results were found as compared with experiments. Moreover, the fields of heat release, species mass fraction and temperature distribution in the centerline of the combustor were investigated.

After the TFC model was calibrated, the best value of constant A that matches the experiment was A = 0.37. All numerical simulations were performed in STAR CCM+ v10.02 and v12.04 software. The turbulent flame speed U_t was derived from the Zimont formula, and the results showed that the flame location and topology were influenced solely by Re_λ, as suggested by the derived new equation for U_t.

The results showed that combustion occurs in the wrinkled and corrugated flamelet regions on the Borghi diagram. At a low Re_λ value, the flame topology in the TFC model was wrinkled and symmetrical with respect to the vertical axis of the combustor, whereas at medium and large Re_λ values, the flame topology exhibited cusps. By contrast, the flame topology behaviour in the CFM model was not constant at different Re_λ and was like a mushroom shape, and the flames moved toward inlet

regions by increasing Re_λ. In addition, in the LES model, the V-shape and the corrugated wings of the flame were formed.

The flame changed topology and location at different turbulent flow conditions of amplitude of pulsation and frequency. The flame topology investigation for jet flow combustor can be used to modulate effectively well the gas turbine burner design or other turbulent combustion studies. The investigation of the flame topology in the combustor with various turbulent flow conditions is important in controlling the flame location to reduce emissions and increase power efficiency, or even design pioneering production techniques related to flame.

ÖZET

Bu tezde, çalkantılı alev kapama (TFC) modeli ve kararlı durum akışı olarak türbülanslı önceden karıştırılmış alevlerin koherent alev modeli (CFM) kullanılmıştır. Ayrıca, kararlı olmayan akış olarak büyük eddy simülasyonu (LES) modeli kullanılmıştır. Taylor mikro skalası Re_λ, türbülans uzunluk skalası l_t türbülans şiddeti Ti temelli Reynolds sayısı ve yanma üzerindeki TFC model A'nın sabiti gibi farklı türbülans parametrelerinin etkileri, sürekli tepki veren akış için modellenmiştir. Buna ek olarak, salınım A_o'nun genliği ve frekans f gibi sinüzoidal dalganın özellikleri, alev topolojisinin davranışını ve yalın propan-hava yanmasının jet akış yanma odasının alev konumunu göstermek için dengesiz tepki akışı için kullanılır. Simülasyonlar sabit giriş hızı ve eşdeğerlik oranında 3, 5 ve 9 kW termal yüklerle elde edilir. İlerleme değişkeni (c) için taşıma denklemleri Reynolds ve Favre ortalamaları cinsinden gösterilmiştir ve farklı türbülanslı akış koşullarında ısı salınımını hesaplamak için ortalama reaksiyon hızı terimleri kullanılmıştır. Sonuçlar, yakıcı performans çalışmalarından elde edilen mevcut deneysel veriler ile karşılaştırılmıştır. Aktif ızgara türbülansının etkisi altındaki önceden karıştırılmış yanma işlemi, sayısal olarak incelenmiştir ve sonuçlar deneylerle karşılaştırılmıştır. Deneylerde, enine ve uzunlamasına aktif ızgaralar türbülansa neden olmuştur. Deneyler, 3, 5 ve 9 kW 'lık bir giriş gücünde önceden karıştırılmış bir gaz alevi üretmek için gerçekleştirilmiştir. CFM, TFC ve LES modelleri gibi türbülanslı yanma modellemeleri, sırasıyla sabit ve kararsız durum akışları olarak farklı türbülanslı akış koşullarında simülasyon yapmak için uygulanmıştır. Deneylerde elde edilen türbülanslı akış koşulları, giriş bölgesinde türbülans (ϵ) ve türbülanslı kinetik enerjinin (k) yayılma oranı ile belirlenmiştir. Tüm simülasyonlar, propanın yanma koşullarını

tahmin etmek için 0,625 ve 0,588 eşdeğerlik oranlarında türbülanslı reaksiyon akışlarını simüle etmek için kullanılmıştır. Isı bırakma alanı deneysel vakalarla karşılaştırılmak için kullanılmıştır. Simülasyonlar ve deney sonuçları arasında kabul edilebilir bir anlaşma bulundu. Alev topolojisi, CFM modelindeki türbülansa TFC modeli ile simüle edilene göre daha hassastır ve alev bölgesi, Re_λ artırarak giriş bölgesine doğru hareket etmiştir. Her iki modelde de, bir Taylor mikro skalasına (Re_λ) dayalı Reynolds sayısını temel bir parametre olarak kullanılmıştır. Ek olarak, LES modelinde, türbülans, A_o ve f gibi bir sinüzoidal dalganın özelliklerini belirleyerek elde edilmiştir. Alev topolojisini ve farklı türbülanslı akış koşullarındaki alev yerini tahmin etmek için üç sayısal model kullanılmış ve deneylerle karşılaştırıldığında üç farklı sonuç bulunmuştur. Ayrıca, yanma alanının merkezi hattındaki ısı yayılımı, tür kütle fraksiyonu ve sıcaklık dağılımı alanları incelenmiştir.

TFC modeli kalibre edildikten sonra, deneyi eşleştiren sabit A'nın en iyi değeri A = 0.37 olarak bulunmustar. Tüm sayısal simülasyonlar STAR CCM + v10.02 ve v12.04 yazılımlarında gerçekleştirilmiştir. Çalkantılı alev hızı U_t Zimont formülünden türetilmiştir ve sonuçlar, alev konumu ve topolojinin, U_t için türetilmiş yeni denklem tarafından önerilen Re_λ tarafından etkilendiğini göstermistir.

Sonuçlar, yanmanın Borghi diyagramındaki kırışmış ve oluklu flamelet bölgelerinde meydana geldiğini göstermiştir. Düşük bir "Re" de, değer TFC modelindeki alev topolojisi buruşturucunun dikey eksenine göre buruşmuş ve simetrik iken, orta ve büyük Re_λ değerlerinde alev topolojisi cusps sergilemiştir. CFM modelindeki alev topolojisi davranışı farklı Re_λ 'da sabit değildi ve bir mantar şekli gibi ve alevler Re_λ artırarak giriş bölgelerine doğru hareket etmistir. Ayrıca LES modelinde, alevin V şekli ve oluklu kanatları oluşturulmuştur. Alev, salınım ve frekansın farklı

türbülans koşullarında topoloji ve yer değiştirildi. Jet akış yakıcıları için alev topolojisi araştırması, gaz türbini brülör tasarımı veya diğer türbülanslı yakma çalışmaları için iyi modüle edilmek üzere kullanılabilir oluğu gözlemlenmistir. Alev topolojisindeki alev topolojisinin çeşitli türbülanslı akış koşulları ile incelenmesi gerekmehtedir.

ACKNOWLEDGMENTS

Firstly, I give my special thanks to Allah, the Almighty, for giving me the strength and the time to continue and finish this work. I also thank Allah for blessing me with many great people who have been my greatest support in my personal and professional life.

Secondly, I would like to express my deepest regards and sincere gratitude to my supervisor Asst. Prof. Dr. Dr. Ing. Ozgur Ertunc for his devotion and honest effort for five years to bring this work into light.

I would like to thank the rest of my thesis monitoring committee, Prof. Dr. M. Pinar. Menguc and Prof. Dr. Ing. I. Bedii Ozdemir for fruitful discussions and useful suggestions to accomplish this work, especially in the unsteady reacting flow part. He also provided me with personal references. I also thank my thesis defense committee for their kind acceptance to examine my PhD work and Dr. M. Sarigul for translating to Turkish language.

My overseas study was made possible and enjoyable with good friends, such as my classmates in Özyeğin University, especially, I. Thamer. Nazzal. In addition, I thank my Turkish friends Suat Yeşil and his brother Husno Yeşil for all their support to me for five years. I would also like to thank my friend Sami Alazawi for his valuable assistance to me and my family in Iraq.

My special appreciation goes to my mother and my family, without the assistance of whom I would not have completed this study.

Finally, I gratefully acknowledge the scholarship provided to me by the Iraqi government (Ministry of Higher Education and Scientific Research, Diyala University),

which provided financial support for five years that allowed me to obtain a Ph.D. in Mechanical Engineering.

TABLE OF CONTENTS

LIST OF TABLES

LIST OF FIGURES

NOMENCLATURE

Roman Symbols	
a	CFM parameter
A	Area [m^2]
A	Constant of TFC model
A_r	Arrhenius coefficient
A_o	Amplitude of pulsation [m/s]
c	Progress variable [-]
$\tilde{c}_\alpha$	Species concentrations [%]
c_p	Specific heat at constant pressure [$J.kg^{-1}.K^{-1}$]
C_μ	Turbulent viscosity coefficient [-]
D	Diameter of the burner [m]
D_t	Turbulent diffusivity [m^2/s]
D_a	Damkohler number [dimensionless]
E_a	Activation energy [kj/mol]
E	Energy [kJ/mol]
f	The frequency [Hz]
G	Flame stretch factor
HR	Heat release[$W.m^{-3}$]
HRR	Heat release rate [$W.m^{-3}$]
ΔH	The enthalpy of the reaction [$J.mol^{-1}$]
h_f	Lower heating value of propane [$kJ.g^{-1}$]
h_i	The enthalpy of species [kJ/kg]
J_i^h	Molecular flux of enthalpy

k	Turbulent kinetic energy [J.kg^{-1}]
k_1	The thermal conductivity of flame holder surface [W/m.C]
Ka	Karlovitz number [dimensionless]
l_t	Turbulent length scale [m]
l_f	Laminar flame length scale [m]
$\dot{m}_1$	Mass flow rate ratio of the mixture in inlet 1 [%]
m	Rate exponents of fuel
n	rate exponents of oxygen
N	Number of the samples
P	Pressure [pa]
R	Universal gas constant [J / mol. K]
Re_t	Turbulent Reynolds number [dimensionless]
Re_λ	Reynolds number based on Taylor microscale [dimensionless]
S_L	Laminar flame speed [m/s]
T	Temperature [K]
T_l	The integral time scale [s]
T_b	Temperature of burned gases [K]
Ti	Turbulent intensity [%]
T_{ref}	Reference temperature [K]
T_{surr}	Surrounding temperature [K]
T_∞	Environment temperature [K]
T_u	Temperature of unburned gases [K]
$\overline{U}$	The mean velocity of the flow [m/s]
U_t	Turbulent flame speed [m/s]
$\tilde{u}$	Fluctuation velocity [m/s]
u′	rms of turbulent fluctuation velocity [m/s]

$\overline{u_i'' u_j''}$	Reynolds stress tensor, i=1,2,3 and j=1,2,3
Y_i	Species mass fraction, , i=1,2,3
Y_{res}	The amount of fuel mass fraction in the end of the combustion
Y_{ft}	The fuel mass fraction in the unburnt gas
$z\alpha_{/2}$	The confidence coefficient

Greek symbols

α	CFM parameter
β_1	CFM parameter in equation 2.46
β	temperature exponent
Φ	Equivalence ratio
δ	The kronecker delta
λ	Excess air ratio
ε	The dissipation rate of turbulence [$m^2.s^{-3}$]
ε_1	The emissivity of the flame holder surface
ρ	The density [$kg.m^{-3}$]
$\bar{\rho}$	Mean density [$kg.m^{-3}$]
ρ_b	Burned density of the mixture [$kg.m^{-3}$]
ρ_u	Unburned density of the mixture [$kg.m^{-3}$]
$\overline{\dot{\omega}_i}$	Reaction rate, , i=1,2,3
ω_{tfc}	TFC reaction rate
ω_{cfm}	CFM reaction rate
Σ	Flame surface density [m^{-1}]
ν	Turbulent viscosity [$m^2.s^{-1}$]
τ_{ij}	Turbulent stress tensor, , i=1,2,3 and j=1,2,3
σ	The standard deviation

σ_1	The Stefan–Boltzmann constant
σ	flame area per unit mass in equation 2.45
θ	Mean quantity of any variable
$\hat{\mu}_\theta$	The estimated mean of θ
(μ_θ)	The real mean of θ
Γ_{Y_f}	Diffusion coefficient of fuel mass fraction
S_Σ	Source term which includes the flame area production by stretch

CHAPTER I

INTRODUCTION

1.1 General

The world is facing considerable challenges related to the dependence on fossil fuels to meet global energy consumption requirements; more than 70% of world energy is based on fossil fuels. More than half of that is supplied by oil, which is almost entirely used for transportation purposes. Given the uses of energy required for domestic and industrial uses by burning fossil fuels and energy production, the means of combustion is expected to remain dominant for many future decades. Therefore, the reduction of the pollutant emission for power-producing devices by reducing the impact of combustion on the environment is expected by increasing the efficiency of combustion devices and reducing pollutant emissions [1].

The combustion phenomenon deals with converting chemical energy of the reacting fuel into heat energy by a chemical reaction. One of the most important thermodynamic facts to know about chemical reactions is the change in heat or energy content related with the reaction at specific temperatures and an appropriate state of the reactants and products. This change is known either as the heat or as the energy of reaction at the specific temperature [2]. Every mole of fuel combusted will generate an amount of energy from the formation of the species that releases heat.

Turbulent flows are common in various applications, such as smoke from combustion processes in spark-ignition engines, furnaces and gas turbines. In most

engineering applications, the flow is turbulent. Turbulent flow is an irregular flow in which the different quantities show a random variation with space coordinates and time. These applications are dependent mainly on fossil fuels. Turbulence and combustion are complicated areas of study. Three types of turbulent combustion are used, namely, non-premixed, partially premixed and fully premixed. Depending on the air intake into the fuel flow, non-premixed flame occurs when the fuel stays separate from the air until it burns. Premixed combustion occurs when the air and fuel are premixed before they enter the zone of combustion. Turbulent premixed combustion is the main interest in the present study.

Combustion commonly occurs within the turbulent region. Combustion was enhanced by increasing the surface area and the mixing process because of increases in the turbulence [3]. Furthermore, heat release from combustion enhances the transition to fully turbulent flow. Therefore, to simulate turbulent combustion, the various models must be experimentally investigated and validated. Turbulent premixed combustion modelling is essential for various engineering applications because it helps in improving these technologies to reduce emissions and increase power efficiency. The effects of the turbulent flow field properties of flames are significant because they extremely increase the flame propagation velocity (turbulent flame speed, U_t) [4]. Turbulence can be generated by using an active regular or fractal grid that is placed on the upstream flame region to develop velocity field [5–10]. The influence of turbulence on combustion is determined by subjecting the flame front to the activity of the eddies to increase the flame surface area, namely, the wrinkling flame [11].

The turbulent combustion models used in this study are coherent flame model (CFM), turbulent flame speed closure (TFC) and large eddy simulation (LES) models

for the reproduction of a turbulent premixed flame under the effect of various turbulent conditions. A common (k–ε) model can model the turbulence [12–17]. The turbulence levels are specified by the turbulent kinetic energy k, dissipation rate of turbulence ϵ (including turbulent intensity Ti and turbulent length scale l_t) and Reynolds number based on Taylor microscale Re_λ [18]. Turbulent intensity has a generally critical effect on the flame surface properties of the diffused flame in the reaction zone below the flame holder surface.

To understand the behavior of the flame location and flame topology in the jet flow combustor with various Re_λ values at a constant thermal load and at a constant equivalence ratio, we investigated the flame front location by using the heat release in the steady reacting flow. By contrast, the characteristics of sinusoidal wave such as frequency f and the amplitude of pulsation A_o for unsteady reacting flow were used to generate turbulence in the combustor and then calculate flame location. In the experiments, the transverse and longitudinal active regular grids generated the turbulence. A lean premixed flame from propane–air mixture of, 3, 5 and 9 kW thermal load was investigated. The CFM and TFC models were implemented in STAR CCM+ v10.02 for steady reacting flow, and the LES model was used for unsteady propane combustion in STAR CCM +v 12.04. Then, numerical results were used for comparison with the experiments with respect to dimensionless Re_λ, and the characteristics of sinusoidal wave.

1.2 Turbulence and combustion interaction

The laminar combustion is used in certain furnaces, candles and lighters, whereas the turbulent combustion modelling and studying is used to improve the

functional systems, which include reduced fuel consumption, reduced pollutant formation, and increased efficiency. The combustion rate is increase by the effect of turbulence on combustion. The heat release from the combustion depends on the concepts of interaction between the turbulence and combustion as shown in Figure (1.1). The applications that include strong turbulence–chemistry interactions are necessary to address a model of coupling between combustion and turbulence. Combustion with turbulence is a complex process that involves a large range of length and chemical time scales. The chemical phenomena-controlling flames are associated with density gradients, temperature and mass fractions and occur in short times over thin layers. The full description of chemical mechanisms in turbulent flames may require hundreds of reactions and hundreds of species that lead to large numerical difficulties. Many definitions of turbulence are used, although they share similar concepts. Bradshaw defined turbulence as "a three-dimensional time-dependent motion in which vortex stretching causes velocity fluctuations to spread to all wavelengths between a minimum determined by viscous forces and a maximum determined by the boundary conditions of the flow" [19, 20].

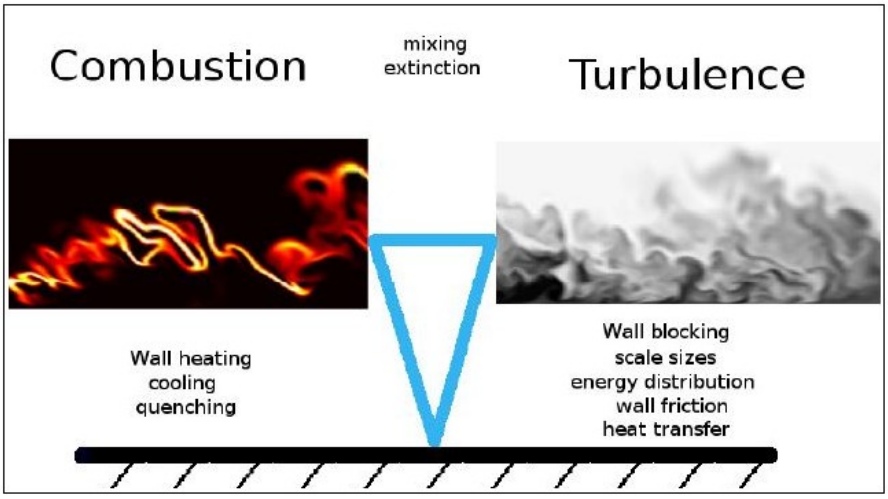

Figure 1.1 The interaction between the wall, turbulence and combustion [20].

Turbulent combustion addresses a number of challenges with respect to numerical simulation because of the complex interaction of chemical reactions and fluid flows. Bray et al. [21] studied the interaction between the turbulent and premixed combustion in spark ignition engines. They studied the interaction from two sides, firstly from the terms of the transport equations of the flux components and Reynolds stress. Secondly, a laminar flamelet form described the mean reaction rate terms. They found that the Reynolds flux and Reynolds stress transport equations that contained turbulent transport terms, are locked over presumed relationship between third order and second order conditioned turbulence quantity in product and reactant.

Belardini et al. [22] studied the interaction between turbulence and complex chemical kinetics in rail diesel engines. The interaction was applied in parallel combustion simulation based on CHEMKIN-2. In addition, even though the turbulence-chemistry interaction did not affect the parallelism in the combustion solver, it produced a large computational analysis.

Steinberg et al. [23] studied the interaction between turbulent flow and premixed flame experimentally by using the particle image velocimetry technique. This method was used to evaluate the flow range and flame front situation at high temporal and spatial resolution. They used methane/air of the Bunsen flame in the combustion with equivalence ratio 0.7 and bulk velocity 1 m/s. They used the analysis of the flame surface density and the strain rate expression. They found that the turbulent structures are accountable for the generation of the flame surface density are those of the concentration of the fluid dynamic strain rate but not by the vorticity, which contrasts with the concept of the flame wrinkling caused by vortices. They also found a high

strain rate on the flame due to the interaction contained strong strain rate structures that interacted with the flame for long periods. As the interaction time of the strain-rate structures increased, the quantity of the flame surface produced, and the measurement of the flame wrinkling increased.

1.3 Numerical Approaches for Turbulent Combustion

The processing of the turbulence condition is significant in turbulent combustion modelling [3]. In general, the turbulent combustion approach may be classified into three essential types: (i) Reynolds averaged Navier–Stokes (RANS), (ii) LES and (iii) direct numerical simulation (DNS). Each type has advantages and disadvantages. The DNS of turbulent flames has a huge cost and needs complex post-processing, but it is a more accurate method; thus, all scales of the turbulence are resolved [1], and the differences between the RANS, LES and DNS are shown in Figure (1.2) [24]. Given the considerable development of computer technology, CFD simulations have become a widespread standard in the industry, thereby forming a baseline tool for turbulent combustion. The numerical simulations are replacing the analytical techniques for turbulent reacting flow processes, but numerical simulations of combustion remain complex [25]. This extensive dependence on the CFD codes rather than experiments raises the issue of the reliability of the results obtained from these codes [26]. In this study, we used only RANS for steady and LES for unsteady reacting flow. Other numerical approaches are used for the processing of turbulence such as detached-eddy simulation (DES) and hybrid RANS-LES approach. For additional detail, comprehensive reviews of these approaches are found in the review papers by Wagner et al. [27] and Sagaut [28].

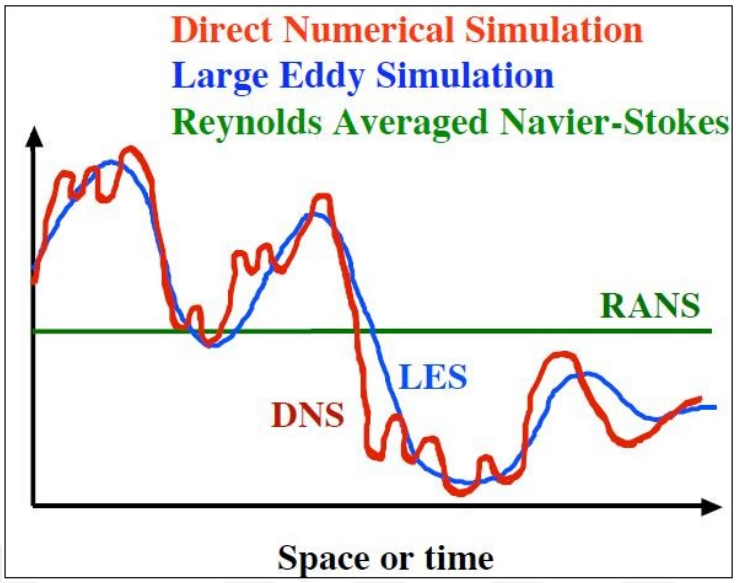

Figure 1.2 The difference between DNS, LES and RANS [24].

1.3.1 RANS Approaches

The concept of the averages of time governing equations and flow variables were introduced in the RANS approaches. However, RANS simulations do not resolve each parameter of the turbulent fluctuation directly and introduce several unclosed expressions from the time-averaging method. The entire impact of the turbulent fluctuation and these unclosed expressions on the average flow variable must be modelled [3]. The complication of turbulence prevents the RANS model to represent all turbulent flows parameters, and thus, the modification of the simulation is warranted. In this study, TFC and CFM models were used in the RANS approach. The RANS model considers the minimal computational cost approach, as opposed to the LES and DNS models. Different models have been suggested; for example, Yasari et al. [29] used RANS simulation with flame speed closure (FSC) and turbulent FSC (TFC)models to study the influence of turbulence on premixed combustion for five sets of experiments as detailed below.

1. ONERA flames at high temperatures and turbulence.
2. Conical PSI flames under high turbulence, pressures and temperatures.
3. Orleans flames at the room temperature.
4. Bunsen flames.
5. V-shaped flames at weak turbulence.

In all simulations, they used a single value of the FSC and TFC constant models of (A=0.5) and the standard turbulence ($k-\varepsilon$) model. They also studied the effect of the equivalence ratio on the reaction rate and flame structure. They predicted the thickness of the mean flame for FSC models from the maximum slope of the Favre-averaged progress variable c̃, and they found the turbulent flame closure model predicts the maximum slope of the Favre-averaged progress variable better than does the FSC model.

The collection between the TFC and the simple developed model of turbulent scalar flux was used by Sabelnikov and Lipatnikov [30] to compute the mean reaction rate of the premixed combustion. They used one dimension, the planar dimension, and the flames propagated in the frozen turbulence region. They combined the two models to solve the problem of the decrease of the reaction rate in trailing edges of the flames, especially when the Favre-averaged progress variable approached unity at the large ratio of the turbulent and laminar flame speed. They used the modifying model of turbulent scalar flux and determined the turbulent scalar fluxes and velocities in six different impinging jet flames. They found the mean thickness of the flame brush from the maximum gradient of the Favre-averaged progress variable $\tilde{c}$.

The TFC model for premixed combustion with the computational model for gaseous combustion by using one transport equation for a reaction progress variable c explained by Dinkelacker and Holzler [31]. The turbulent flame speed based to reaction rate of the progress variable c and computed for all positions of the flame brush. The heat release for the model is coupling with the flow field by the mean density and Favre averaged reaction progress variable. They used V-shape burner type of the turbulent premixed combustion with the conditions of the chemical properties and turbulent flow at the constant (A = 0.52) and different flow rates and equivalence ratios. In addition, the width of the flame applied to a simple turbulent diffusion simulation. The Laser-Doppler-Anemometry was used to measure the conditions of the inlet of the integral length scale. The turbulent burning velocity fluctuation, the mean flow velocity at 5 mm above the end of the combustor and the instantaneous density measurements with the technique of the planar laser-induced Rayleigh scattering were used to measure the mean progress variable. They used the following approaches of the reaction source that contained the progress variable:

1. $\overline{w_c} \sim |\nabla \bar{c}|$ Gradient approach
2. $\overline{w_c} \sim \bar{c}.(1-\bar{c}\,)/\mathrm{L}$ Parabolic approach

They found the deviation in the integral reaction rate for a gradient approach was independent of the width of the flame brush but proportional with the parabolic approach at constant length scale.

Lipatnikov and Chomiak [32] used the FSC model for premixed turbulent combustion. They studied the effect of pressure on flame speed in SI engines and used the constant of the FSC model (A=0.4) for all tests. They implemented multi-

dimensional numerical simulation of FSC model for FIRE code for four-valve engine combustion chamber at different conditions. They applied this model, which developed by Zimont as a reference with the development of turbulent diffusivity for spherical expanding turbulent flames.

The numerical simulations of a laboratory scale rod stabilized V-shaped flame by Manickam et al. [33] were implemented by using TFC model and an algebraic flame surface wrinkling (AFSW) reaction model. They found that the angles of flames predicted by the AFSW model are in good agreement with the experiment results, and propane combustion in TFC model shows minimal deviation.

Flohr and Pitsch [34] used the TFC modelling with RANS and LES context of the gas turbine combustor of the premixed combustion. They modelled a simple jet premixed from the burner to investigate the burner responsible for forced excitations. They based the TFC model on solving the transport equation of the reaction progress variable. In addition, the model achieved with reaction rate contains a turbulent flame speed, and the relationship between the inflow rate and heat release was indicated. Their experiment showed the good agreement of a self-excited instability technique at the same frequency in terms of its phase angle between the integrated heat release rate and the incoming flow rate.

The effect of high Damkohler and Reynolds numbers; that is, high turbulence investigated by Zimont [35] in premixed combustion burners that operated at high turbulence when velocity pulsation is are higher than flamelet combustion speed. He used intermediate steady propagation (ISP) flames of the turbulent flame closure TFC model to analyze the turbulent premixed flames at constant turbulent speed that is

controlled by chemistry, molecular processes, turbulence diffusion and flame width. The flame thickness at Richardson's law of turbulent diffusion and Kolmogorov small scale is discussed. He concluded the results as follows:

1. Combustion occurred on the intermediate steady propagation flame in turbulent time scale, $\tau_t\, D_a^{-1} \;<\; t \;<\; \tau_t\, D_a$.
2. At high Reynolds numbers, the turbulence that contains a spectrum of vortices, the acceleration of flamelets and the widening process in the combustion region had a natural limiting value. In combustion velocity and equilibrium flamelet thickness in a coordinate system where the flamelet is fixed, heat release because of combustion and the heat fluxes in the front occurs because heat convection and conduction have the same order of magnitude.
3. The flame thickness did not convert when turbulence increased and the combustion flamelet was completely wrinkled because of the combustion extinction that occurred before the mechanism of the combustion was formed.
4. The velocity of flamelet combustion was affected by the sheet region of the flamelet, thereby resulting in the decreased influence of chemical kinetics on turbulent flame speed.
5. One value of the empirical constant parameter A=0.5 is used for different gas fuel combustion for air excess value that is limited to the turbulent flame speed of ISP flames.

Lean premixed combustion in a gas turbine burner that uses the CFM model was studied by Yilmaz et al. [12]. To stabilize the flame, they used CH_4–air flames with equivalence ratios (Φ) of 0.6, 0.7 and 0.8; $k-\varepsilon$ turbulence model; and perforated flame

holder. They found that flame brush thickness and flame length decrease at increasing Φ values. They also found that modified $k-\varepsilon$ turbulence provides better velocity distribution results than the standard $k-\varepsilon$ in the region above the burner exit.

Heat release from propane and syngas combustion using CFD simulation with STAR–CCM+ software was conducted by Amico et al. [36], they used the standard $k-\varepsilon$ turbulence model and turbulent intensity 10% for numerical simulation in an adiabatic combustion chamber to generate 2.3 kW power. They found that the result of temperature distribution for propane was greater than that for syngas combustion at steady and unsteady conditions. In addition, the emission measurements from syngas in both steady and unsteady conditions were greater than of propane. Kanniche and Zurbach [37] used the CFM and eddy break up (EBU) model for two-dimensional turbulent premixed flames and the standard $k-\varepsilon$ model. They found that heat release rate is better evaluated by the CFM than by the EBU model. One of the products of fuel burning is heat release, which is an essential parameter in the study on turbulent reacting flow.

Heat release distribution is useful in understanding flame surface properties and locations in the combustor domain [38 – 41]. A few researchers have investigated the effect of turbulence on the flame location. Hartung et al. [42] used an ethylene–air mixture in a circular duct burner. The flame front location was recognized by the maximum concentration of the hydroxyl radical but not by the maximum heat release value. Meanwhile, the flame location changed by altering the equivalence ratio from 0.7 to 1.35 [43]. Moreover, the flame location changed by altering Re_λ; the flame front location was investigated by using laser tomography [44].

1.3.2 LES Approaches

The LES model represents a compromise between the RANS and DNS models, in which small structures are modelled when large structures are computed. Thus, in the LES model, a partial resolution of the turbulent fluctuations occurred, thereby leading to increases in computational cost [3]. For many applications of the premixed combustion, the reactions are bounded to propagating regimes, which are considerably thinner than the computational grids used in LES. In those cases, the interaction between the combustion and turbulence is not resolved and must be completely modelled.

The LES model in the premixed combustion elicited considerable interest from different researchers such as Moller et al. [45], who used different unsteady models of LES to flame holder to stabilize the propane flames. Pavel and Pope [46] used LES - PDF simulation for Sandia flame to stabilize the jet flow of CH_4-H_2 flames by using a bluff body.

Battaglia and Zimont [47] simulated a RANS and LES jointed method for turbulent premixed combustion into flameless combustion of a detached gas injection at inlet and strong exhaust gas recirculation. The RANS simulation was performed by stationary information of the average field, whereas LES was performed for non-stationary ones. The approach achieved the mean dissipation rate and the small scale of the turbulence was obtained by Kolmogorov theory. They used a FLOX burner to investigate the flameless non-premixed combustion by using a natural gas as a fuel, and the nominal input power is 13 kW. They concluded that, by using a different injection system, the RANS numerical simulation indicated a more compact flame than did LES simulation. In addition, the LES model, including Kolmogorov scales independent on time subgrid-turbulence viscosity, was used to produce the image of the process instead

of the Smagorinsky model. The results from RANS for the flameless region showed distributed combustion with smooth profiles of the velocity and temperature. In addition, identical instantaneous LES fields demonstrate a significant lack of uniformity of the temperature and clear documented large-scale eddies particularly at the initial part of the combustor. The LES - RANS approach works by using the Kolmogorov scales for modelling combustion intensity and sub-grid turbulence. They concluded that the developed joint LES - RANS model is an efficient timesaving tool for simulations both in the instantaneous and average fields of parameters in boiler and gas turbine burners for premixed combustion type.

1.4 Motivation for the Research

Despite the move toward renewable energy sources in recent years, the combustion of fossil fuels continues to account for the massive majority of energy production worldwide. Climate change requires the reduction in fossil fuel use, which in turn demands the development of new and efficient engine technology. This development depends largely on using numerical simulations. In other words, internal combustion engines are characterized by high flow rates in comparatively small geometries; therefore, turbulent combustion is relied on for quick and efficient energy production. Turbulent combustion addresses a number of challenges with respect to numerical simulation because of the complex interaction of fluid mechanics and chemical reactions. Combustion simulations had advanced a lot over the past few decades. The improvement of modelling attempts, with well-resolved and extremely accurate measurements of velocity, temperature and various species in turbulent flames

is needed. In addition, to understand the interaction between turbulence and combustion, the investigation of flame topology and flame location is of great interest.

A few numerical and experimental studies, such as Wu et al. [48] and Tamadonfar and Gülder [49], examine the effect of turbulence on flame location. A numerical model that predicts flame topology and calculates flame location under the influence of different turbulent flow conditions remains necessary. Based on the literature survey, the following questions motivated this dissertation:

1) At what turbulent level does the flame location move downstream or upstream in the combustor domain at a constant thermal load, i.e., constant inlet velocity?
2) Under which turbulent flow conditions is the flame topology affected?

Understanding the behavior of the flame topology in the combustor with various turbulent flow parameters is important in controlling the flame location to reduce emissions and increase power efficiency or even design novel production techniques related to flame.

1.5 Objectives of the Dissertation

The aim of this thesis is to investigate the turbulence–combustion interaction for the control of premixed combustion with turbulence. The main goal can be achieved after accomplishing the following sub-objectives:

1. To find the best combustion model in the framework of RANS equations, we planned to conduct systematic simulations of selected experimental conditions by using combustion models such as TFC and CFM;

2. To investigate the effect of turbulent kinetic energy and length scales of turbulence on the flame location and topology by using TFC and CFM, while keeping the thermal load constant; and
3. To use LES-based combustion model to test the influence of turbulence generated by oscillating jets on the flame. This approach aims to simulate the experiments as much as possible, in which the turbulence is generated by an active grid.

TFC, CFM and LES were used to calculate the flame location and visualize the flame topology from the heat release of combustion in the jet flow combustor at various turbulence levels without changing the thermal load and geometry. The results were compared with those of existing experiments.

1.6 Thesis Outline

In the practical premixed turbulent combustion, problems include the coupling between combustion and turbulence. The heat liberated from the flame was affected by the turbulence when a premixed flame propagation was in a turbulent flow. The intense interaction between flame reactions and turbulent flow needed sufficient numerical calculation models for turbulent premixed combustion. Therefore, many models exist in CFD code, which are used to simulate turbulent premixed flame such as DNS, RANS and LES. Owing to the huge cost and complex post-processing of the DNS of turbulent premixed flames, and the RANS approach deals with a balanced equation of the Favre-average density. Therefore, the RANS and LES models will be used in this work.

The background and the literature survey are discussed in Chapter 1, as are the objectives of the thesis. The turbulent flame speed is an important parameter in the turbulent premixed combustion, which represents the intensity of burning and is affected by the interaction between the chemistry and turbulence and the small or large dynamic turbulent eddies. In this work, the simulation of the TFC and CFM models with RANS for the reacting flows used for the chemical species, energy, momentum and mass for reacting flows is necessary to describe the main properties of the flow. In addition, the unsteady flow in the LES with EBU reaction modelling is discussed in detail in Chapter 2. In this work, we will manipulate the range of the turbulence intensity and turbulence length scale at different values of input power to control the impact of turbulence on the flame. Thus, we can reach the optimum combustion at the specified condition. The experiment explanation is shown in Chapter 3. The outcome results from steady and unsteady reacting flow to investigate the flame topology and flame location are discussed in details in Chapter 4. The conclusions and the recommendations for future work are elucidated in the last chapter.

CHAPTER II

THEORETICAL BACKGROUND

2.1 Physical and Chemical Processes in Premixed Turbulent Combustion of Gaseous Fuels

The heat released from combustion depends on the concepts of interaction between turbulence and combustion. Turbulent premixed flames involve the interaction of processes, such as chemical reactions, turbulent eddies, and heat transfer. These processes required simplified TFC, CFM, and LES models to estimate the characteristics of the flame. Heat release is a combustion product of CFM and TFC models and is an essential parameter in the study of turbulent reacting flows. Heat release distribution is useful in understanding the properties and locations of flame surfaces in jet flow combustor [43, 44].

One way of attaining heat transfer during combustion is intake form of radiation. Performing coupled simulation with radiation is a challenge in practical situations because of the interaction between combustion and turbulence. According to P. Coelho [50], the influence of radiation on turbulence acts as a dissipation process. The effects of radiative heat transfer increase with temperature, but these effects decrease with the dissipation rate of turbulent kinetic energy. This assumption was matched with J. Li and M. Modest [51], especially at small flame thickness; thus, maximum temperature was dropped to 18 K and the difference in heat release with and without radiation effect is less than 5%. Zimont et al. [52] reported the maximum error in temperature

measurement, which was calculated at less than 70 K when radiation effects were disregarded. Therefore, the effect of radiation on combustion is neglected in the CFM and TFC models. The effect of radiation on combustion will be studied in two cases in terms of the distribution of heat release on the centerline of the combustor of CFM and TFC models.

Lean premixed combustion can potentially reduce pollutant emissions from combustors [21, 22]. Soot may form from burning propane with air at a high equivalence ratio that is generally higher than unity. Yellow flame indicate to soot particles, which are commonly produced under rich fuel conditions in nonpremixed flames [20]. The lean mixture of propane–air reaction includes multiple species in specific proportions, such as C_3H_8, O_2, H_2O, N_2, and CO_2. Lean premixed combustion was operated at high-efficiency and low-emission conditions to reduce burnt gas temperature [26, 29]. The static temperature of the fresh mixture is set to 300 K in the present study. We suppose that soot does not form at a low equivalence ratio. This assumption was enhanced by Zimont et al. [52] and Goh et al. [8]. Yilmaz et al. [12] used 0.6, 0.7, and 0.8 equivalence ratios for a lean premixed combustion in a gas turbine combustor. They found that emission can be reduced to negligible levels at these ratios. They also found that flame location was decreased by increasing the equivalence ratio. In the present study, the equivalence ratio is held constant and lower than unity. Thus, soot formation is not expected.

The CFM and TFC models were designed for one – step reaction [53]; thus, the global one – step reaction for lean propane air mixture was used. This case can sufficiently predict different variables of combustion, such heat release, temperature,

and velocity profile. However, many researchers, such as Yilmaz et al. [12], Nazzal and Ertunc [16], and H. Schmid et al. [43] used one - step reaction in their studies.

Flow is generally turbulent in daily life applications. Flames are affected by turbulent flow because density dropped more than once within a typical flame. In addition, high-density drops and large heat releases are typically localized in thin flame fronts, thereby introducing difficulties in studying the effect of heat release in flame turbulence [19]. The interaction between turbulence and combustion and vice versa is important and should be investigated to understand the effects of turbulence on flame behavior. The interaction problems between turbulent and combustion may be classified into two ways. The first problem concerns with the heat release in flames, which may be affected by turbulence characteristics. These characteristics include mean dissipation rate, root mean square (rms) of turbulent fluctuation velocity, and time and length scales. Heat release increases the magnitude of velocity, thereby increasing heat release rate, which causes the self-acceleration of a turbulent flame. In addition, an instantaneous flame front causes perturbations in flows that wrinkle the flame front. This condition will be discussed extensively in Chapter 4. The second problem concerns the RANS equation in a non-reacting flow, wherein molecular transfer is significantly lesser than the turbulent transfer. In addition, RANS addresses the estimation of the mean quantities that differ from instantaneous values. The mean quantities are practically desirable. This approach requires limitation in the range of time and length scales by applying averaging techniques to the conservation equations. Favre averaging is usually used because of high fluctuations in density due to heat release [50].

In our study of the LES model, we aim to generate turbulence in different ways. The first approach is the use of a long jet flow pipe instead of a short one. The second

method is the use of turbulent parameters in the inlet region, such as turbulent kinetic energy, dissipation rate of turbulent kinetic energy, turbulent intensity, and turbulent length scale. Unfortunately, we failed to generate turbulence using these methods. Finally, turbulence can be generated by setting the characteristics of the sinusoidal wave in the inlet region. Thus, we aimed to simplify the model because LES is an unsteady transient condition and computationally costly.

2.2 Turbulence and Combustion Interaction.

When simulating the turbulent reacting flow by numerically solving the Navier–Stokes equations, averaged quantities should be used [54]. In this chapter, the effect of combustion on turbulence and vice versa is explained by the balance equation for the Favre averaged combustion progress variable. Many researchers have discussed turbulence and combustion interaction from the perspective of the Bray Moss Libby model or RANS and LES approaches. These studies include Bray et al. [55], Ahmed [56], Bray [57], Steinberg et al. [58] and Swaminathan [59]. However, the approach was performed by using the Favre-averaged quantities and density variations [60], as follows:

$$\frac{\bar{\rho}}{\rho_u} = \frac{1}{\left(1+\tilde{c}\left(\frac{\rho_u}{\rho_b}-1\right)\right)} \tag{2.1}$$

$$\tilde{T} = T_u\,(1-\tilde{c}) + T_b\tilde{c} \tag{2.2}$$

$$\tilde{c}_\alpha = c_{\alpha,u}\,(1-\tilde{c}) + c_{\alpha,b}\tilde{c} \tag{2.3}$$

where T_u , ρ_u , $c_{\alpha,u}$ and T_b , ρ_b, $c_{\alpha,b}$ are the temperature, density and species concentrations, respectively, in unburned gases (for reactants $\tilde{c} = 0$) and for burned gases (products $\tilde{c} = 1$).

If the turbulent combustion flame front is moving with turbulent flame speed (U_t) inside a combustor domain, the brush width controlled by turbulent diffusion (D_t) can be described by the following Favre averaged combustion progress variable equation.

$$\frac{\partial}{\partial t}(\bar{\rho}\tilde{c}) + \frac{\partial}{\partial x_j}(\bar{\rho}\tilde{u}_j\tilde{c}) = -\frac{\partial}{\partial x_j}(\overline{\rho u_j{}''c''}) + \frac{\partial}{\partial x_j}\overline{\left(\rho D_t \frac{\partial c}{\partial x_j}\right)} + \bar{W} \qquad (2.4)$$

In modelling of premixed turbulent combustion, to estimate the reaction rate ($\bar{W}$) is the central problem of the model which represent the complexity of the interaction processes. Such a model introduces a differential equation for estimation the normalized as a function of the Damkohler, Reynolds, Zeldovich, Karlovitz and Lewis or Markstein numbers and the density ratio, depending on the rms of turbulent fluctuation velocity (u′) or on the ratio of (u'/S_L) in dimensionless numbers being strong. In addition, at a constant density flow, the interaction between combustion and turbulence is explained in Figure (2.1).

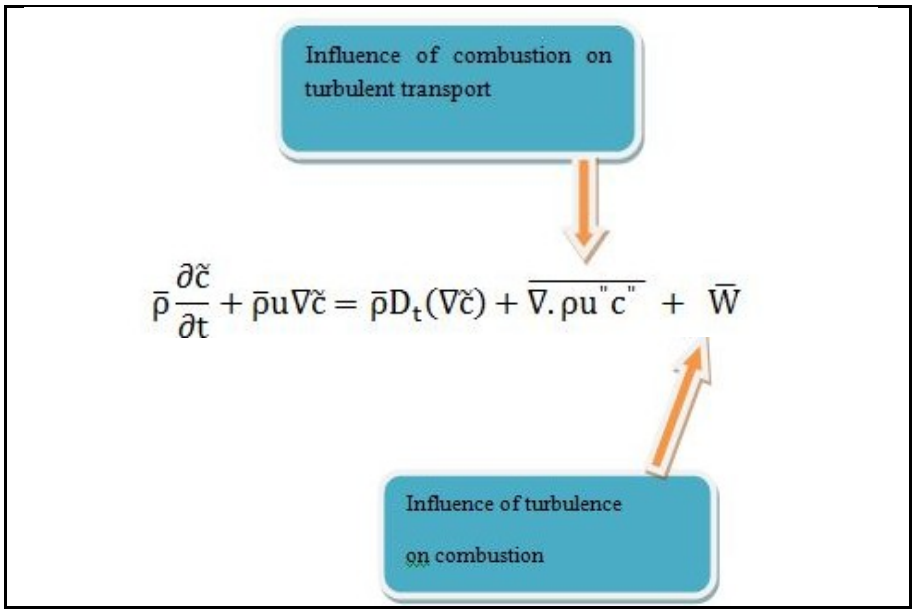

Figure 2.1 Turbulence influenced by combustion and vice versa.

2.2.1 The Influence of Combustion on Turbulence

The effect of combustion on turbulence can be considered by the balance equation for the Favre-averaged combustion progress variable equation as mentioned in Equation (2.4).The effect of the combustion on a turbulent flow is explained in two ways. Firstly, the heat release of the flame is changed and affects the turbulence properties, such as the mean dissipation rate $\bar{\varepsilon}$, RMS turbulent velocity u′ and time scale and length scale. The value of velocity is increased by the heat release, thereby increasing the heat release rate that causes self-acceleration of a turbulent flame. Secondly, in the mean Navier–Stokes equation as in Equation (2.5), the components of the Reynolds stress tensor $\overline{u_i''u_j''}$ are higher than the components of the viscous stress tensor $\overline{\tau_{ij}}$ [19].

$$\frac{\partial}{\partial t}(\bar{\rho}\tilde{u}_i) + \frac{\partial}{\partial x_j}(\bar{\rho}\tilde{u}_i\tilde{u}_j) = -\frac{\partial}{\partial x_j}(\overline{\rho u_i'' u_j''}) - \frac{\partial \bar{p}}{\partial x_j} + \frac{\partial \overline{\tau_{ij}}}{\partial x_j} \tag{2.5}$$

The effect of combustion on turbulence required to close the turbulent scalar flux $(\overline{\rho u'' c''})$ in Equation (2.4) and the turbulence properties, such as rms turbulent velocity (u′), that are used by a model of the reaction rate $\bar{W}$ as shown in Figure (2.1) and Equation (2.6) are determined [19].

$$\frac{\partial}{\partial t}(\overline{\rho u_i'' c''}) + \frac{\partial}{\partial x_j}(\tilde{u}_j\,\overline{\rho u_i'' c''}) = -\frac{\partial}{\partial x_j}(\overline{\rho u_i'' u_j'' c''}) - \overline{\rho u_i'' u_j''}\frac{\partial \tilde{c}}{\partial x_j} - (1-\tilde{c})\tau S_L \bar{W}\bar{n}_i +$$

$$\bar{\rho}\bar{c}(1-\tilde{c})\left[\overline{\left(\frac{1}{\rho}\frac{\partial p}{\partial_{x_i}}\right)}_u - \overline{\left(\frac{1}{\rho}\frac{\partial p}{\partial_{x_i}}\right)}_b\right] - \overline{\rho u_j'' c''}\left[\frac{\partial \tilde{u}_i}{\partial_{x_J}} + \frac{\bar{W}\delta_{ij}}{\bar{\rho}(1-\tilde{c})}\right] \tag{2.6}$$

where n_i, $\frac{\partial p}{\partial_{x_i}}$ and δ_{ij} are the normal vector acting on the unburned mixture, the pressure gradient and the mean flame brush thickness, respectively. In addition, the rms of the turbulent velocity is written as:

$$\acute{u} = \sqrt{\frac{\overline{\rho u_j'' u_j''}}{3\bar{\rho}}} \tag{2.7}$$

At a high Reynolds numbers, the mean molecular diffusion term is neglected in Equation (2.4); then, the averaging value of the turbulent velocity is as follows:

$$\nabla . \bar{u} = \frac{\tau}{\rho_u} \overline{W} \tag{2.8}$$

2.2.2 Influence of Turbulence on Combustion

In turbulent premixed flame, the instantaneous reaction rate depends on the instantaneous temperature and temperature pulsations; therefore, the reaction rate cannot be estimated to be utilizing the average temperature. Therefore, the standard disturbance method cannot be used, and an advance model is required to close the mean rate of product formation. Numerous approaches can be followed in the analysis of Lipatnikov and Chomiak [61]. In addition, several models can be classified depending on the progress variable term (see appendix A).

1. Algebraic model.
2. Presumed PDF model.
3. Self-similarly developing premixed turbulent flame model.
4. Flame surface density and scalar dissipation rate model.

Therefore, the simplified of the reaction rate of TFC, CFM and LES models are required to study the flame characteristics inside the combustor, which will be discussed later.

2.3 Governing Transport Equations

2.3.1 General Form

In combustion, large density variations happen. Therefore, the density-weighted averaging procedure, i.e. Favre averaging, is appropriate for all the flow and combustion quantities, for example, velocity can be written as follows [60]:

$$\tilde{u} = \frac{\overline{\rho u}}{\bar{\rho}} \tag{2.9}$$

In addition, the fluctuations from the Favre-averaged mean are calculated as follows:

$$u^{"} = (u - \tilde{u}) \tag{2.10}$$

The number of atoms in the combustion chamber as a whole does not change as mass conservation. A recognized approach to depict turbulent premixed combustion is by scalar variable c. This reaction progress variable *c* propagates reacting species and represents the combustion, which is zero in reactants and has unity in products [13]. Moreover, we need mean values of reaction space variables that consider turbulent fluctuations at any spatial site [57]. Then, the general form of Reynolds averaging and Favre averaging of reacting flow conservation equations is written as [1, 19].

- Mass $\frac{\partial \bar{\rho}}{\partial t} + \frac{\partial \bar{\rho}\tilde{u}_i}{\partial x_j} = 0$ (2.11)
- Momentum $\frac{\partial \bar{\rho}\tilde{u}_j}{\partial t} + \frac{\partial \bar{\rho}\tilde{u}_j\tilde{u}_i}{\partial x_j} = -\frac{\partial \bar{\rho}\widetilde{u_j^{"}u_i^{"}}}{\partial x_j} + \frac{\partial \bar{\tau}_{ij}}{\partial x_j} - \frac{\partial \bar{p}}{\partial x_i} + \bar{\rho}g_i$ (2.12)
- Species $\frac{\partial \bar{\rho}\tilde{Y}_i}{\partial t} + \frac{\partial \bar{\rho}\tilde{Y}_i\tilde{u}_j}{\partial x_j} = -\frac{\partial \bar{\rho}\widetilde{Y_i^{"}u_J^{"}}}{\partial x_j} - \frac{\partial \bar{\tau}_{ij}}{\partial x_j} + \overline{W}$ (2.13)
- Energy $\frac{\partial \bar{\rho}\tilde{E}}{\partial t} + \frac{\partial \bar{\rho}\tilde{u}_j\tilde{E}}{\partial x_j} = -\frac{\partial \bar{\rho}\widetilde{E^{''}u_j^{''}}}{\partial x_j} - \frac{\partial}{\partial x_j}\overline{\left(\rho D_t \frac{\partial E}{\partial x_j}\right)} + HR$ (2.14)

  where $E = h - \frac{P}{\rho} + \frac{1}{2}u_i u_i$ and HR is the heat released from the combustion.

2.3.2 TFC Model

When we describe the physical model of premixed combustion at strong turbulence and fast chemistry and present the equations, we used the RANS and Favre averages. The creation of products and HR are results of chemical processes described with a single progress variable c, which defines the normalized mass fraction of products. The TFC model was designed for one - step reaction, therefore global one - step reaction for propane was used [57]. Due to lean premixed combustion was used in TFC model soot does not form [52], which will be discussed in Chapter 4. The transport equation for the fuel mass fraction, Y_f and the source term, ω_{tfc} are written as [53].

$$\frac{\partial \rho Y_f}{\partial t} + \nabla.\left(\rho u Y_f\right) = \nabla.\left(\Gamma_{Y_f} \nabla Y_f\right) + \omega_{tfc} \tag{2.15}$$

$$\omega_{tfc} = \rho_u U_t \left|\nabla Y_f\right| \tag{2.16}$$

where U_t, and Γ_{Y_f} are turbulent flame speed and diffusion coefficient of fuel mass fraction respectively.

In the TFC model, the reaction rate is important to investigate the flame topology, which will be discussed in Section 2.4. For the source term, U_t depends on the local turbulence parameters and physico - chemical characteristics of the combustible mixture. To simplify TFC model, and derive a new expression of the U_t depending on the strength of turbulence some assumptions should be considered theoretically [52]:

1. The flame flow is one-dimensional.
2. Density and turbulence parameters are constant before combustion.
3. Neglect the radiation effect in the energy equation.

Then, the transport equation for progress variable Equation (2.15) becomes:

$$\frac{\partial \tilde{c}}{\partial t} = \frac{\nu_t}{S_C}\frac{\partial^2 \tilde{c}}{\partial x^2} + U_t\left(\frac{\partial \tilde{c}}{\partial x}\right) \quad (2.17)$$

Equation (2.17) describes the combustion as a wave moving with the turbulent flame speed, and the wave width is increased due to the turbulent diffusion. This equation is apparent if the 1-D transport equation for ($\tilde{c}$) is expressed in a coordinate system $\acute{x} = \mathrm{x} + \mathrm{U_t}\,\mathrm{t}$ moving with the front. Then, we integrate Equation (2.17) between x = -∞ (unburnt mixture) and x = ∞ (burnt gas) in a coordinate system moving with the turbulent flame speed to form the mass conservation equation.

$$\rho_u U_t = \rho_b\,(\tilde{u}_b + U_t) \quad (2.18)$$

In TFC model, the turbulent flame speed is expressed in terms of turbulence parameters and chemical characteristics of the combustion. Large-scale turbulent vortices wrinkle the thickness of the flame and control the turbulent combustion area width, whereas for small scales, the turbulent concentrates the transfer processes inside the flame and estimates their propagation velocity $\mathrm{Un_t}$ and thickness $\delta \mathrm{n_t}$. In the turbulent combustion mechanism, the whole flame area depends on the completing spectrum of turbulence and is estimated by its integral characteristic and thickened flame, by using Kolmogorov scales and dimensional analysis for small-scale turbulence; then, the velocity of the 'thickened' front (Un_t) can be written as [52]:

$$Un_t \sim D_a^{-0.5}\ \acute{u} \quad (2.19)$$

where

$$D_a = \frac{\tau_t}{\tau_c}, \qquad \tau_t = \frac{l_t}{\acute{u}}, \qquad \tau_c = \frac{D_t}{S_L^2} \quad (2.20)$$

$$\delta n_t \sim D_a^{-1.5}\ l_t \quad (2.21)$$

where D_a is the Damkohler number; τ_t, l_t and τ_c denote the turbulent time, length scales and chemical time scale, respectively; and $\mathrm{S_L}$ represents the laminar flame

speed [63, 64]. In this study, all simulations will be achieved at powers of 3, 5 and 9 kW and turbulent intensities (Ti) of 10%, 15%, 20% and 25% with a turbulent length scale (l_t) of 0.01 m and will be examining the influences of turbulent and combustion parameters on the flame topology and location.

By using the factor ($\frac{\bar{A}}{A_0}$) (instantaneous flamelet sheet area for the unit of cross-sectional area), the turbulent flame velocity U_t is greater than the velocity of the thickened front Un_t, i.e.

$$U_t \sim Un_t \left(\frac{\bar{A}}{A_0}\right) \sim Un_t \frac{\Sigma}{\Lambda} \tag{2.22}$$

where $\Sigma^2 = \overline{(z - z^-)^2}$ indicates the inequality in the flame position due to turbulent convection and Λ refers to the microscale of the random flame front surfaces.

$$\Sigma^2 \sim D_t\, t \sim l_t t\acute{u} \tag{2.23}$$

where (D_t) denotes the turbulent diffusion and time (t) is in the range between

$$\tau_t \leq t \leq \frac{l_t}{Un_t} \sim \tau_t D_a^{-0.5} \tag{2.24}$$

In addition,

$$\Lambda \sim (\delta n_t t\acute{u})^2 \tag{2.25}$$

For dimensional analysis and constant consideration and by combining Equations (2.19), (2.21), (2.23) and (2.25), we can obtain

$$\frac{\bar{A}}{A_0} \sim \left(\frac{l_t}{\delta n_t}\right)^{0.5} \sim D_a^{0.75} \tag{2.26}$$

Then, from Equations (2.19), (2.21) and (2.22), we can achieve

$$U_t = A\, D_a^{0.75}\, D_a^{-0.5}\, \acute{u} \tag{2.27}$$

or $U_t = A D_a^{0.25}\, \acute{u}$

where A is a constant of the TFC model.

$$U_t = A\acute{u}\left(\frac{\frac{l_t}{\acute{u}}}{\frac{D_t}{S_L^2}}\right)^{0.25} \tag{2.28}$$

The turbulent flame speed is written as [53]:

$$U_t = AG\left(l_t{}^{0.25} S_L^{0.5} D_t^{-0.25} \acute{u}^{\,0.75}\right) \tag{2.29}$$

where G is the flame stretch factor and D_t represents the unburnt thermal diffusivity of the unburned mixture.

Numerous researchers have used different values of the TFC model constant A. In this study, Chapter 4 explains the effect of constant A on the flame topology of propane–air lean premixed combustion. Zimont et al. [52] implemented the TFC model for a CFD code-based finite volume that is supported by gas turbine burner experiments and that sets the default value of the constant A as 0.52. Several researchers have used this value in their studies. The constant A plays an important role in a turbulent flame speed equation and thus on flame properties [18, 19, 65]. Turbulent flame speed U_t is considered to be the core of the TFC model and is derived by analyzing the flame structure performed in the premixed combustion [66]. Flame properties include different factors, such as flame location, flame speed, flame thickness and temperature. The flame speed can develop from laminar to turbulent conditions. The flame location can be characterized by temperature or progress variables [65, 67]. The constant A of the TFC model is influenced by turbulent intensity, Ti, and thus flame topology.

The relationship between the rms of u' and turbulent kinetic energy can be written as [18, 68].

$$k = 1.5(u')^2 \tag{2.30}$$

where k and ε are used to describe the turbulent length scale, l_t, mathematically.

$$l_t = \frac{k^{1.5}}{\epsilon} . \frac{{C_\mu}^{0.75}}{\kappa_v} \tag{2.31}$$

where κ_v and C_μ represent the Von Karman constant and turbulent viscosity coefficient, respectively.

The turbulent intensity is indicated to the turbulence grade in the turbulent combustion and defined as the ratio between the rms values of u' and mean velocity of flow $\overline{U}$.

$$Ti = \frac{u'}{\overline{U}} \tag{2.32}$$

The high turbulence level and Reynolds number can be achieved by active grids [69]. Re_λ is used to classify the strength of the turbulence [5] and is a Reynolds number based on the Taylor microscale. In a homogeneous isotropic turbulent flow, Re_λ is approximated as [18]

$$Re_\lambda = k\sqrt{\frac{20}{3\nu\epsilon}} \tag{2.33}$$

The turbulent intensity generally refers to the turbulence level, which is the ratio between the mean velocity of the flow and the rms of velocity fluctuations u′ [16, 70]. We used all these parameters to derive a new expression of the turbulent flame speed, U_t, which is defined as a function of Re_λ. The Reynolds number based on the Taylor microscale, Re_λ, which includes turbulent intensity elucidates the impact of turbulence on flame specially at wrinkled and corrugated flamelet regions [71 – 76].

The laminar and turbulent flame speeds are important parameters used in the CFM and TFC model and from Equations (2.29 – 2.33). Thus, we can derive a new expression of the turbulent flame speed U_t depending on the strength of turbulence (Re_λ) as:

$$U_t = 0.4217\ AG\left(\nu^{0.375} S_L^{0.5} D_t^{-0.25} {Re_\lambda}^{0.75}\right) \quad (2.34)$$

The effect of turbulence on turbulent flame speed can be represented solely by Re_λ, which will be discussed in Chapter 4. The constant A in Equation (2.34) was set at 0.37 in all simulations depending on our prior investigation [77]. Damkohler was the pioneer to derive the turbulent flame speed theoretical expression. The two various regimes of premixed turbulent combustion are set, namely, small- and large-scale turbulences. To understand these two regimes, we will discuss a new regime diagram called Borghi diagram in different reaction zones as shown in Figure (2.2) [63, 64 and 78].

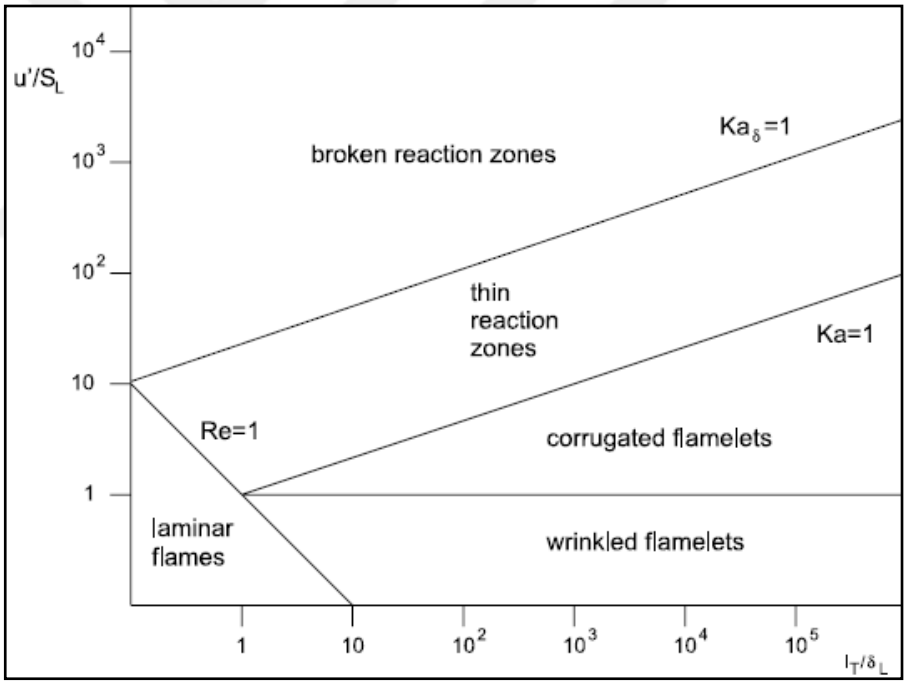

Figure 2.2 Borghi diagram for premixed turbulent combustion [78]

Some of the cornerstone results from turbulence theory concerning the premixed turbulent combustion regimes are from Zimont [79], Pope [80] and Peter [81]. They defined the regimes of premixed turbulent combustion in terms of length scale and velocity ratios. The diagram contains two main areas: laminar in the left corner below

the line (Re = 1) and turbulent area above the unity Reynolds number line. The two logarithmic axes of the diagram represent the manometer and denominator of the turbulent Damkohler number as expressed in Equation (2.45) and can be rewritten as:

$$D_a = \frac{\frac{l_t}{l_f}}{\frac{\acute{u}}{S_L}} = \frac{\text{length scale ratios}}{\text{velocity ratios}} \tag{2.35}$$

Moreover, if the flame thickness l_f, turbulent intensity $\acute{u}$ and turbulent length scale l_t are introduced, then the turbulent Reynolds number is written as [82]:

$$Re = \frac{\frac{l_t}{l_f}}{\frac{S_L}{\acute{u}}} \tag{2.36}$$

Kolmogorov theory presented that the energy transferred from the large eddy of the integral scale is equal to the energy dissipation at the Kolmogorov scale. Then, the Kolmogorov length (η), velocity (u_η) and time (t_η) scales can be written as [82]:

$$\eta = \left(\frac{\nu^3}{\varepsilon}\right)^{0.25} \tag{2.37}$$

$$u_\eta = (\nu\varepsilon)^{0.25} \tag{2.38}$$

$$t_\eta = \left(\frac{\nu}{\varepsilon}\right)^{0.5} \tag{2.39}$$

where ν is the kinematic viscosity and ε denotes the dissipation rate. In addition, with the Kolmogorov length, velocity and time scales defined, we write two turbulent Karlovitz numbers, which represent the boundaries of the reaction zones in the Borghi diagram as [78]:

$$Ka = \left(\frac{l_f}{\eta^2}\right)^2 = \left(\frac{{u_\eta}^2}{{S_L}^2}\right) = \left(\frac{t_f}{t_\eta}\right) \tag{2.40}$$

Moreover, when the reaction zone thickness (δ) is appropriate, then the second Karlovitz number is written as:

$$Ka_{\delta} = \left(\frac{{l_{\delta}}^2}{\eta^2}\right) = \delta^2 K \quad \text{Where} \quad l_{\delta} = \delta \; l_f \tag{2.41}$$

In the Borghi diagram, we notice that the boundaries of interest are the line of the unity velocity ratio (i.e. $\frac{\acute{u}}{S_L} = 1$), which separates between the wrinkled and corrugated flamelet areas, and the line denoted by the unity second Karlovitz number (i.e. Ka_{δ} = 1), which separates between broken and thin reaction zones.

In addition, the unity Karlovitz number (i.e. $Ka = 1$) separates between the thin reaction zone and corrugated flamelets areas.

The first area in the turbulent region is the wrinkled flamelet area, where $u' < S_L$; the turbulent intensity (u') of even the large eddies is not large enough to contend with the progress of the laminar burning velocity (S_L) flame front, which is dominating over the flame front corrugated by turbulence.

The second area in the turbulent region is the corrugated flamelet regime, which is characterized by Ka < 1, which means that the flame thickness is less than the Kolmogorov length scale, indicating that the entire diffusion flame structure is entrench with eddies of the size of the Kolmogorov scale, where the flow is quasi-laminar. Therefore, the flame is not perturbed by turbulent fluctuation and stays quasi-steady. In addition, the border between corrugated and thin reaction zone regimes is calculated by Ka = 1, which is the flame thickness equivalent to the Kolmogorov length scale. Moreover, the burning velocity is equal to the Kolmogorov velocity and the flame time is equal to the Kolmogorov time scales.

The third turbulent region is the thin reaction zone, which is characterized by $Ka_\delta < 1$ and $Ka > 1$, because the Kolmogorov length scale (η) is less than the flame thickness (l_f), and then the small eddies of size η are able to enter into the reaction preheat zone. In addition, the small eddies remain larger than the inner layer thickness (l_δ) and cannot sneak into the reaction preheat zone.

The last turbulent region is the broken reaction zone where Kolmogorov eddies are less than the inner layer thickness (l_δ). The eddies have to enter into the inner layer and perturb it with the outcome that chemistry break down because enhancement the heat loss to the preheat zone followed by the loss of radicals and decrease the temperature. When this case occurs, the flame will be extinguished, and the oxidizer and fuel will inter-diffuse and mix at low temperatures where combustion reactions have turned off. Thus, the discussion of the Borghi diagram shows the relationship between dimensionless numbers and turbulence scales from one side and velocity ratio in turbulent combustion regimes on the other side; for further details, see Peter [78, 82] , Tamadonfar and Gülder [83], P. Siewert [84] and numerous others.

2.3.3 CFM

The CFM provides solution for both flame structure and fluid dynamics and solves the reaction rate of transport Equation (2.15) in terms of flame area density and fuel mass fraction. The same assumptions that used to simplified TFC model were used here. Therefore, transport Equation (2.15) is written in the fuel mass fraction term as follows [53].

$$\frac{\partial \rho Y_f}{\partial t} + \nabla.\left(\rho u Y_f\right) - \nabla.\left(\Gamma_{\mathrm{Y_f}} \nabla Y_f\right) = \omega_{cfm} \tag{2.42}$$

The chemical reaction rate in propane reaction is the mass of the species (*i*) produced per unit time and volume [57, 71]. In CFM, the flame area density is solved using the chemical reaction rate of the species transport equation [53].

$$\omega_{cfm} = -(\rho_u S_L \Sigma)(Y_{ft} - Y_{res}) \tag{2.43}$$

where ρ_u is the density of the unburned mixture, S_L denotes the laminar flame speed and Σ refers to the flame area density. In addition, *c* represents progress variable, which can be written as:

$$c = \frac{Y_{ft} - Y_{res}}{Y_{ft}} \tag{2.44}$$

where Y_{res} represents the amount of fuel mass fraction in the end of the combustion and $Y_{ft}$is the fuel mass fraction in the unburnt gas. Hence, for totally burned case Y_{res}=0.0 and *c*=1, and for totally unburned case Y_{res}= Y_{ft} then *c*=0.0.

To solve the transport equation of the flame area density (σ) which represents the flame area per unit mass; we can use this formula [16, 53].

$$\frac{\partial(\rho\sigma)}{\partial t} + \nabla.(\rho u\sigma) - \nabla.(\rho\Gamma_\sigma \Delta\sigma) = S_\Sigma + \nabla.(\Gamma_\sigma \sigma \Delta\rho) \tag{2.45}$$

The source term, S_Σ which includes the flame area production by stretch and can be calculated from this equation [16, 53].

$$S_\Sigma = \alpha K_t \Sigma - \beta_1 \frac{\rho_u Y_{ft} S_L (1 + a\sqrt{k}/S_L)}{\rho Y_f} \Sigma^2 \tag{2.46}$$

where $\alpha, \beta_1 \; and \; a$ are represent the CFM parameters equal to 1.5, 1 and 0.1, respectively [68].

Equation (2.46) indicates that the net flame stretch is a function of the turbulent kinetic energy and dissipation rate of turbulent kinetic energy (*K*–*ε*) model. For the

FAD, the turbulence effect is represented in terms of the flame stretch factor, which is a function of the K-ε model. Therefore, flame stretch (K_t) in Equation (2.46) is calculated as.

$$\Gamma_K = \frac{K_t}{\epsilon/_k} = f(\frac{\acute{u}}{S_L}, \frac{I_l}{\delta_l}) \tag{2.47}$$

where, I_l integral length scale and δ_l is the thermal laminar flame thickness.

Finally, Γ_K has this formula.

$$\Gamma_K = \Gamma_p - B.\Gamma_q \tag{2.48}$$

where, Γ_p and Γ_q are the flame production and quench due to the stretch. In addition, $\acute{u}$ and I_l can be calculated from Equations (2.30) and (2.31), respectively.

The CFM model was designed for one- step reaction and the transport equation of the species was used to describe the reactive flow [53]. Since the test cases include only lean premixed combustion soot formation is not expected [56]. In the CFM model, the reaction rate is important to investigate the flame topology, which will be discussed in Section 2.4.

2.3.4 LES Model

In the previous sections, the propane reaction at steady-state conditions from two different models, such as TFC model and CFM, with different input parameters was discussed. In this section, the LES model, which is an unsteady technique, of the propane reaction is described. In this model, the turbulent length and time scales at large values are solved, and the small-scale motions are modelled [53]. In the LESs, the difficulties appear as a flow upstream in the combustion chamber area. Moreover, LES uses a wall subgrid scale, which computes implicit kinetic energy and turbulent

viscosity. The reaction in LES is an eddy breakup type. The hybrid reaction is one - step reaction calculating the reaction rate and is represented by the minimum value calculated by turbulent mixing and finite-rate chemical kinetics. As LES is an unsteady mechanism technique, the time step is an important parameter to control the combustion rate and reach the coverage solution, which will be discussed later. The unsteady mechanism technique includes the combustion instability and ignition limit. The objective of the unsteady mechanism is to release the modelling constraints that are difficult in the RANS model [85]. In addition, to avoid stretching the mesh, the ratio of turbulent kinetic energy to subgrid kinetic energy is larger than 20 [53].

2.3.4.1 LES Transport Equations

In the context of LES inside the combustor domain, the vortices are formed beyond the inlet region depending on the amplitude of pulsation and the frequency of the inlet sine wave velocity as shown in Figure (2.3), which is presented here by the line integral convolution of velocity streamline. The pressure has dropped characteristics of a decaying swirl flow in the region beyond active grids forming the vortices in this region. Figure (2.4) depicts the time histories of the total mass flows entering the combustor for inlets 1 and 2 at mean velocities $\overline{U}_1$ = 0.079 m/s and $\overline{U}_2$ = 1.25 m/s and fluctuation velocities A_{o1} = 0.106 m/s and A_{o2} = 0.188 m/s, respectively, with frequency f = 100 Hz. The total mass flow rate ratio passing inlets 1 and 2 has unity, and therefore, the total mass flow rate in the inlet region is constant. The set of transport equations used in the LES model is obtained by arranging into a form of unsteady RANS equations, which are applicable for transient conditions. Then, the subgrid scale filtering equation for species can be written as [53]:

$$\frac{\partial(\rho)\tilde{Y}_i}{\partial t} + \frac{\partial(\rho)\tilde{Y}_i\tilde{u}_j}{\partial x_j} = \frac{\partial}{\partial x_j}\left[\left(D_t + \frac{\mu_t}{\sigma_k}\right)\frac{\partial \tilde{Y}_i}{\partial x_j}\right] + \bar{\omega}_{LES} \tag{2.49}$$

The filtered reaction rate $\bar{\omega}_{LES}$ as a type of eddy breakup reaction rate can be calculated directly from an Arrhenius expression and by using filtered values of the mass fractions and temperature as [86]:

$$\bar{\omega}_{LES} = A_r T^{\beta} \exp\left(-\frac{E_a}{RT}\right)[Y_{C3H8}]^n[Y_{O2}]^m \tag{2.50}$$

where A_r, β, E_a, R, m, n and $[Y_i]$ are the Arrhenius coefficient, temperature exponent, activation energy, universal gas constant, rate exponents of reactants and mass fraction of species, respectively.

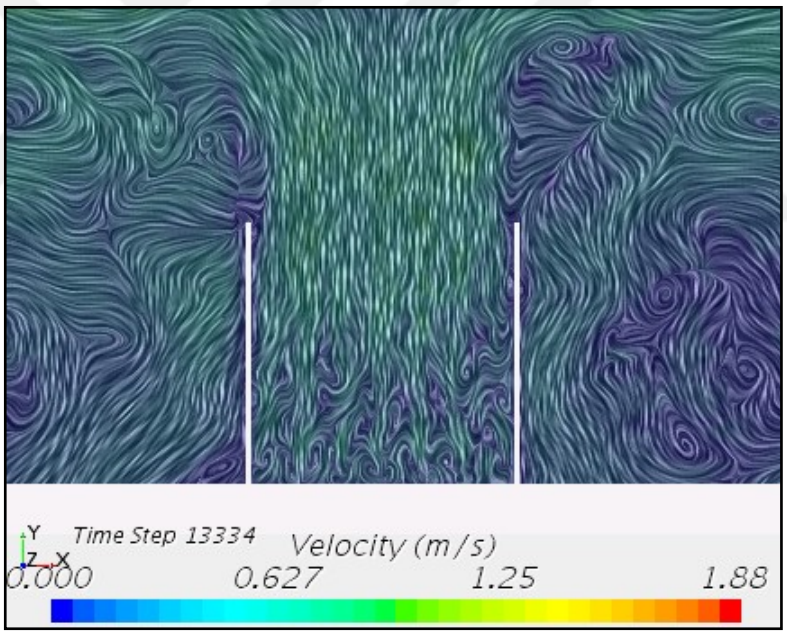

Figure 2.3 Vortices formed in the region beyond active grids at t = 4s and mass flow ratio 10% in inlet 1 and f =100 Hz and A_o = 0.15 m/s.

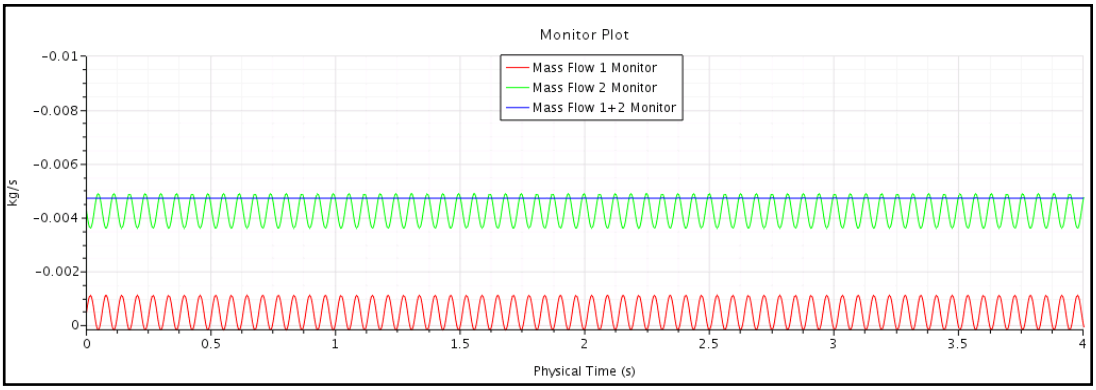

Figure 2.4 Mass flow rate of the fuel and air mixture in inlet 1and inlet 2 during the combustion duration at t = 4 s with frequency of 100 Hz and mass flow rate 10% in inlet 1 and amplitude of pulsation of 0.15 m/s.

2.4 Heat Release

One way to visualize the flame is to look at the level of *HR* from the combustion. *HR* is an essential value to investigate the turbulent and laminar reacting flows. Practically, the precise distribution of *HR* inside the combustor is beneficial to discern the flame and its location [22]. However, *HR* is impacted by modifying turbulent intensity. As a result of burning fuel, such as propane, one of the products is *HR*, which is an important parameter in the study of turbulent combustion interaction. The distribution of *HR* in the jet flow combustor region is useful in understanding the flame topology and their locations [4, 23 – 25]. In this study, two main calculations related with *HR* are performed. The first is performed with steady reacting flow with the TFC model and CFM, and the second calculations are related with unsteady reacting flow with the LES model. However, when the hydrocarbon fuel (C_3H_8) is burning, numerous species and radical species will be created, but only carbon dioxide and water are the final combustion products as in Equation 2.51. In addition, the burned gas should consist only of water, carbon dioxide, oxygen and nitrogen; therefore, the

completely chemical energy bound in the fuel is transformed to thermal energy. This transformation is called *HR*. The reaction is used as CFM, TFC and eddy breakup reaction types in the LES model. Because of one – step reaction was designed for CFM and TFC models therefore, the one – step global reaction of propane is set as follows [87 – 92]:

$$C_3H_8 + 5(O_2 + 3.76N_2) \leftrightarrow 3CO_2 + 4H_2O + 18.8N_2 + HR \quad (2.51)$$

Radiation transfer may be calculated from a steady reacting flow solution to investigate wall heat fluxes for example, because of interactions between combustion and turbulence perform coupled simulation in practical situations is a challenge [86]. Despite of this, two simulations in TFC and CFM models are performed to show the effects of radiative heat transfer as explained in Chapter 4. And when the effect of radiation is disregarded, the energy equation in terms of enthalpy can be written as [93]:

$$\frac{\partial \rho h}{\partial t} + \frac{\partial (\rho u_i h)}{\partial x_i} = \frac{DP}{Dt} - \frac{\partial J_i^h}{\partial x_i} + \tau_{ij}\frac{\partial u_i}{\partial x_i} + \omega_i \quad (2.52)$$

$$h = \sum_{i=1}^{N}\left\{Y_i\left[h_i + \int_{T_{ref}}^{T} C_{p,i}TdT\right]\right\} \quad (2.53)$$

where h is the enthalpy, J_i^h denotes the enthalpy molecular flux and τ_{ij} represents the turbulent stress tensor and T_{ref} = 298.15 K indicates the reference temperature. The temperature is then calculated from the enthalpy in accordance with the state equation. In addition, h_i refers to the low heating value of the fuel and is 46.39 kJ/g for propane. If we consider radiation effect on the flame holder region, then the heat conducted to the outer surface of the flame holder is lost to the environment by convection and radiation. Then the heat transfer can be expressed as.

$$-k_1\frac{\partial T}{\partial r} = h[T_{ro} - T_\infty] + \varepsilon_1\sigma_1[T_{ro}^4 - T_{surr}^4] \quad (2.54)$$

From Equations 2.16 and 2.43 related to the reaction rates of TFC and CFM models respectively, the heat release formula can be written as:

$$HR = \sum_{i=1}^{N} \omega_i \, h_{\,i} \tag{2.55}$$

In the TFC model, the reaction rate is proportional to the gradient of the mean progress variable, Equation 2.16, and the first model was found by Zimont et al. [52], followed and improved by Zimont and Lipatnikov [35] and Lipatnikov and Chomiak [32, 61]. While in CFM model, the reaction rate is proportional to the flame area density for which a balance equation is derived and closed, Equation 2.43. In this issue, we have the model of Kanniche and Zurbach [37] and Candel et al. [38]. Therefore, different flame shapes were observed in CFM and TFC models.

By considering the coupling relation between the species mass fractions and temperature, the final expression of HR can be written as [53, 71]:

$$HR = \sum_{i=1}^{n} h_i \; \omega_{cfm} \qquad \text{(CFM)} \tag{2.56}$$

$$HR = \sum_{i=1}^{n} h_i \; \omega_{tfc} \qquad \text{(TFC Model)} \tag{2.57}$$

$$HRR = \sum_{i=1}^{N} h_i \; \bar{\omega}_{LES} \qquad \text{(LES Model)} \tag{2.58}$$

Therefore, from equations of heat release, one can notice that the difference between CFM and TFC model is the reaction rate and can be written as in Equations 2.16 and 2.43 and subsequently we have different solutions of transport equation of species and will be giving different flame shapes as explained in Section 4.3.

2.5 Turbulent Premixed V-Flame

In the LES model, the flame will be formed as a V–flame shape in the combustion domain. A V-flame is formed by inserting either a wire or a hot surface in a flow of downstream premixed mixture [94, 95]. Dinkelacker and Holzler [31] studied a lean methane-air, V-shaped flames stabilized by a wire placed above the exit of the burner with a diameter of 40 mm. Turbulence was generated by a perforated plate placed 70 mm below the burner exit. In this study, the hot surface of the flame holder is used. The wire creates a wake region in which the flame can propagate to stabilize itself, whereas the combustion will start from the energy released from the wire. When the flow is laminar, the flame propagates against the entering fuel and air mixture, and a premixed V-shape flame is formed [96, 97]. While in a turbulent flow, the wings of the flame are corrugated by velocity fluctuations and the V-flame shape is recovered in the mean *HR* profile. This profile is of interest because grid turbulence may be generated in the entering fuel and air mixture flow, so combustion occurs in a well depicted spatially when decaying turbulence. Different V–flame shapes under different turbulent sine wave velocity parameters will be investigated in Chapter 4.

CHAPTER III

EXPERIMENTAL AND NUMERICAL SETUP

3.1 Experimental Setup

The models described in previous chapters were tested against an experimental data for lean premixed propane fuel [98]. Simulations were performed using TFC model, CFM and LES model presented in Chapter 2 and were compared with each other and with experiments. In addition, all the simulations were conducted for turbulent reacting flows at equivalence ratios of 0.588 and 0.606 to estimate the combustion conditions of propane. The experiments were performed to generate a premixed flame at inlet powers of 3, 5 and 9 kW from the jet flow combustor. Lean premixed combustion under the influence of active grid turbulence is computationally investigated, and the results are compared with experimental data.

3.2 Experimental Configuration

The experimental study used for the validation of the simulation methodology was lean premixed propane combustor configuration as depicted in Figure (3.1) and Figure (3.2) [98]. This experiment was selected for its relatively simple geometry and boundary conditions but complex flow patterns resembling those in a gas turbine combustor and for the availability of detailed measurements that map the species, temperature and velocity fields within the combustor. The experimental study consisted

of three essential tests for 3, 5 and 9 kW conducted under various operating turbulent conditions.

The combustion experiments were conducted using an active grid, which comprised an array of moving square wings attached to rods and an axisymmetric burner. The active grid generated a high turbulence level with a low flow rate. Ten motors controlled the wings' rotation. Experiments were performed to generate a premixed flame at equivalence ratios (Φ) of 0.588 and 0.606 and approximate Re_λ values of 70, 90 and 110. Table (3.1) presents the turbulent specifications and inlet flow conditions. The inlet diameter of the burner is 100 mm. The chamber height is 550 mm. The flame holder has a diameter and thickness of 200 and 5 mm, respectively, and lies above the burner exit by 100 mm. Air and fuel were mixed before being injected into the chamber and the mixture at the inlet included C_3H_8, O_2 and N_2. The mixture flowed at a constant inlet velocity, that is, constant thermal load. After mixing, the flow was transmitted through a flame barrier and a pipe that encompassed the transverse and longitudinal active grid to generate turbulent conditions. In the experiment, the flame topology was depicted as low, medium and highly turbulent depending on the Re_λ. The increase in turbulent conditions enhanced the heat transfer in the reaction zone for the small eddies of the premixed mixture [63]. The experiments were performed at room temperature and atmospheric pressure. Images extracted from videos were used to capture the flame phenomena. The flame images and their averages can only be used to compare with the numerical simulations due to the limited data of experiments. Turbulence downstream of the active grid was measured with hot wire anemometer in the absence of combustion. The images were captured using a colored digital camera.

Each image is 576 × 720 pixels, representing the flame topology at a specific Re_λ. Table (3.1) lists the flow conditions and dimensions specified in the experiment.

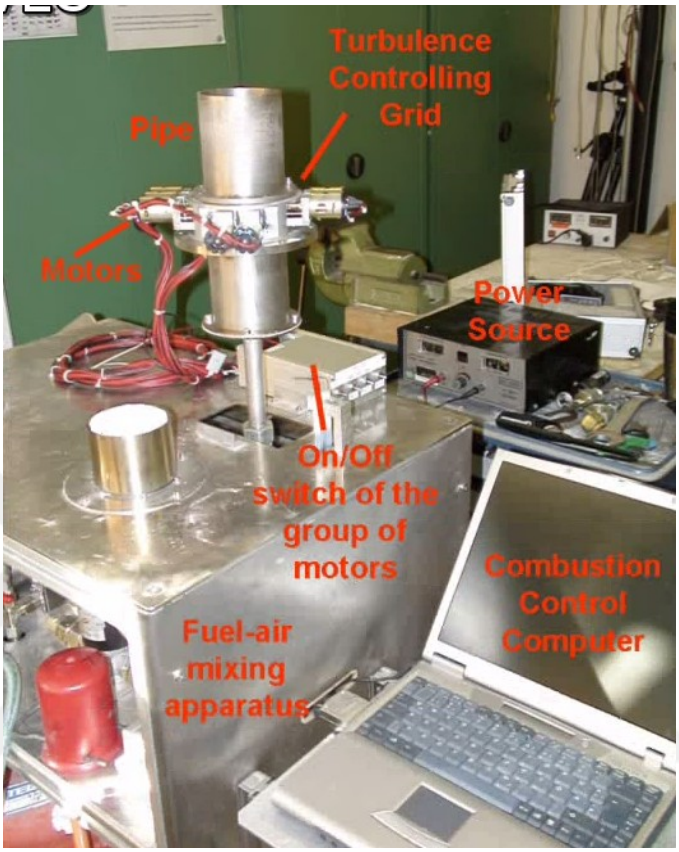

Figure 3.1 Experimental apparatus [98].

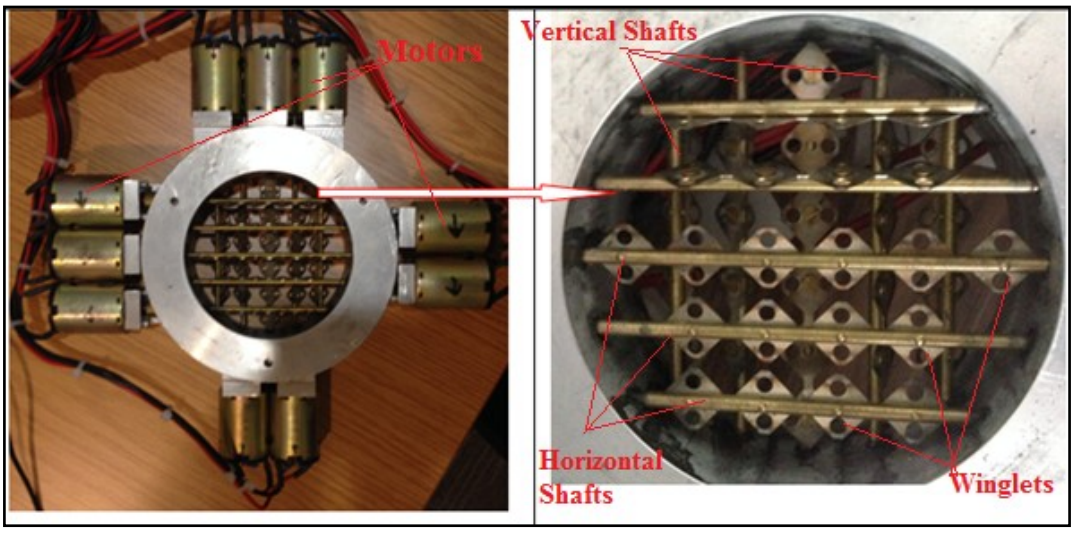

Figure 3.2 Active regular grids with motors [98].

Table 3.1 Inlet flow conditions at different thermal loads.

Power (kW)	Y_{C3H8}	Y_{O2}	Y_{N2}	Inlet mean velocity (m/s)	Equivalence ratio	Re_λ	Excess air ratio (lambda)
3	0.0392	0.2352	0.7255	0.17	0.606	5 10 20 30 40	1.65
5	0.0382	0.2355	0.7264	0.29	0.588	40	1.7
9	0.0382	0.2355	0.7264	0.52	0.588	20 70 90 110 150	1.7

3.2.1 Active Grid Generate Turbulence

In this study, the transverse and longitudinal active regular grids moved by 10 motors generated turbulence. The design of the active grid as shown in Figure (3.2) follows that of Mydlarski and Warhaft [5] and Kang. et al. [99]. The active grid consists of two rows, with five vertical and five horizontal rotating shafts in each row. The shafts are composed of 3 mm diameter round brass. The first, second, fourth and fifth vertical and horizontal shafts have four square flaps (winglets), and the third shaft (centre) has six square flaps, so the total number of grids in the two rows is 44. In addition, the grid size is $0.01 \times 0.01\ m^2$ composed of 1 mm-thick aluminum plate. Each shaft is

independently driven by a 1/4 hp AC motor and each motor is controlled by an inverter. The control signal is generated by a PC and sent to the inverters. The main objective of the active grids is to generate upstream turbulent flow even in low inlet velocity.

3.3 Experimental Results

Images extracted from videos were used to capture the flame phenomena. The flame images and their averages can only be used to compare with the numerical simulations due to the limited data of experiments. Turbulence downstream of the active grid was measured with hot wire anemometer in the absence of combustion. The images were captured using a colored digital camera. Each image is 576 × 720 pixels, representing the flame topology at a specific Re_λ. Figure (3.3) shows the experimental instantaneous snapshot flame images of a premixed gas mass flow rate at a different Re_λ and 300 K. The images represent the flame topologies and locations at different Re_λ values, which can be comparison with numerical results. The images exhibit an average of 63 instantaneous snapshots of the flame performed by ImageJ techniques with one frame for the first reaction and another frame for the second reaction. Generally, the flames are blue and corrugated and move upstream toward the burner exit by increasing Re_λ due to complete fuel burning. The flame may flash back with a further turbulence increase. The flame barrier prevents this incident. However, the gas is stopped to prevent the active grid, located above the flame barrier, from being damaged. In addition, sufficient amount of oxygen in the fuel molecule of premixed gas facilitates the oxidation of the fuel, thereby increasing the homogeneous combustion area below the flame holder and preventing soot formation.

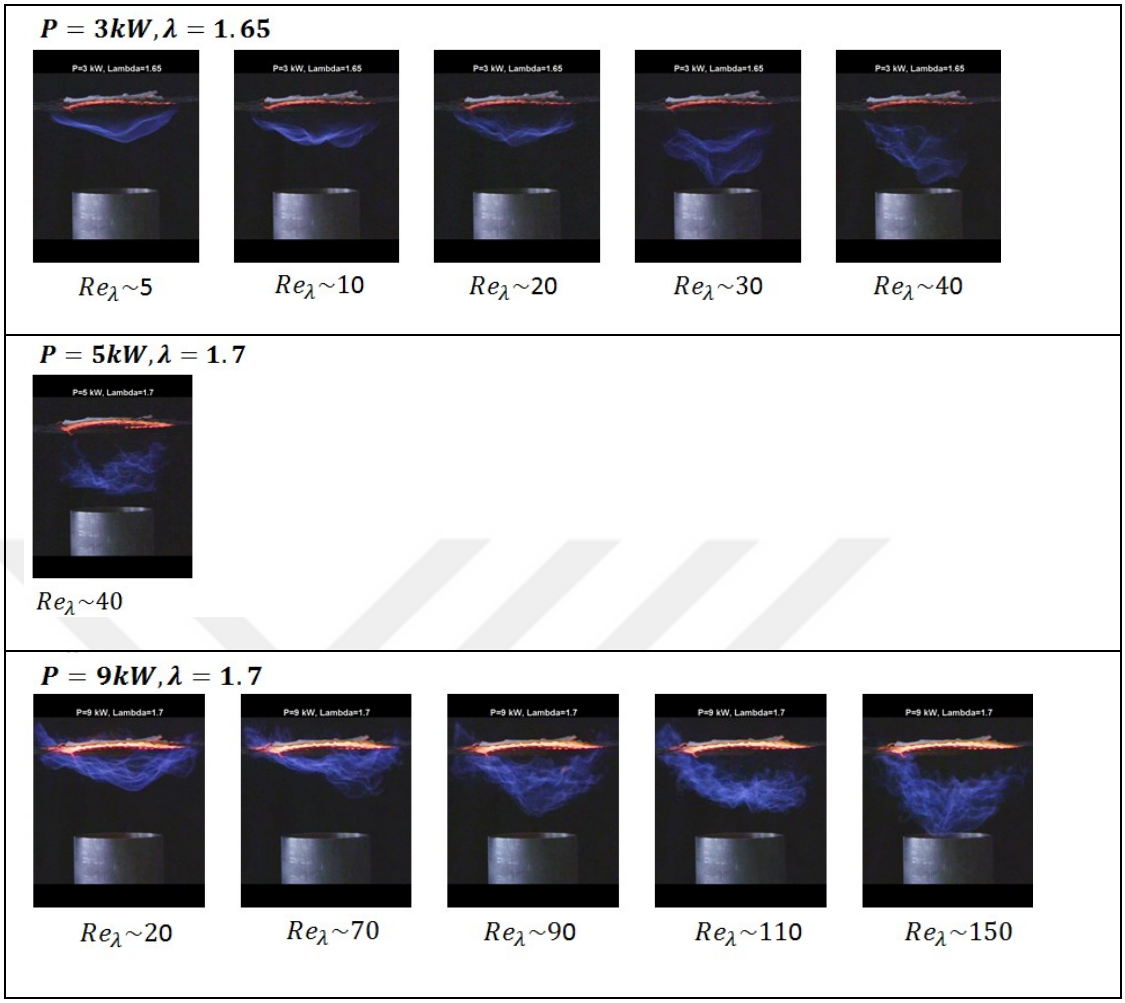

Figure 3.3 Instantaneous snapshots of experimental flame images at different excess air ratios at different Re_λ values [98].

Figure (3.4) shows the experimental averaged flame images of a premixed gas mass flow rate at 5.0868 g.s^{-1} and an excess air ratio (lambda = 1.7) at a different Re_λ, 300 K and thermal load of 9 kW. The images represent the flame topologies and locations at different Re_λ values (i.e. Re_λ = 70, 90 and 110). The images represent an average of 63 instantaneous snapshots of the flame performed by ImageJ techniques. Generally, the flames are blue and corrugated due to complete fuel burning and move upstream toward the burner exit by increasing Re_λ. The flame may flash back with a further turbulence increase. The flame barrier prevents this incident. However, the gas is

stopped to prevent the active grid, located above the flame barrier, from being damaged. In addition, sufficient amount of oxygen in the fuel molecule of premixed gas facilitates the oxidation of the fuel, thereby increasing the homogeneous combustion area below the flame holder and preventing soot formation.

Re_λ = 70 Re_λ = 90 Re_λ = 110

Figure 3.4 Average of 63 instantaneous snapshots of experimental flame images at excess air ratio (lambda = 1.7) and the stages of increasing Re_λ at P = 9 kW.

3.4 Numerical Setup

By using the mean velocity $\overline{U}$ and fluctuation velocity (represented here by the amplitude of pulsations, A_o), the inlet sine wave velocity equation can be written as in Equation (3.1) to generate the turbulence in the combustion system.

$$U(t) = \overline{U} \mp A_o \sin(2\pi f t), \tag{3.1}$$

In addition, the mean velocity can be calculated from the state equation as:

$$\dot{m} = \rho A U \tag{3.2}$$

Through the calibrated mass flow rate ratio in inlets 1 ($\dot{m}_1$) and 2 ($\dot{m}_2$), the frequency f and the amplitude of pulsation A_o, the turbulence can be generated in the inlet region and then transferred inside the jet pipe flow during the cold flow period.

After the fuel–air mixture is reached, the hot surface of the flame holder is used, the combustion occurs and then the V– shape flame is formed.

Figure (3.5) shows the cross section of the combustor used for all of the simulations. The burner diameter is 0.1 m. The combustion chamber height is 0.55 m and the diameter is 0.51 m. In the steady-state case (CFM and TFC model), the inlet region is one region, whereas in the unsteady-state case (LES model), the inlet region is divided into two regions as A_1 and A_2 with a ratio of A_1/A_2 = 1.765 to generate turbulence. The grid is an unstructured polyhedral mesh with 301,594 cells for the TFC model and CFM and 1,271,418 cells for the LES model. The cell size measurement and refinement were performed in the combustion chamber domain as follows; the inlet, pipe jet flow and flame holder regions were 0.0131 m for TFC and CFM and 0.0078 m for LES and the regions near the wall were 0.016 m. In addition, coarse meshes were used for the regions near the walls, and fine meshes were utilized for the reaction and inlet regions due to computational cost and time. The boundary conditions of all the combustor parts, such as the velocity inlet (CFM and TFC model) or mass flow inlet (LES model) conditions in the inlet region and the pressure outlet in the outlet regions were applied. For the CFM and TFC model, the adiabatic wall case for others parts of the combustor was used even though this assumption is generally correct, whereas in the LES model, the convection boundary condition was utilized for the top, bottom and surrounding regions. The realizable, $k-\epsilon$, two-layer mode was used for turbulence modelling [87].

To initialize a new TFC simulation, the Reynolds number based on the Taylor microscale, Re_λ, is set as the experiment value for 3, 5 and 9 kW thermal loads. Turbulence in the inlet region progressively fills the domain and ultimately becomes

fully developed. The turbulence in the steady case, i.e. TFC model and CFM, is set by the dissipation rate of turbulence and turbulent kinetic energy as in Equation (2.33). However, in the unsteady reacting flow, i.e. LES model, is set by characteristics of the sinusoidal wave. The velocity field in the LES model is set by the sinusoidal velocity as in Equation (3.1) [88]. The computational time step (*dt*) was selected by computing a generalized The convective time scale (CFL) number as [89]:

$$CFL = \frac{u\Delta t}{\Delta x} + \frac{v\Delta t}{\Delta x^2} \tag{3.3}$$

The implicit unsteady solver time step is 0.3 ms and used for all LES simulations, and the corresponding CFL is less than 0.5.

The averaging time of for all mean quantities is 3.66 s out of 4 s of total simulation time. Averaging starts after the fresh mixture reaches the flame holder region. Combustion occurs due to the hot flame holder with an initial temperature set to 1700 K. Fresh mixture takes 0.34 s to reach the flame holder region. Combustion occurs within 3.66 s and flow forms the vortices behind the inlet region. They are transferred to the combustion region and boundaries of the combustor. The statistical accuracy of the mean quantities is assessed using the number of independent samples within 3.66 s of computation time. Integral time scale T_l of the reacting flow in the jet flow combustor can be calculated as:

$$T_l = \frac{D}{\overline{U}} \tag{3.4}$$

where, $\overline{U}$ (0.53 m/s) is the average value of the inlet velocity and *D (0.1 m)* is the inlet diameter of the burner. Hence, T_l is approximately 0.2 s. Therefore, sampling rate can be estimated as:

$$The\ sampling\ rate = \frac{1}{2T_l} \approx 2.5\ Hz \tag{3.5}$$

The number of independent samples is approximately 9 at 3.66 s. The statistical uncertainty of any mean quantity (θ) can be described as:

$$\frac{\hat{\mu}_\theta}{\mu_\theta} = 1 \pm z\alpha_{/2} \frac{1}{\sqrt{N}} \frac{\sigma[\hat{\mu}_\theta]}{\mu_\theta} \approx 1 \pm z\alpha_{/2} \frac{1}{\sqrt{N}} T_i \tag{3.6}$$

where $z\alpha_{/2}$ is the confidence coefficient for a confidence interval of $(1-\alpha)$. The second term is the deviation of the estimated mean of θ ($\hat{\mu}_\theta$) from the real mean of θ (μ_θ) value. σ is the standard deviation estimator. Thus, T_i is turbulence intensity if θ is the velocity [105]. Statistical uncertainty can be approximated with number samples $N = 9$ and 95% confidence and $T_i = 0.28$ at around 18% using T_i for all variables. If this level will be reduced to below 10%, the number of independent samples should be 36 and the average time of computation should be around 14 s as see in Figure (3.6). This simulation would last for 105 s (more than 30 days) because 4 s of simulation costs 30 h in a 28–core workstation. This computation time cannot be afforded for the number of tests conducted in this study.

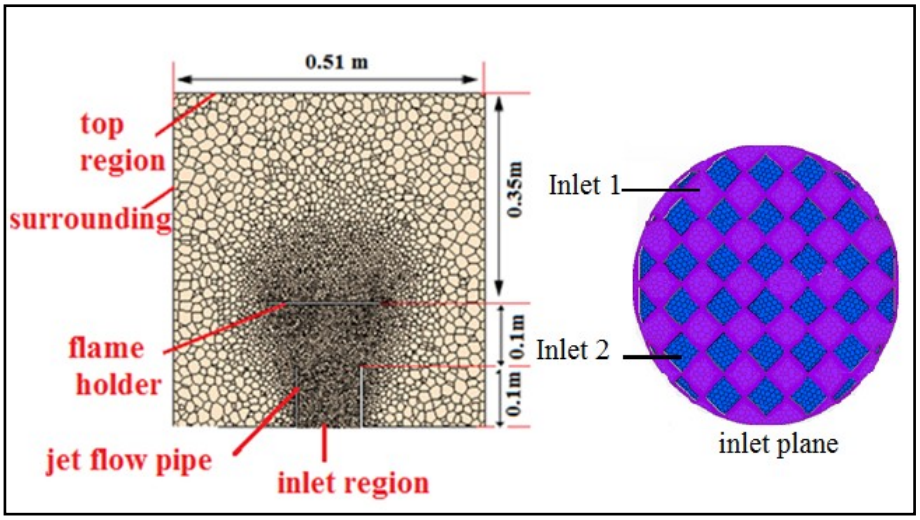

Figure 3.5 Left: cross section of the combustor and the refinement mesh in the reaction region and jet flow region, right: inlet 1 and inlet 2 which represent the active grids in the computational analysis.

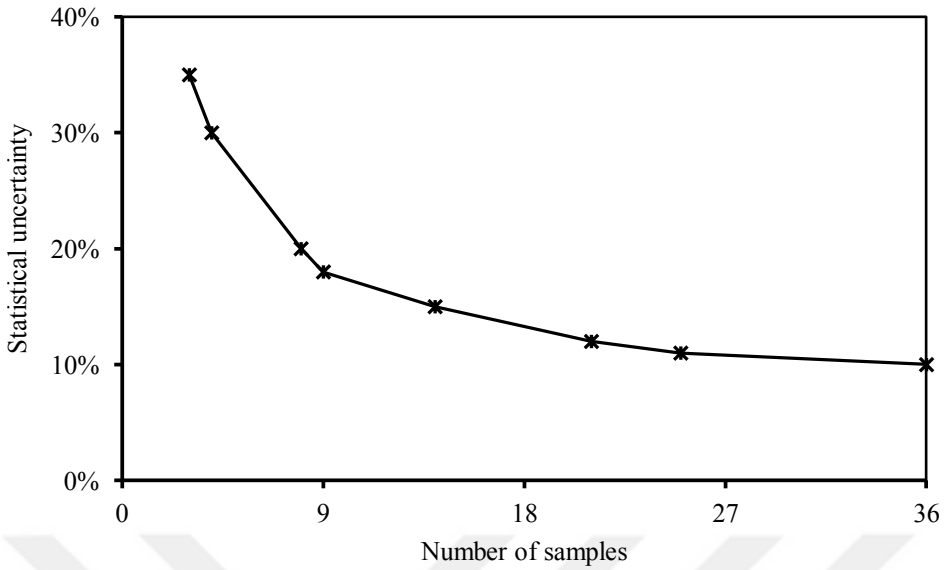

Figure 3.6 Statistical uncertainty distribution at a given independent samples.

CHAPTER IV

RESULTS OF NUMERICAL SIMULATIONS

4.1 Introduction

Simulations of steady reacting flows were performed using two primary models, such as TFC model and CFM, under the same computational turbulent factors. In addition, LES for unsteady reacting flows was performed and results were compared with the experiments. All the simulations are conducted for lean premixed combustion at equivalence ratios of 0.588 and 0.606 to estimate the flame characteristics. The influence of the factors, such as Re_λ, turbulent intensity, turbulent length scale, turbulent kinetic energy and turbulent dissipation rate, of turbulence on the flame topology and location was computationally investigated, and the results are compared with experimental data for steady reacting flow. In addition, the influence of the characteristics of the sinusoidal wave for unsteady reacting flow is considered for this purpose. Understanding the behavior of the flame topology in the jet flow combustor with various turbulent flow parameters at a constant thermal load, i.e. constant inlet velocity and equivalence ratio, which is determined by the *HR*, is important in controlling the flame location. This flame location obtained from *HR* in a jet flow device is used to improve this technology to control the flame location and thickness, which might be applied on the design of combustion chambers.

4.2 Calibration of TFC Model

In the beginning of this study, the TFC model was calibrated for a lean premixed combustion under the influence of turbulence only for 5 kW. The calibration was conducted under various flow conditions, such as the TFC constant A from 0.1 to 0.5 step 0.1 and different turbulent intensities (Ti) 10%, 15%, 20% and 25% with a turbulent length scale (l_t) of 0.01 m. The TFC constant A is an essential parameter in the premixed combustion. The TFC model was calibrated by varying constant A until the simulation reproduces the flame as in the experiments. Then, the simulations were extended for 3 and 9 kW for the same computational factors. The results showed that the flame topology and location are highly modified by changing constant A and turbulence intensity from weak to strong turbulence. Furthermore, the heat transfer and turbulent flame speed in the reaction zone of the jet flow combustor are enhanced through the increase in turbulence level. Table (4.1) lists the comparison for the model constant used in the literature.

Table 4.1 Comparison of using the TFC constant model.

Constant of TFC model (A)	Reference No
0.4	[41]
0.5	[38, 44, 60, 103]
0.52	[40, 13, 101]
0.65	[102, 104]
1	[43]
0.1-0.5 (0.37)	This work [77]

All numerical simulations are compared with the experiments. Table (4.2) presents the inlet flow conditions at an input power of 5 kW and different turbulent intensities. Each value of turbulent intensities represents a single value of constant A.

Experimental flame images are only available to compare with the numerical simulation and to obtain the average of a set of neighborhood images. The images represent an average of 63 instantaneous snapshots of the flame using ImageJ software with the first frame for the first reaction and the second frame for the second time, as shown in Figure (4.1). The flame color is blue due to the sufficient amount of oxygen in the fuel–air mixture and the total fuel consumption in the burning operation. The flame is confined in the reaction region between the flame holder and burner exit. The flame is corrugated shape and not stretched into the inlet region.

Table 4.2 Inlet flow conditions at an excess air ratio (lambda=1.7).

Power (kW)	Equivalence ratio (Φ)	Inlet velocity m/s	Propane mass fraction	Oxygen mass fraction	Nitrogen mass fraction	l_t (m)	Ti %	constant A
5	0.5556	0.2966	0.0361	0.2360	0.7279	0.01	10	0.1
								0.37
								0.5
							15	0.1
								0.37
								0.5
							20	0.1
								0.2
								0.3
								0.32
								0.35
								0.36
								0.365
								0.369
								0.37
								0.38
								0.4
								0.5
							25	0.1
								0.37
								0.5

The fuel mass fraction contour in Figure (4.2) shows the main results of the calibration in terms of the mass fraction of fuel at different values of constant A and at constants Ti = 20% and l_t = 0.01 m. The 12 simulations clearly represent the effect of constant A. At low values of constant A and moderate turbulence (Ti = 20%), the flame topology diffuses outside the flame holder region. The flame is gradually moved down inside the combustor domain toward the inlet region. The last case in Figure (4.2)

presents the proper mass fraction results found at moderate turbulence. Then, we find that the best value of constant A is 0.37 matching with the experiments [77].

After selecting the proper value of constant A, the study is expanded to 10% (low), 15% (moderate) and 25% (high) turbulence intensities. The fuel mass fraction contour in Figure (4.3) depicts the flame topology at a constant length scale and different constant A values, i.e. A = 0.1, 0.37 and 0.5 and Ti of 10%, 15% and 25%. At a low turbulence and constant A value, the flame moves outside the flame holder region; however, when constant A increases to 0.5, the concave flame topology is enclosed inside the pipe jet flow region. At A = 0.37, the flame topology fits the experimentally observed flame.

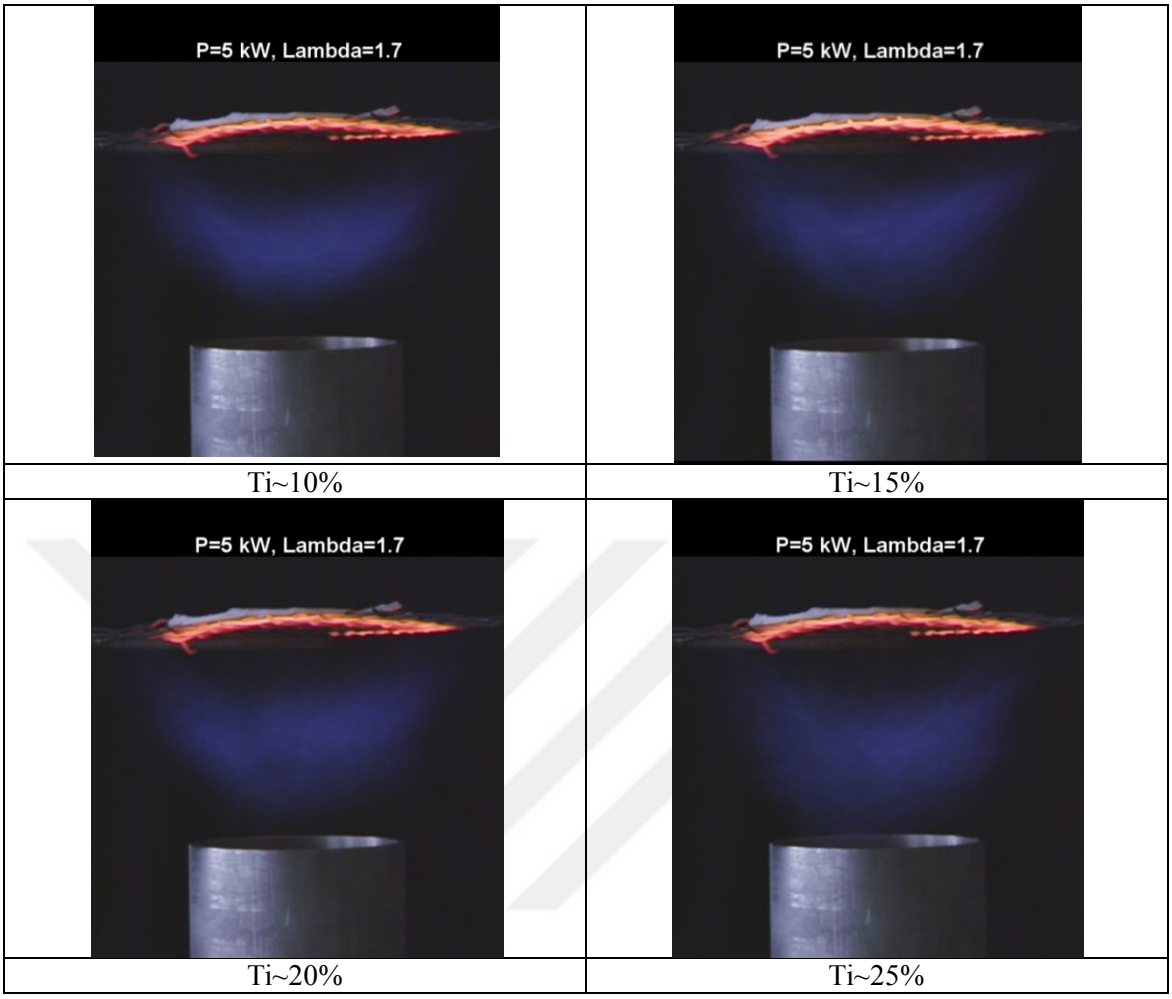

Figure 4.1 The average of 63 instantaneous snapshots of experimental flame images shows the increasing in turbulent intensity at thermal load of 5kW.

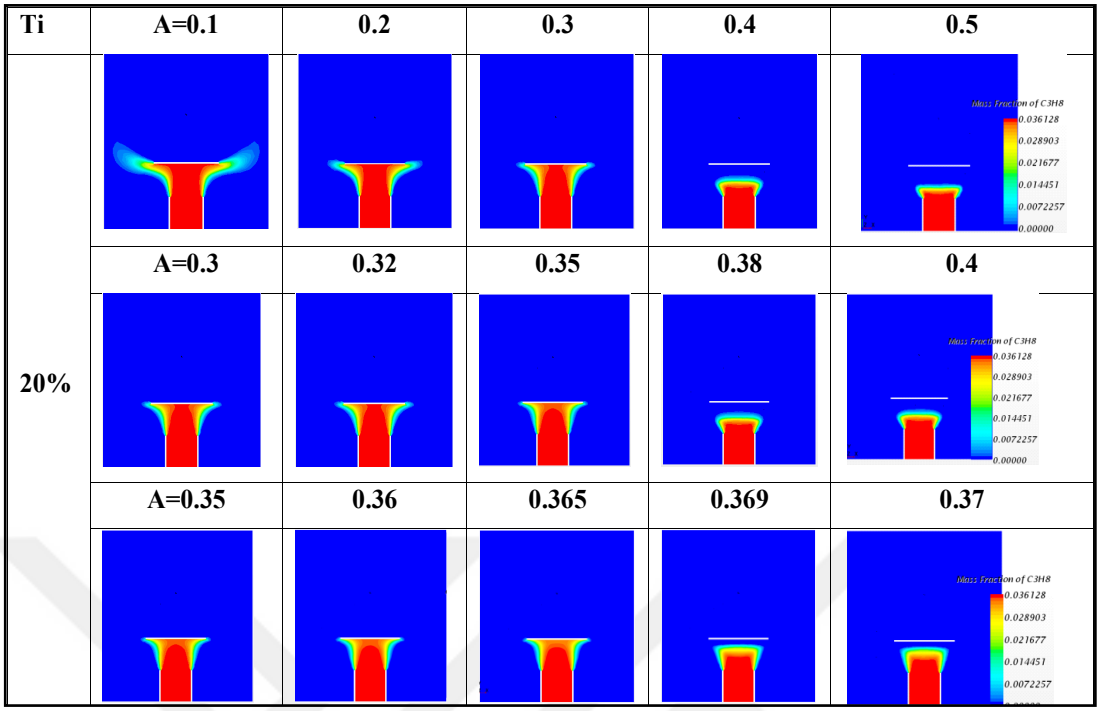

Figure 4.2 Fuel mass fraction at different constant A and *Ti* =20%, and l_t = 0.01m, P = 5kW.

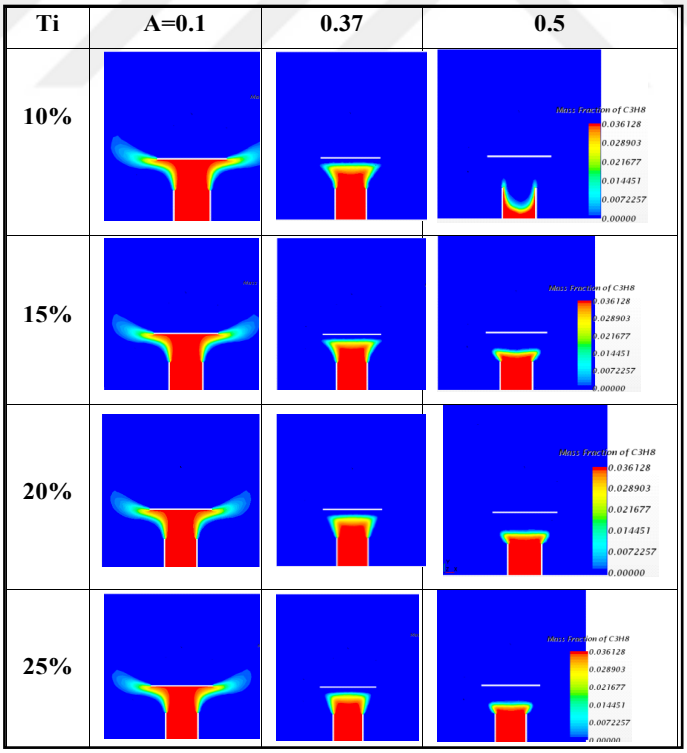

Figure 4.3 Fuel mass fraction at different constant A and turbulent intensity *Ti* and l_t = 0.01m, thermal loads of 5kW.

Figure (4.4) depicts the heat released from the propane flame of 5 kW at different turbulence values Re_λ = 70, 90 and 110 at the inlet. The *HR* curves show that the flame location noticeably moves toward the inlet region at increasing Re_λ. When turbulence is increase flame moves downwards towards the inlet region with increasing Re_λ. At a given *HR* value, the flame location decreases toward the burner exit region, i.e. y = 0 m, by increasing turbulence, which exactly conforms to the experimentally found behavior.

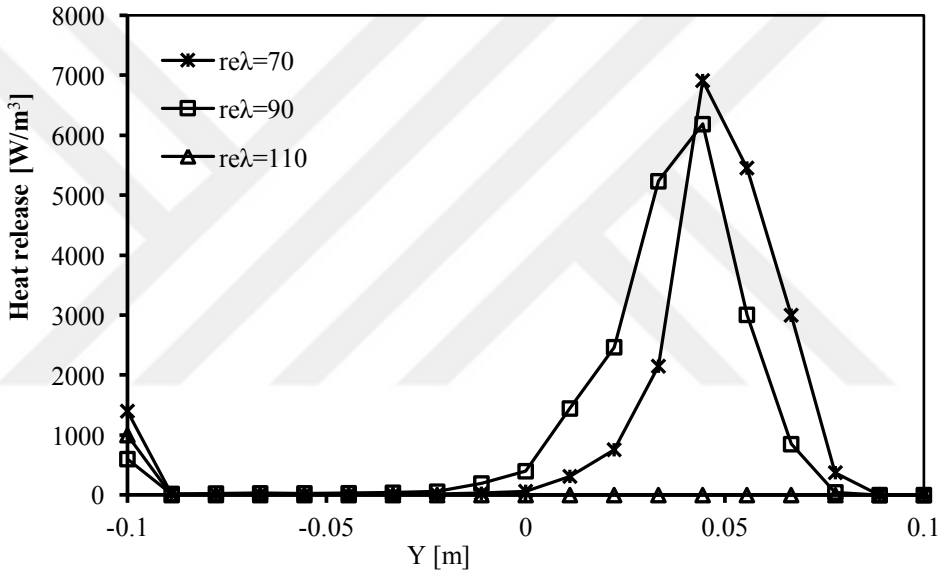

Figure 4.4 Heat release in the axial direction of the combustor at A =0.37 and different Re_λ for thermal load 5 kW.

Figure (4.5) presents the temperature distribution in the axial direction of the combustor at a normal line to the flame surface at A = 0.37 and l_t = 0.01m of 9 kW thermal load. In all simulations, the peak temperature reaches 1740 K. A growing trend is observed in the average temperatures obtained in the zone below the flame holder. No significant difference is found among the average temperature profiles of propane–air flames at Re_λ = 70, 90, 110 and 130 at y = 0.0 m, that is, at the burner exit. However, differences at y = 0.05 m are observed in the TFC model. Therefore, an increase of Re_λ

changes the turbulent conditions from weak to strong cases thereby is pulling combustion toward the inlet. The improved mixing between the premixed propane–air mixtures causes this result. From Figure (4.5), at y = 0.05 m, the increase of turbulent level enhances the temperature in the reaction zone by a factor of 12% when turbulence shifts from weak to medium and by a factor of 2% when turbulence changes from medium to strong.

To show the effect of radiation on combustion, we stabilize the distribution of heat release on the centerline of the combustor of CFM and TFC models. Figure (4.6) shows the heat release distribution along the centerline of the combustor with and without radiative heat transfer from the flame holder region of the CFM and TFC models. The average of heat release from combustion with radiative effect is less than 1.5% and 2% for the condition without radiative effect for the CFM and TFC models when radiation heat transfer is considered. Thus, all simulations are performed without the assumption of radiation effect on the flame holder. However, this assumption resulted in less than 5% error. Therefore, radiation effect is ignored from all combustion simulations for the CFM and TFC models. This assumption was enhanced by P. Coelho [50] who maintained that the influence of radiation on turbulence acts as a dissipation process. In addition, the effects of radiative heat transfer increase with temperature, but these effects decrease with the dissipation rate of turbulent kinetic energy. This assumption was matched with J. Li and M. Modest [51] in terms of small flame thickness; thus, maximum temperature was dropped to 18 K and the difference in heat release with and without radiation effect is less than 5%. According to Zimont et al. [52], the maximum errors in temperature measurement are calculated at less than 70 K when radiation effects are disregarded.

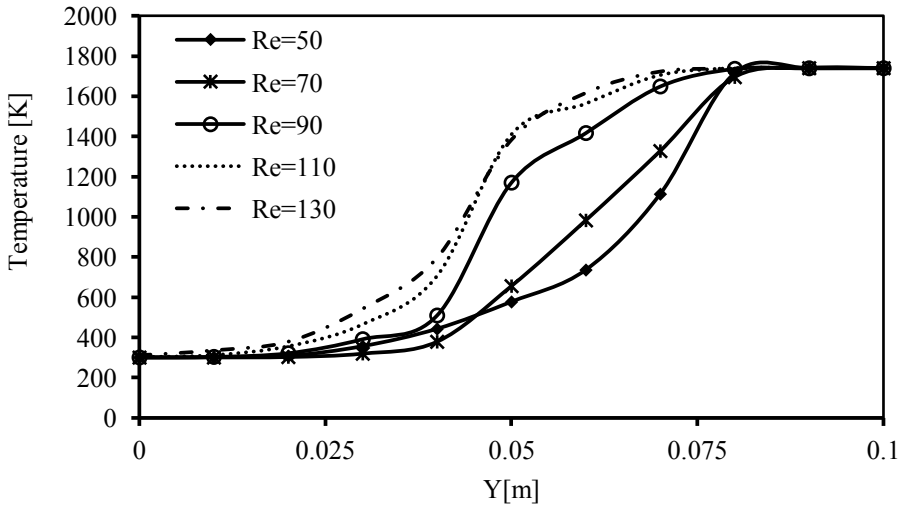

Figure 4.5 Temperature distribution extracted from the simulations conducted by TFC model at different Re_λ for thermal load 9 kW.

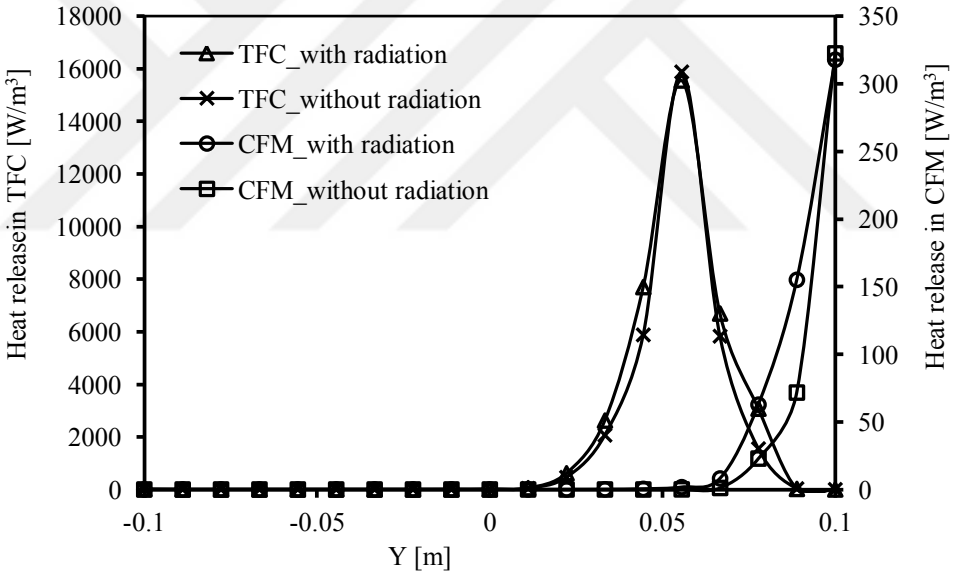

Figure 4.6 Heat release calculated by the CFM and TFC models with and without radiation effect on the flame holder at Re_λ = 70 and 9 kW.

4.3 Flame Topology Simulated by CFM and TFC Models

4.3.1 Grid Independency Analysis

After choosing the appropriate value of 0.37 for constant A, a grid dependency analysis based on the flame location was conducted. Figures (4.7) and (4.8) depict the flame locations calculated by the CFM and TFC models from the maximum heat released value along the centerline of the combustor at Re_λ=70 with different grid numbers. Various grid numbers, from M1 (i.e., coarse mesh) to M9 (i.e., fine mesh), were tested in the jet flow combustor domain to check the optimal mesh density. Table (4.3) represents the grid numbers and flame locations from the grid independency analysis. In CFM, the flame location decreased gradually with an increase in grid number from M1 to M3 but did not vary with a decrease in mesh size after M4. Therefore, the flame location converged at a solution and became independent of the mesh size. The same process occurred with the TFC model. From approximately 300,000 grid cells, for mesh size M4 onwards, the flame location did not vary for both models to an extent that would have influenced the derived conclusions. Therefore, the subsequent simulations were performed using M4 for 301,594 grid cells, as shown in Figure (2.5).

In addition, the deviations in the flame locations were 2 and 3 mm between the coarse and fine meshes of the CFM and TFC models respectively. While, for LES model, Figure (4.9) show the results of the grid independency study based on the flame location at mass flow rate of 30%, frequency 200 Hz and amplitude of pulsation of 0.3 m/s. Flame locations are calculated at various grid numbers from coarse mesh of 169,216 cells to finer mesh of 2,336,858 cells. The flame location is decreased by

increasing mesh numbers until 1,303,315 cells and converged to a solution and became independent of the mesh size. The total number of the cells is 1,331,305 cells, which is satisfied of the grid independency study based on the flame location calculated from the mean heat release rate on finer mesh and used in all test examined.

Table 4.3 Grid independency analysis results.

Mesh number	Cell number
M1	174592
M2	235976
M3	268836
M4	301594
M5	340595
M6	437730
M7	568607
M8	774058
M9	981745

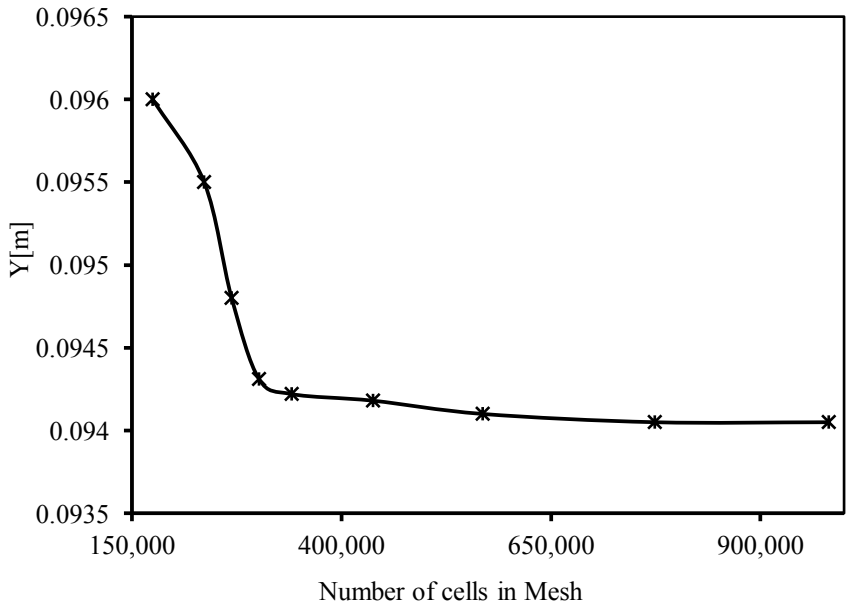

Figure 4.7 Flame locations at Re_λ 70 with different number of the mesh in CFM.

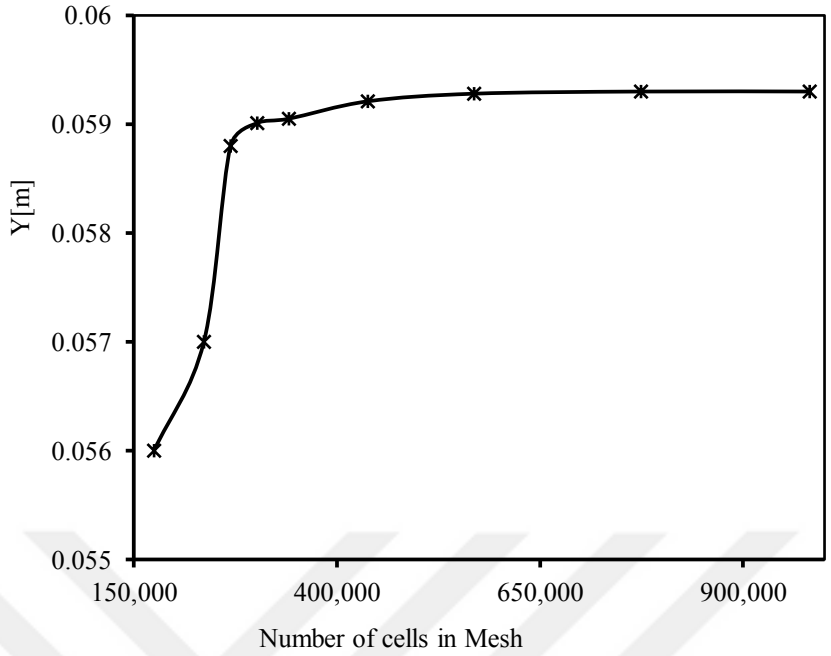

Figure 4.8 Flame locations at Re_λ = 70 with different number of the mesh in TFC Model.

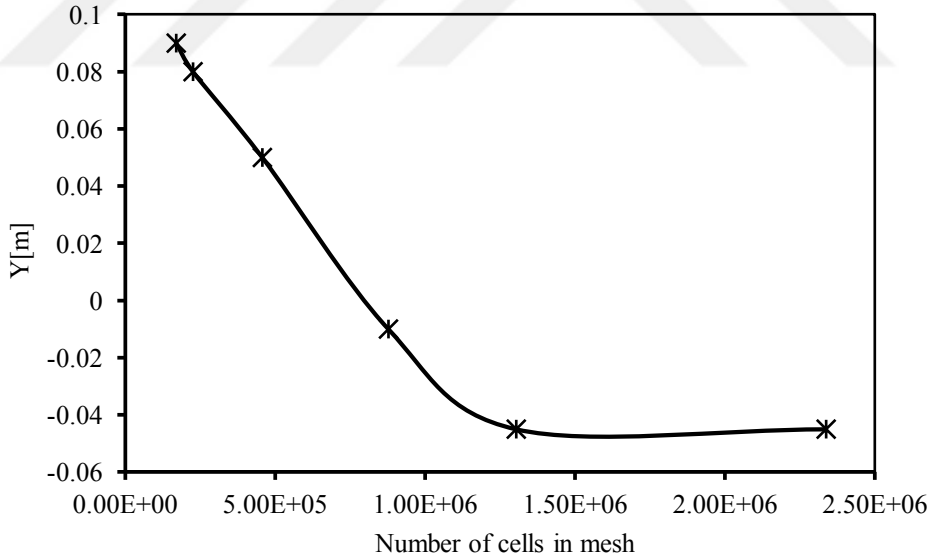

Figure 4.9 Flame locations with different number of the mesh in LES model, at mass flow rate of 30% frequency 200 Hz and amplitude of pulsation of 0.3 m/s.

4.3.2 Regimes of the Combustion

The CFM and TFC models were used to simulate the premixed combustion of the propane–air reaction as steady reacting flow cases. The turbulent combustion regimes can be characterized by considering the relationship between the turbulent and chemical reaction scales. This relationship involves several dimensionless numbers in the analysis. One such number is the Karlovitz number (Ka), which is a key parameter in the Borghi diagram [68]. Ka is the ratio between the chemical time scale and the smallest turbulent time scale [103]. The effect of changing the turbulence level on flame location can be understood by investigating the flame behavior in the regions of the premixed turbulent combustion diagram, which is known as the Borghi diagram. In this study, the lean premixed combustion occurs in the wrinkled and corrugated flamelet regions. Figure (4.10) presents the flame locations on the Borghi diagram in the flamelet regions in this study.

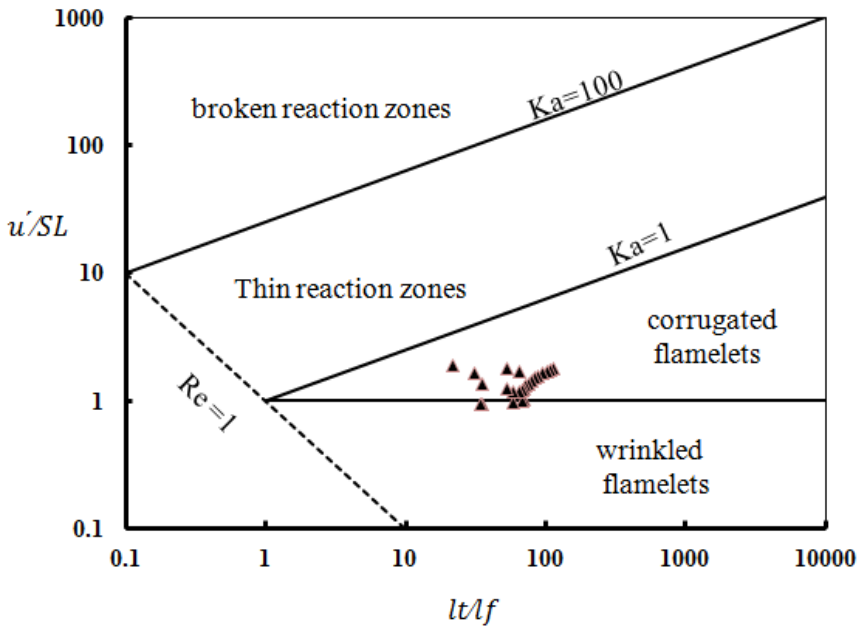

Figure 4.10 Flame locations on the premixed turbulent combustion regime (Borghi diagram [68]).

4.3.3 TFC Model

4.3.3.1 Effect of Re_λ

To investigate the effect of turbulence on combustion, TFC model was examined under the influence of different turbulence levels. All numerical simulations were conducted using the STAR-CCM+ v10.02 software [53]. The flame topology was investigated by setting the turbulence level parameters k and ϵ at the inlet region for Re_λ evaluation according to Equation (2.33). The inlet flow conditions of the turbulence levels for different thermal loads of 3, 5 and 9 kW are listed in Table (4.4). For the comparison between the CFM and TFC models, numerical simulations were conducted at different levels of Re_λ, similar to the experiments listed in Table (3.1).

Figure (4.11) shows the flame topology of the TFC model is symmetric and remains in contact with the burner exit. In addition, although Ti remains constant at 50% at three different Re_λ values, the turbulence length scale l_t is large at Re_λ = 110. The TFC model showed less sensitivity to the changes in l_t. Furthermore, the distribution of velocity streamlines is present in all combustor domains and significantly shows that the flame location minimally affects the recirculation zone behind the flame holder and the flame is weakly spread towards the inlet region.

The heat released from the combustion for thermal loads 9 kW at different turbulence levels are presented in Figure (4.12). The maximum heat release is increased by increasing turbulence level until Re_λ =110, after that it has decrease due to high turbulence was generated i.e. Re_λ =150. The flame is stretch towards the inlet region by increasing Re_λ. As indicated by the heat release distribution along the centerline of the jet flow combustor, the flame location gradually moves downwards towards the inlet

region with increasing Re_λ. This outcome exactly conforms to the experiment results (Figure 4.1).

Table 4.4 Inlet flow conditions at k = 0.0878 [J/kg] and thermal loads of 3, 5, and 9kW.

Re_λ	l_t (m)	ϵ ($m^2.s^{-3}$)
5	0.000193	134.755
10	0.000772	33.688
20	0.003089	8.4222
30	0.006950	3.7432
40	0.012356	2.1056
70	0.037840	0.6875
90	0.062552	0.4159
110	0.093442	0.2784
130	0.130510	0.1993
150	0.173756	0.1497

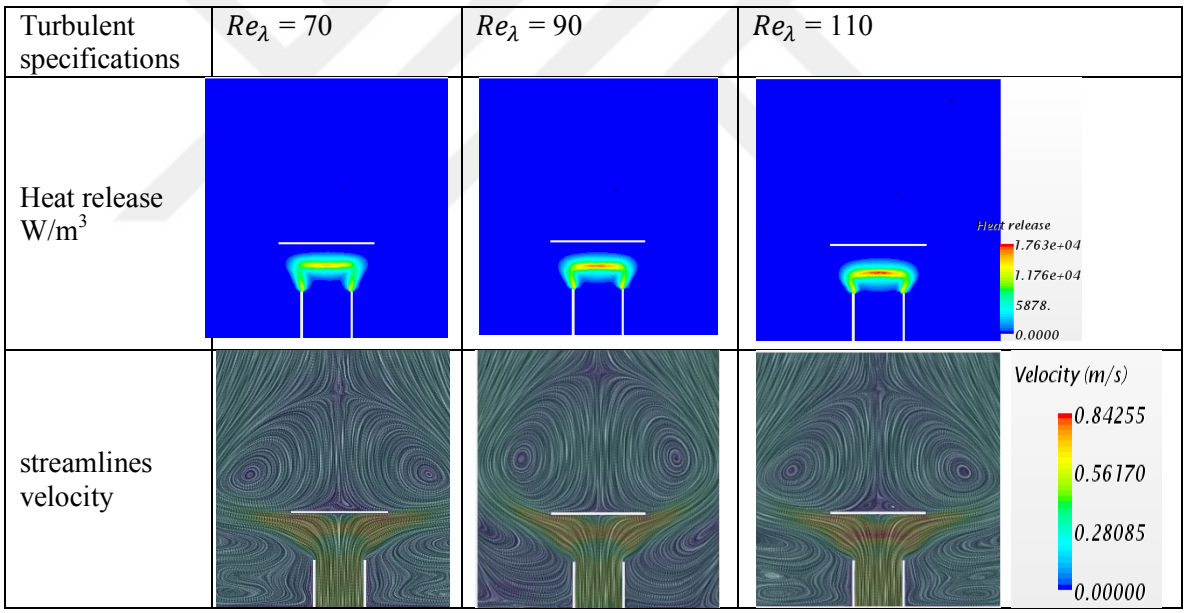

Figure 4.11 The average heat release and velocity streamline contours of TFC model at different Re_λ and 9 kW [106].

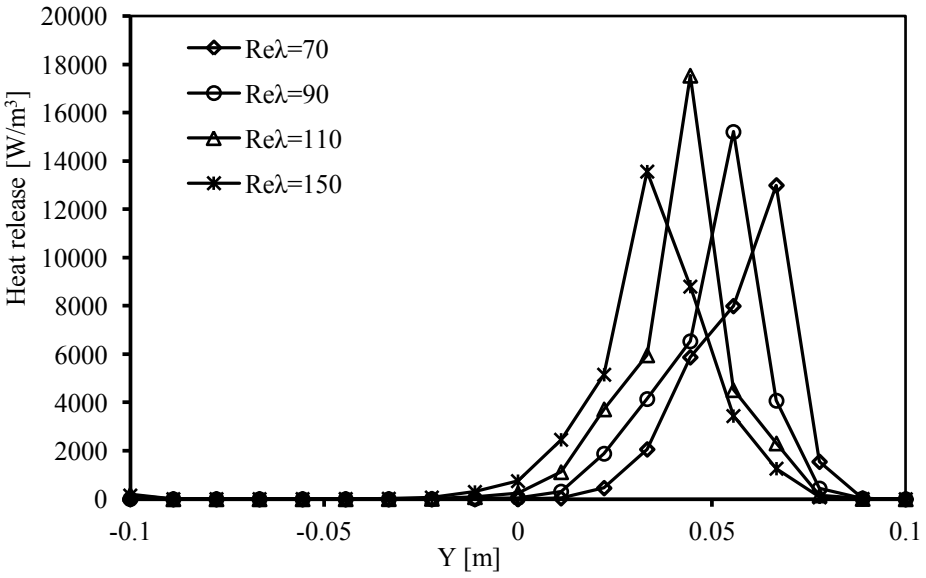

Figure 4.12 Axial distributions of heat release from the combustion of TFC model at different Re_λ and 9 kW.

4.3.3.2 Species Concentration Profiles

The distributions of the species mass fraction along the centerline of the combustor at different Re_λ values are shown in Figures (4.13) and (4.14). At different turbulence levels of Re_λ =5, 10, 20, 30, 40, 70, 90, 110 for thermal loads 3, 5 and 9 kW, the species distributed along the centerline of the combustor include O_2 and CO_2. The concentrations of O_2 and CO_2 respectively decrease and increase more rapidly in the reaction region at *y*=0.04 m at a low turbulence level (i.e. Re_λ =5) for a thermal load of 3 kW than those for thermal loads of 5 and 9 kW. The same trend occurs when the turbulence level is increased up to Re_λ = 90. Therefore, this effect is diminished and appears to be constant at 3 kW, as shown in Figures (4.13 G) and (4.14 G), and at 3 and 5 kW, as shown in Figures (4.13H) and (4.14H). The flame topologies are shown in Figures (4.12, 4.13 and 4.14). The flame location moves towards the inlet region when the turbulence level is increased, especially at a low thermal load (i.e. 3 kW), and the effect is less at 9 kW.

At Re_λ =70, the concentration of C_3H_8, O_2, CO_2 and H_2O at the end of combustion of TFC model is shown in Figure (4.15). The concentration of C_3H_8 is totally consumed in the combustion while concentration of O_2 is not zero due to lean condition of the equivalence ratio i.e. Φ= 0.588 and soot does not form, this is Reinforced our previous hypothesis. The concentration of the species that participated in the reaction of the jet flow combustor seems constant even with increasing turbulence level. Therefore, the soot concentration was not noticeable due to lean propane combustion and blue color was dominated. As in the experiments, because of lean combustion, not all oxygen participates in the combustion, but a sufficient amount of oxygen in the fuel molecule of premixed gas facilitates the oxidation of the fuel; thus, the homogeneous combustion area is increased, and soot formation is prevented.

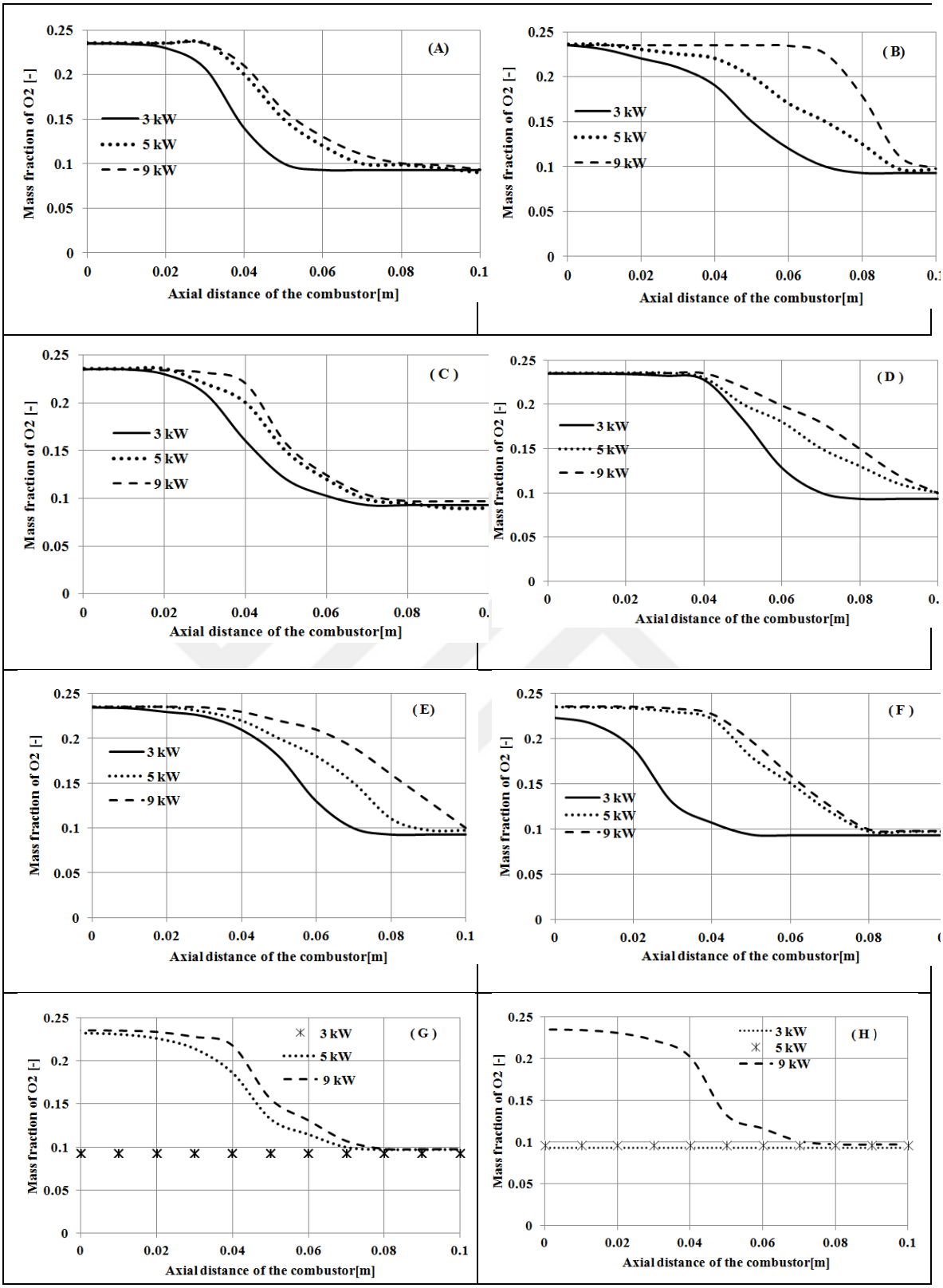

Figure 4.13 Axial distributions of O_2 mass fraction from the combustion of TFC model at: (A) Re_λ=5, (B) Re_λ=10, (C) Re_λ=20, (D) Re_λ=30, (E) Re_λ=40, (F) Re_λ=70, (G) Re_λ=90, (H) Re_λ=110, and thermal load 3, 5 and 9 kW.

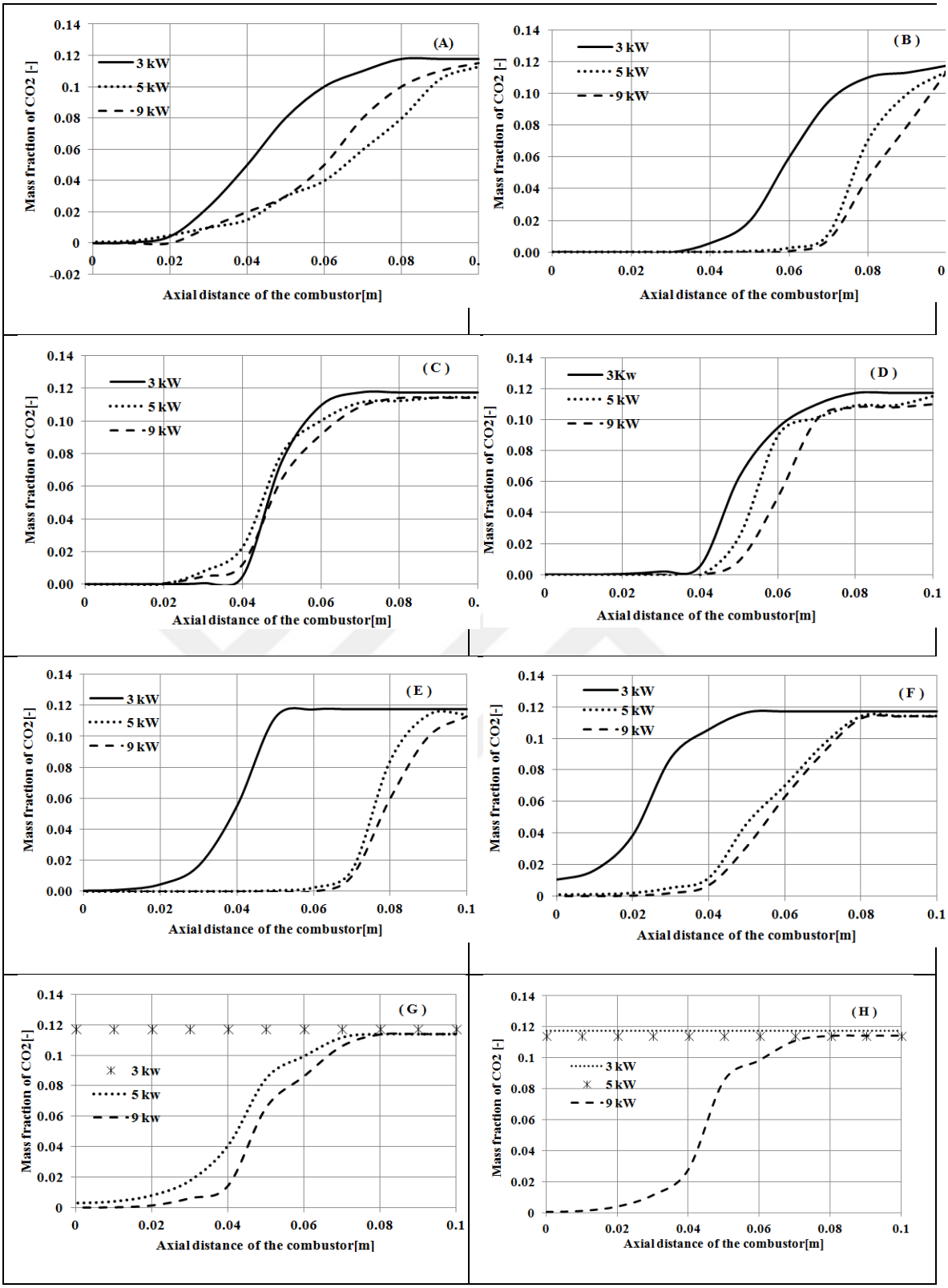

Figure 4.14 Axial distributions of CO_2 mass fraction from the combustion of TFC model at: (A) Re_λ=5, (B) Re_λ=10, (C) Re_λ=20, (D) Re_λ=30, (E) Re_λ=40, (F) Re_λ=70, (G) Re_λ=90, (H) Re_λ=110, and thermal load 3, 5 and 9 kW.

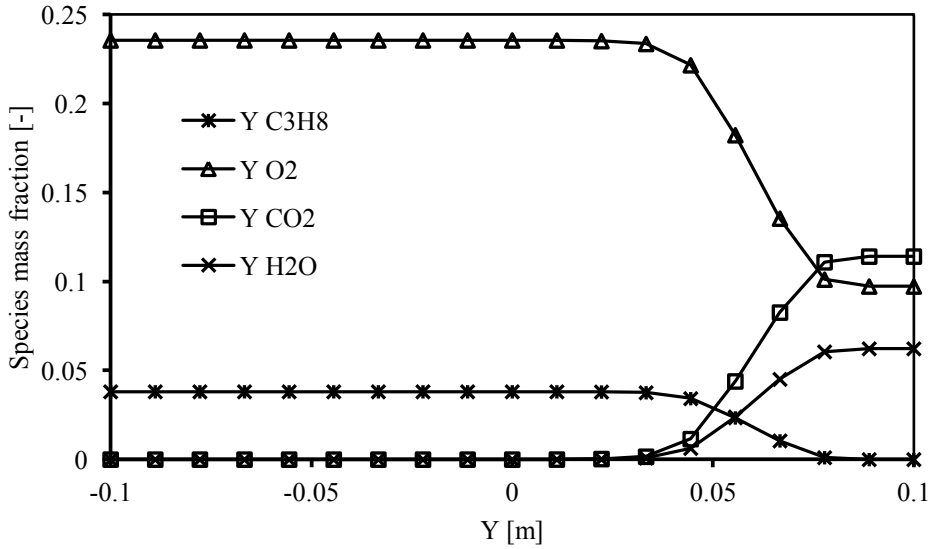

Figure 4.15 Axial distributions of mass fraction of C_3H_8, O_2, CO_2 and H_2O for TFC model at Re_λ =70 and 9 kW.

4.3.3.3 Turbulent Kinetic Energy Profiles

The effects of velocity distribution on the flame topology and location were also studied. Figure (4.16) shows the distribution of the mean flow velocity in the axial direction of the combustor at different Re_λ values and 9 kW. In general, in the inlet region (i.e. y = −0.1 m), the mean velocity of 0.484 m/s gradually increases to approximately 0.5 m/s at the burner exit and then decreases due to an expanded area. After combustion, the average velocity increases rapidly to the maximum value, then decreases to the minimum value at the stagnation point in the flame-holding zone (i.e. y = 0.1 m). The distribution of the turbulent flame speed *Ut* along the centerline of the combustor of the TFC model at different Re_λ values, k = 0.0878, and 9 kW is shown in Figure (4.17). The turbulent flame speed increases with Re_λ at a constant k in the inlet region, in accordance with Equation (2.34). In all the test cases, U_t initially decreases from the turbulence dynamics as expected, then increases within the flame zone. The increase in U_t that occurs within the zone of the combustion starts at y = 0.02 m above

the burner exit. The maximum heat released value can be determined by changing *Ut* and subsequently the flame location.

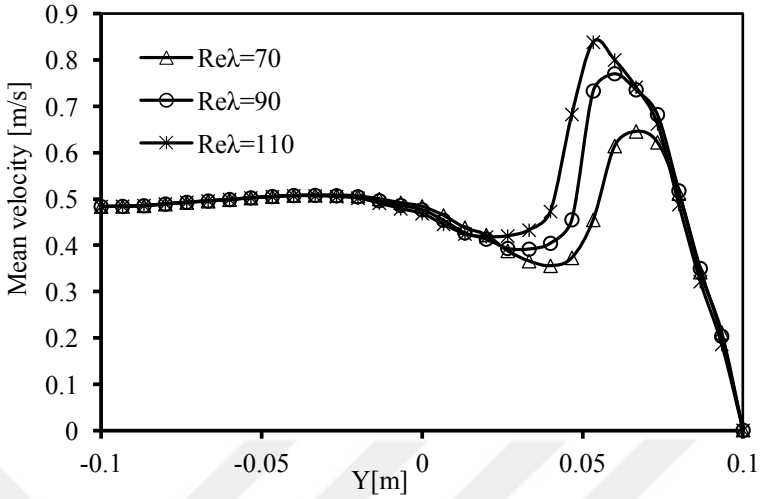

Figure 4.16 Mean velocity distribution along centerline of the combustor of TFC at different Re_λ for 9 kW.

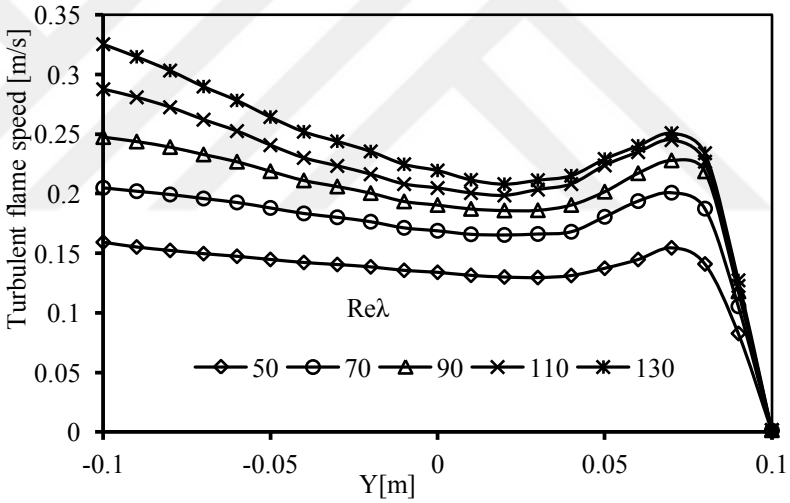

Figure 4.17 Turbulent flame speed **d**istribution along centerline of the combustor of TFC at different Re_λ for 9 kW.

The turbulent kinetic energy TKE or k, distribution along the centerline of the jet flow combustor is depicted in Figure (4.18) at various Re_λ values and 5 kW. In general, the TKE behind the inlet region decays from turbulence dynamics and then rises within the flame region. At low turbulence, the effect of TKE diminishes. By

contrast, at $Re_\lambda > 40$ the effect of TKE is very noticeable in the hot flow region (i.e. $y >$ 0.05 m).

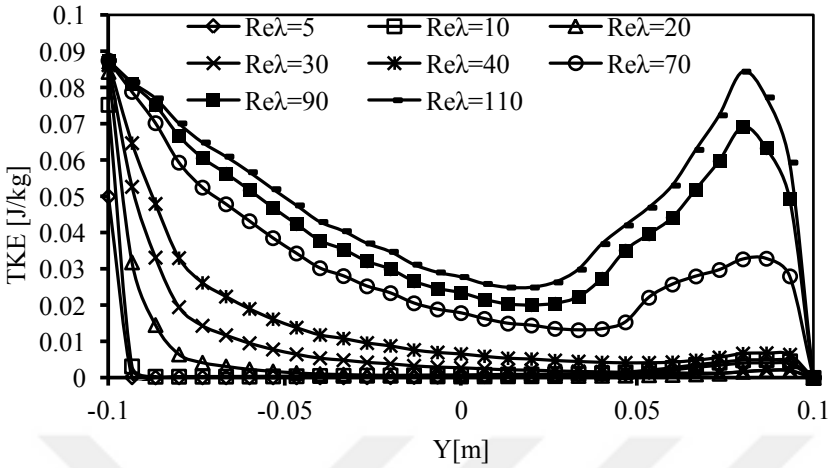

Figure 4.18 Axial distributions of TKE of TFC model at different Re_λ and thermal load 5 kW.

The influences of turbulent kinetic energy on the flame topology and location were examined by conducting simulations with k = 0.0878, 0.13, 0.26 J·kg^{-1} at the inlet, Re_λ=110 and 9 kW. Figures (4.19) and (4.20) show the developments of k and *HR* respectively. In Figure (4.19), despite the variation of k values in the inlet region (i.e., y = –0.1 m) and Re_λ = 110 (high turbulence), the highest k value (i.e. 0.26 Jkg^{-1}) decreases more rapidly in the cold flow region than 0.0878 Jkg^{-1} and 0.13 Jkg^{-1} do. However, they have the same trend in the hot flow region, particularly in the region below the flame holder at the y value range of 0–0.1 m after combustion occurs. Thus, the flame topology and location are not affected by the change in k values or turbulence dissipation rate when Re_λ is constant. Only the maximum value of *HR* decreases with an increase in k, as shown in Figure (4.20). These results confirm Equation (2.34), which indicates that the turbulent flame speed can vary depending on Re_λ. Only this variation can determine the flame location.

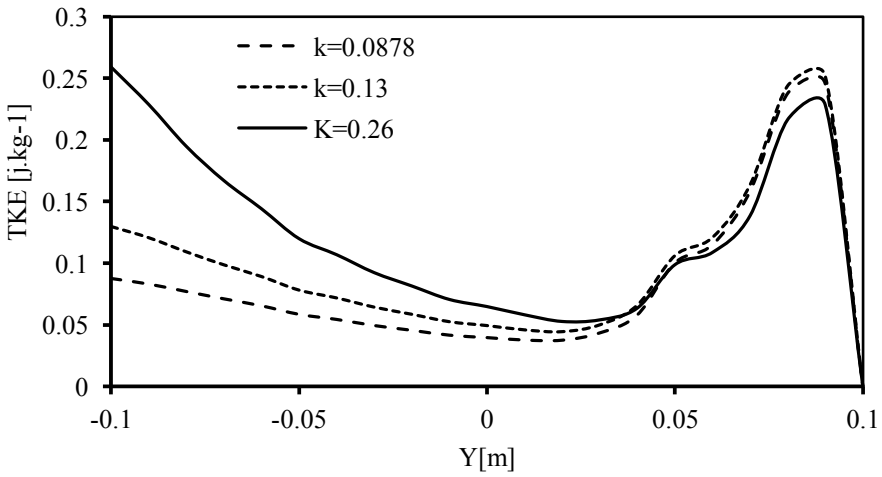

Figure 4.19 TKE distribution in the axial direction of the combustor by the TFC model at Re_λ = 110 for 9 kW.

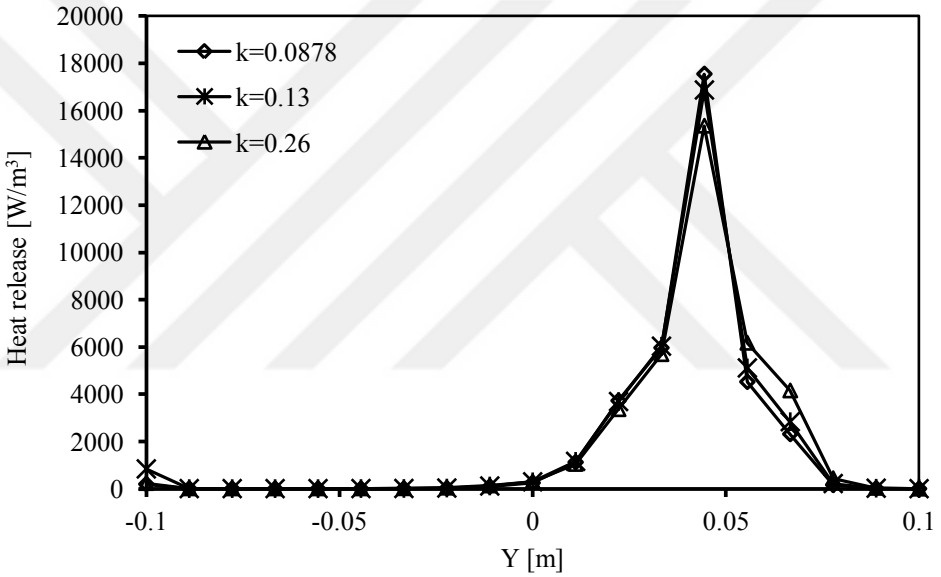

Figure 4.20 *HR* calculated by the TFC model at Re_λ =110 and different *k* for 9 kW.

4.3.4 CFM

4.3.4.1 Effect of Reλ

Figure (4.21) shows the flame topology in CFM in the jet flow combustor. The flame topology appears as a mushroom and has weak diffusion towards the inlet region when Re_λ = 70 than in high-turbulence cases. When turbulence is increased (i.e. Re_λ = 90 and 110), the flame moves downwards towards the burner exit (i.e. y = 0 m). In addition, the distribution of the velocity streamlines is present in all combustor domains, similar to the results obtained by the TFC model, and the flame location is affected by the recirculation zone behind the flame holder. When the turbulence level is increased, the flame topology moves downwards towards the inlet region upstream flow in the jet flow combustor. This result confirms the experimental results. The contours of heat release seem to be approximately different from that existing on our previous work [106] because we considered the amount of fuel mass fraction in the end of the combustion (Y_{res}) is equal to be zero.

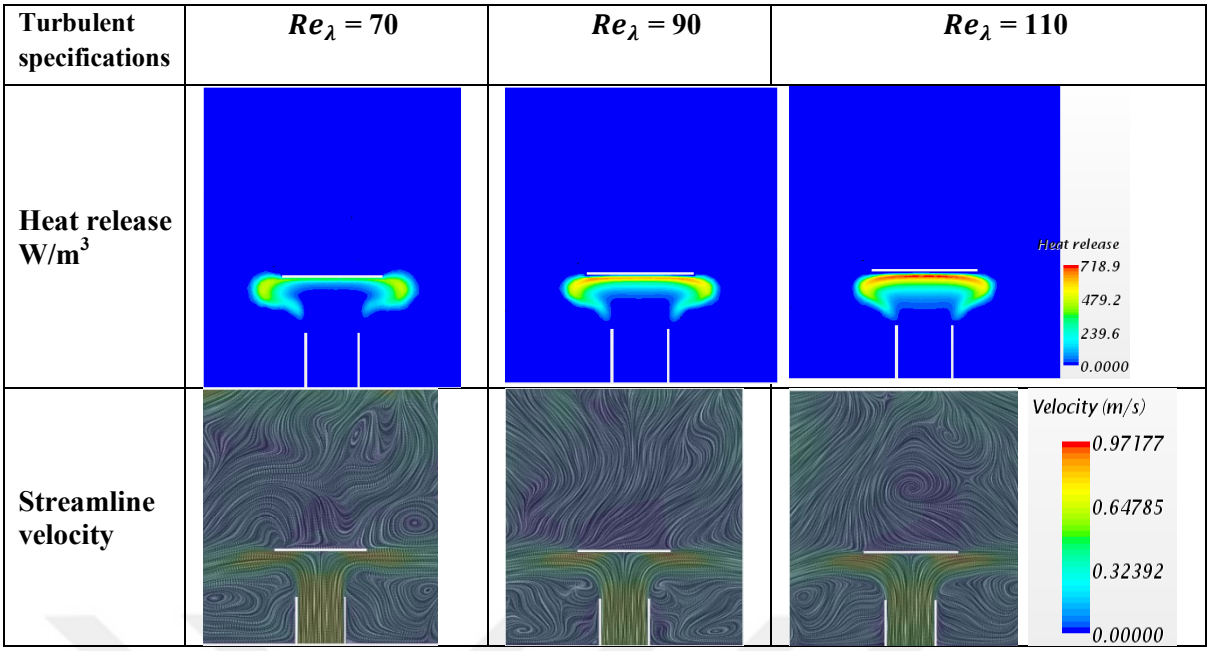

Figure 4.21 The average heat release and velocity streamline contours of CFM model at different Re_λ and 9 kW [106].

This section also focuses on the dependency of the flame topology on thermal loads, set as 3, 5 and 9 kW , with r =0.0, 0.04, 0.11, 0.16 m, which are the positions of the four line probes of the combustor, and different turbulence levels. These positions were chosen because the behavior of the CFM flame inside the entire domain of the combustor is not constant at different Re_λ values. The values of the heat released in the line probe at r =0.0 m are monitored. The distribution of heat release along the axial direction of the combustor at different turbulence level is shown in Figure (4.22). We notice from the Figure, the maximum heat release was increased by increasing Re_λ and the flame moves towards the inlet region. The flame location from the moment the maximum heat is released shifted downwards towards the inlet region, which is an agreement with the experiments as shown in Figures 3.3 and 3.4.

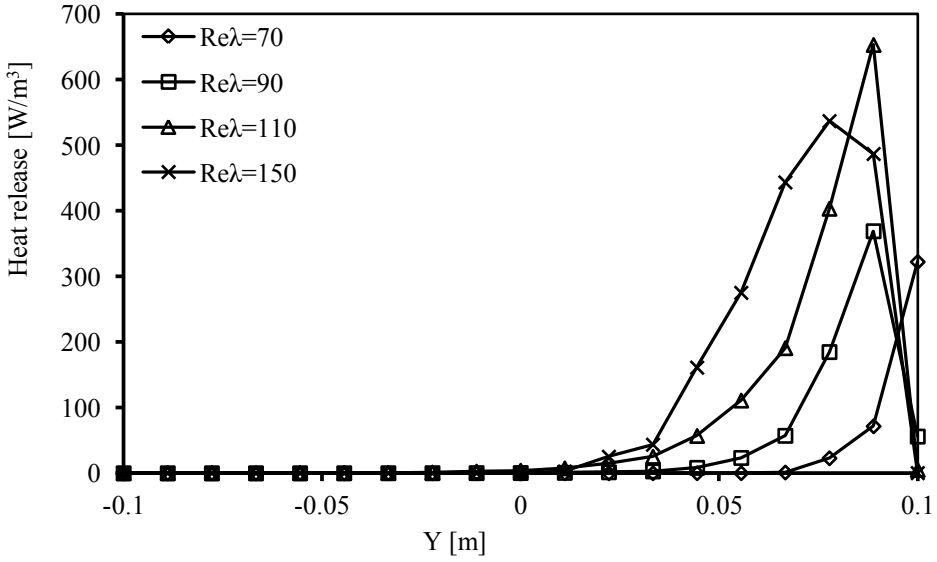

Figure 4.22 Axial distributions of heat release from the combustion of CFM model at different Re_λ and thermal load 9 kW at r=0.0 m.

The axial distributions of the temperatures from the combustion in CFM at different turbulence levels and thermal loads of 3, 5 and 9 kW are depicted in Figures 4.23 (A–H). The static temperature is 300 K for all simulations. As shown in Figure 4.23 (A), at a low turbulence level (i.e. Re_λ= 5) the maximum temperature from the combustion at 5 kW and r = 0.16 m is 1460 K when y = 0.095 m and the flame location is near the flame holder region. The maximum temperature of the combustion (i.e. 1277 K) at 9 kW thermal load occurs in the reaction region when the turbulence levels are increased from Re_λ= 10 to Re_λ= 30 at r = 0.16 m and y = 0.08 m. When Re_λ is further increased to 40, the temperature from the combustion at 3 kW increases rapidly in the reaction region and reaches the maximum value of 1800 K at y = 0.0 m along the centerline of the combustor, but the enhancement is less at 9 kW , as shown in Figure 4.23 (E). The temperature increases gradually at 5 kW and reached the maximum value of 1100 K at y = 0.065 m and r = 0.18 m. When the turbulence level is increased to Re_λ=70, 90, 110, as the flame stretched towards the inlet region, the temperature at 3 kW rapidly increases to the maximum value of 1800 K, whereas the temperature

gradually increases to the maximum value at 9 kW along the centerline of the combustor. The temperature profile is affected by increasing the turbulence level from the low to the medium level due to the mixing process but seems to be constant at a high turbulence level.

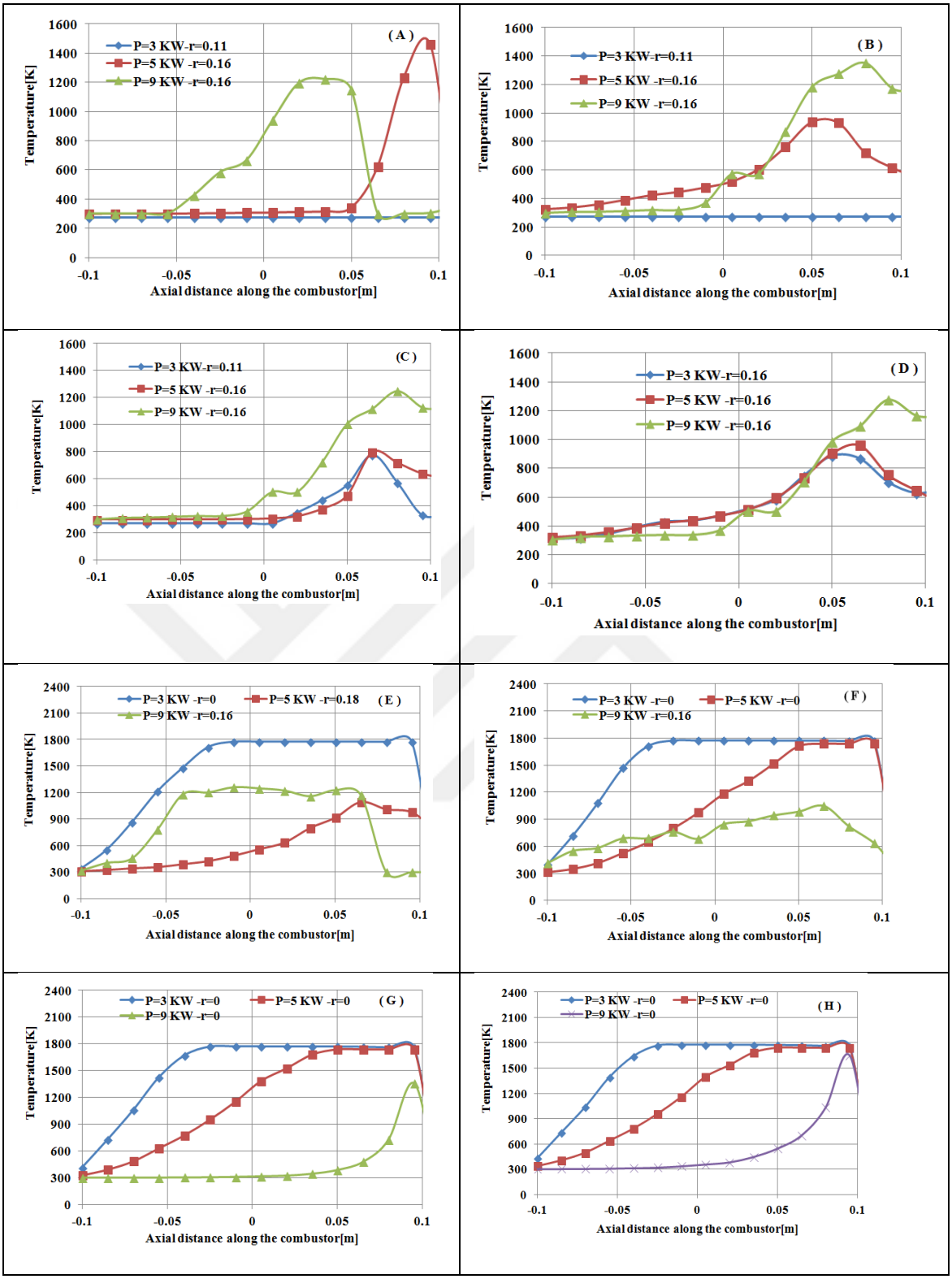

Figure 4.23 Axial distributions of temperature from the combustion of CFM model at: (A) Re_λ = 5, (B) Re_λ =10, (C) Re_λ =20, (D) Re_λ =30, (E) Re_λ =40, (F) Re_λ =70, (G) Re_λ =90, (H) Re_λ =110, and thermal load 3, 5 and 9 kW at r =0.0, 0.04, 0.011, 0.16 and 0.18 m.

4.3.4.2 Species Concentration Profiles

The species mass fractions of the lean combustion, namely the O_2 and CO_2 profiles, in the combustor are shown in Figure (4.24). The O_2 concentration profile on the left side of Figure (4.24) is more widely spread in the reaction region at a low Re_λ. When the turbulence level is increased, the flame location moves downwards towards the inlet region. Similarly, for the CO_2 concentration at low turbulence levels (i.e. Re_λ=5, 10, 20, 30 and 40), the flame topology is more widely spread below the flame holder region. When the turbulence level is further increased to Re_λ = 70, 90 and 110, the flame topology is weakly spread in the reaction region, and the flame location moves downwards towards the inlet region. Given that the combustion is lean, the content of O_2 by the end of the combustion is not zero at different turbulence level. That mean the soot does not form due to sufficient amount of oxygen as shown in Figure 4.15. As shown in Figure (4.24), the flame topology is affected, and the flame location moves downwards towards the inlet region when the turbulence level is increased from weak to high, further verifying the experimental as shown in Figures (3.3) and (3.4).

Re_λ	Mass fraction of O_2	Mass fraction of CO_2
5	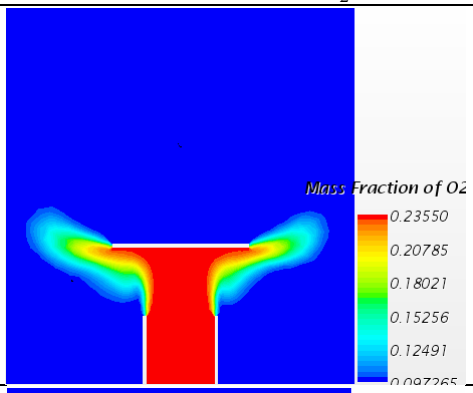	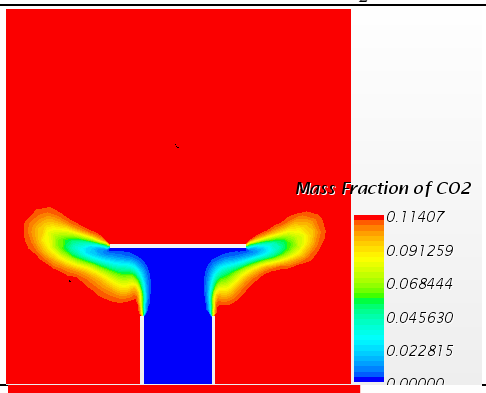
10	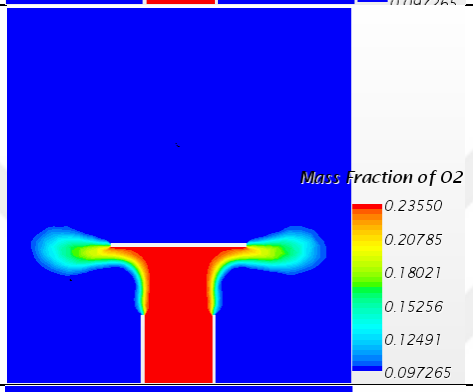	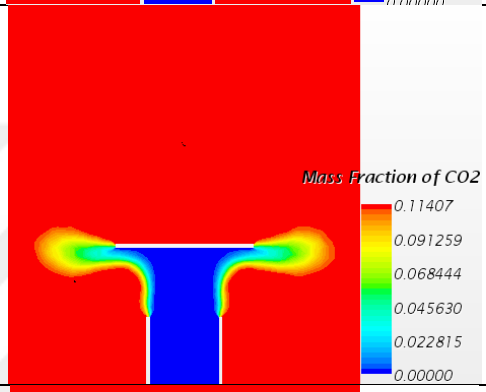
20	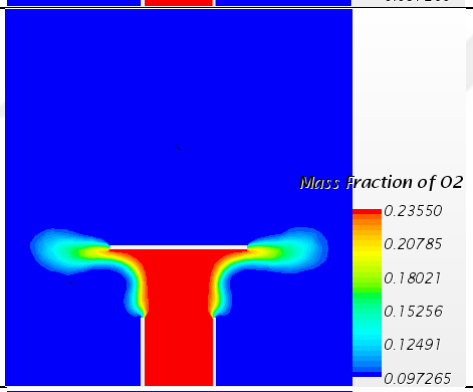	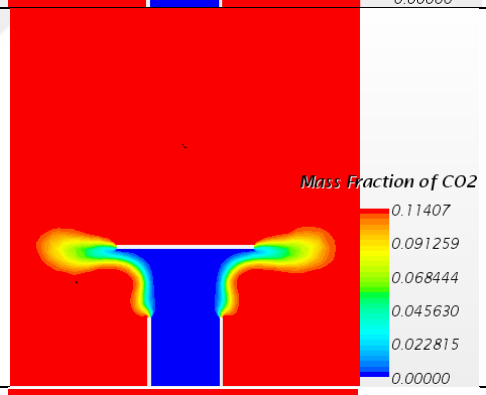
30	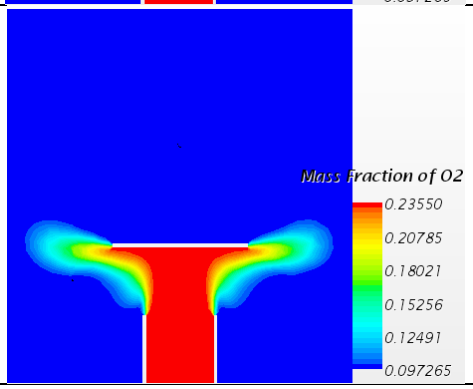	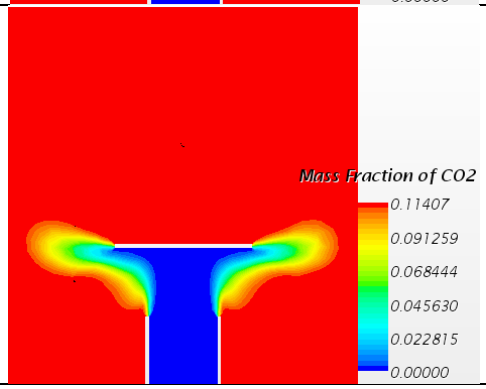

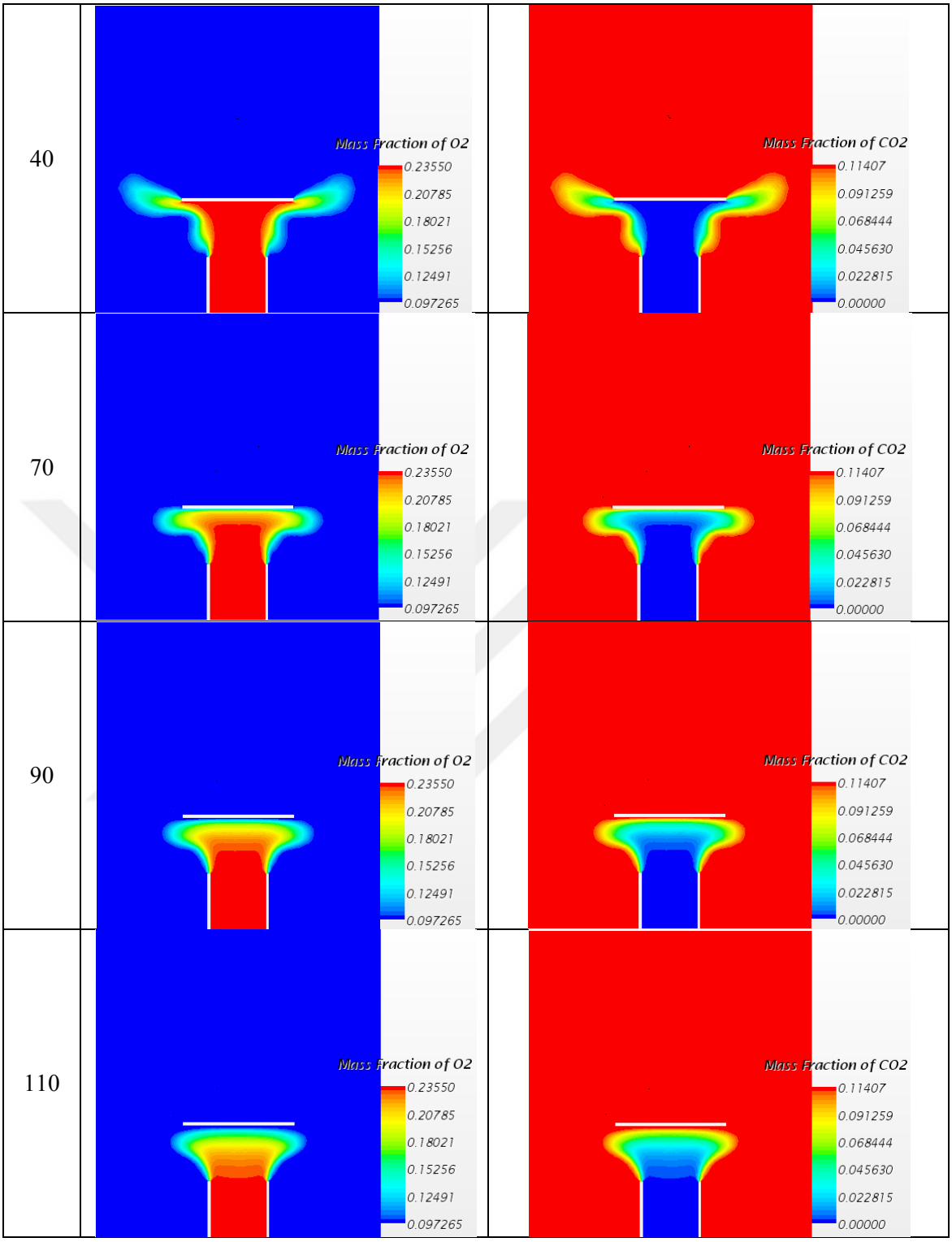

Figure 4.24 Mass fractions of O_2 and CO_2 of CFM model at different Re_λ and thermal load of 9 kW.

4.3.4.3 Turbulent Kinetic Energy Profiles

The distribution of turbulent kinetic energy (k) along the centerline of the combustor (i.e. r = 0 m) at different Re_λ values are shown in Figure (4.25). At a low turbulence level, the effect of k diminishes, whereas the effect of k is clear when Re_λ reaches 40 in the region above the exit jet pipe flow (i.e. y = 0.05 m), as shown in Figure 4.25 (E). The maximum value of k is recorded at 5 kW in the region below the flame holder at Re_λ =110. The behaviour of k behind the inlet region decays from turbulence dynamics as expected, and then rises within the flame region after combustion occurs. By increasing k value, that mean increasing in turbulent flame speed and heat release from the combustion and subsequently flame moved toward inlet region as provided in experiments and was illustrated in Equations (2.30-2.34 and 2.55).

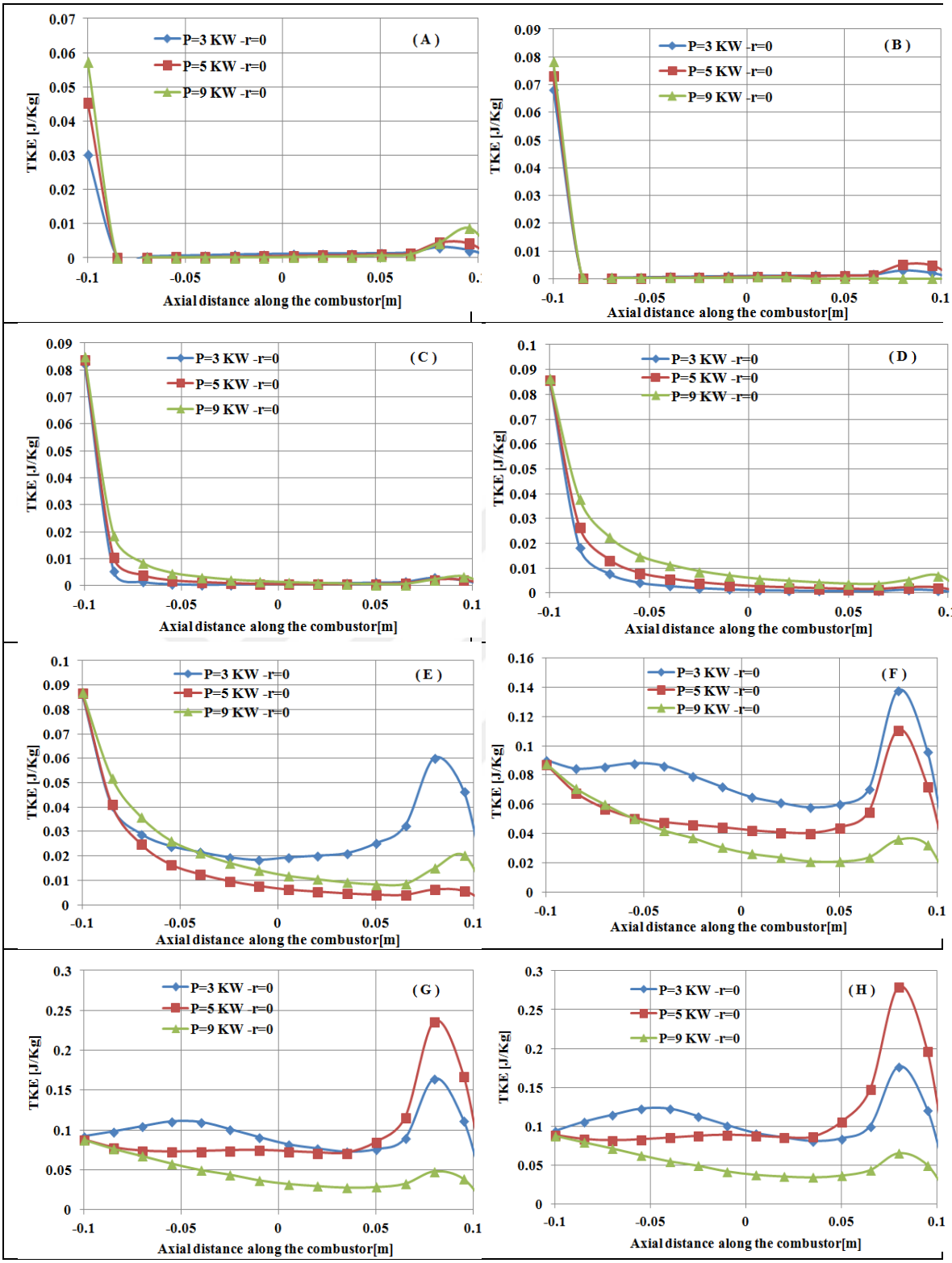

Figure 4.25 Axial distributions of turbulent kinetic energy of CFM model at: (A) Re_λ = 5, (B) Re_λ =10, (C) Re_λ =20, (D) Re_λ =30, (E) Re_λ =40, (F) Re_λ =70, (G) Re_λ =90, (H) Re_λ =110, and thermal load 3, 5 and 9 kW

4.4 Determination of Flame Location

Flame location is calculated along the centerline of the combustor above the burner exit of the CFM and TFC models to understand the interaction between turbulence and combustion. The reaction rate of propane flame in Equations 2.16 and 2.43 is an important factor that influences the heat release of chemical reaction. Figure (4.26) shows flame topology in the CFM and TFC models at Re_λ=110 and thermal load of 9 kW. The contour of heat release is used to show the influence of turbulence on combustion. The flame in CFM is mushroom-shaped, which contains more diffusion into the inlet region than that in the TFC model by increasing Re_λ. The flame in the TFC model is symmetric and in contact with the burner exit; this result is similar to the finding of Muppala et al. [13] who used five 5 models to study flame locations for methane–air flame in a swirl burner. They found that the five reaction models showed a small difference in the flame location in the centerline of the combustor. The Bray-Moss-Libby model showed a flame shape that differs from than of the TFC model. The position of maximum heat release in the line probe of TFC model is less than that of CFM. Hence, flame is anchored approximately between (10–90) mm and (0.0–70) mm above the burner exit for the CFM and TFC models, respectively.

Figure (4.27) shows the logarithm scale of reaction rate distributions (source terms in Equations 2.16 and 2.43) along the centerline of the combustor of the CFM and TFC models. The reaction rate in the TFC model starts early and the reaction rate rapidly increases to a maximum value due to the activation of reaction. This reaction rapidly decreases due to the depletion of the reactant. CFM gradually increases along the centerline of the combustor. The reaction rate in the TFC model is greater than that of the CFM. Flame is expanded and the mixture of the fuel and oxidizer pushes the flame away from the burner exit when the reaction rate is not fast as in the case of CFM

simulations. This reaction produces the flame seen in Figure (4.26). These experiments did not option sufficient measurement to perform a comparison.

The reaction rate of CFM is a function of flame area density. The latter is a function of turbulent kinetic energy as explained in Equations 2.43, 2.46 and 2.47. We solve a transport equation of flame area density, which involves transported quantity. Turbulence influences the generation of transported quantity, which then influences fuel consumption. In the TFC model, fuel consumption rate (source term) is directly linked to turbulence. Therefore, the effect of turbulent kinetic energy on combustion is compared for the CFM and TFC models at high turbulence level. This tendency indicated the increase in reaction rate (Figure 4.27) due to an increase in turbulent kinetic energy (TKE) as shown in Figure (4.28) at Re_λ=110, for 9 kW. TKE in the TFC model is five times greater than that in the CFM in the reaction region. Thus, more turbulence is generated.

Besides identifying the reason for the difference in flame location in the CFM and TFC models, we are interested in studying the distribution of gradient progress variable in the centerline of the combustor at Re_λ = 110 for 9 kW as shown in Figure (4.29). The figure shows the maximum values of $|\nabla \tilde{c}|$ are 51 and 34 at y = 0.044 and 0.088 m in the reaction regions of TFC and CFM, respectively. This result is indicated the flame position above burner exit of CFM, which is higher than TFC model for the same turbulence parameters. The influence of local burning velocity is discussed to study the difference in flame shapes between the CFM and TFC models. The speed of the local laminar flame seems constant in the CFM and TFC models. These results is illustrated in Figures (4.30), which is represented by laminar flame speed distributions in the centerline of the combustor at Re_λ = 110 and thermal power of 9 kW.

We also used different flames locations. The shape of the flame also differs as shown in Figure (4.31). The species mass fraction of the CFM and TFC model at 9 kW with high turbulence level are depicted in this figure. The flame shape in CFM resembles a mushroom and is more convex than the TFC model in the reaction region.

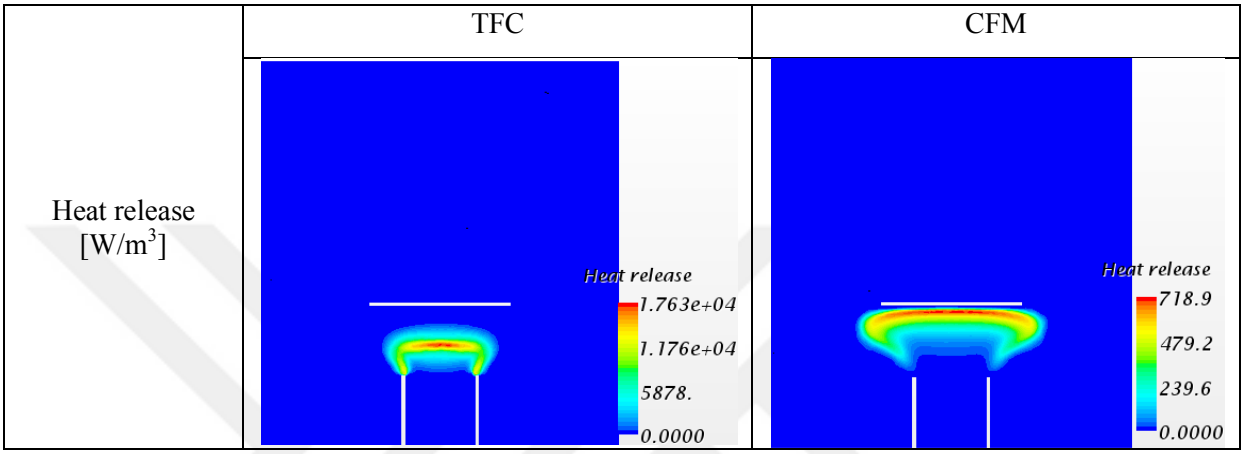

Figure 4.26 Heat release of the CFM and TFC models at Re_λ =110 and thermal load 9 kW.

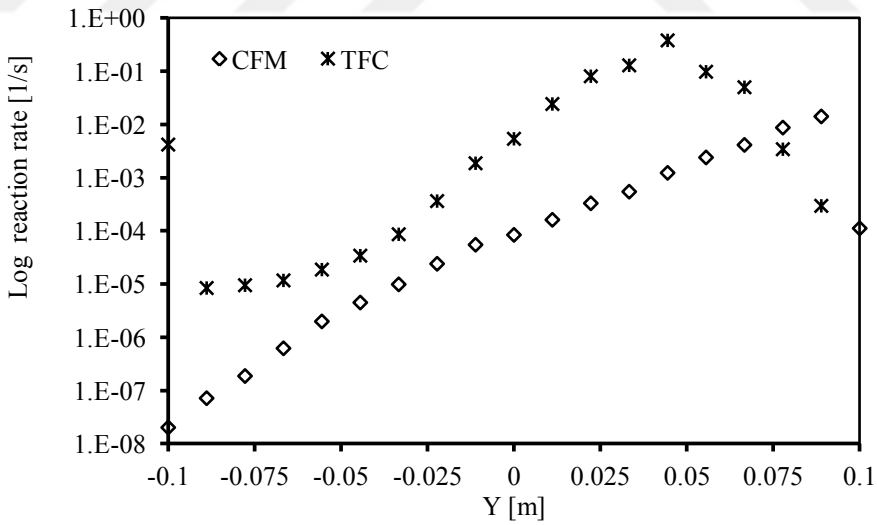

Figure 4.27 Logarithm scale of reaction rate distributions of CFM and TFC model at Re_λ =110 of 9 kW.

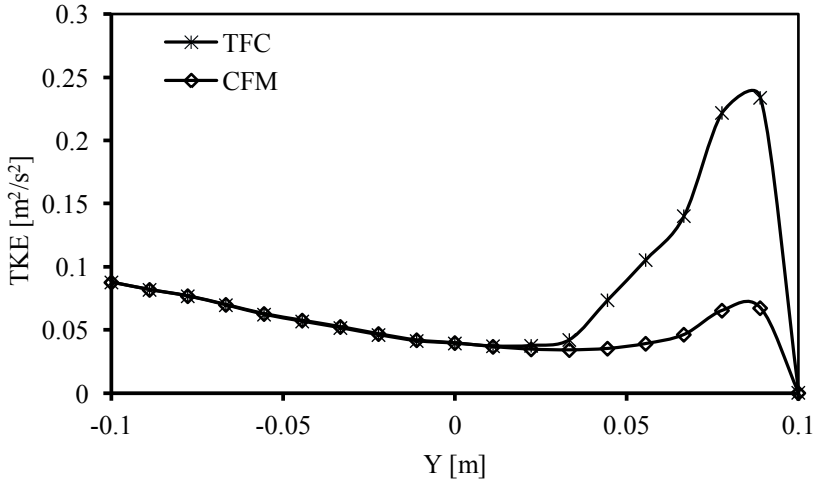

Figure 4.28 TKE distribution of TFC and CFM models at Re_λ =110 of 9 kW.

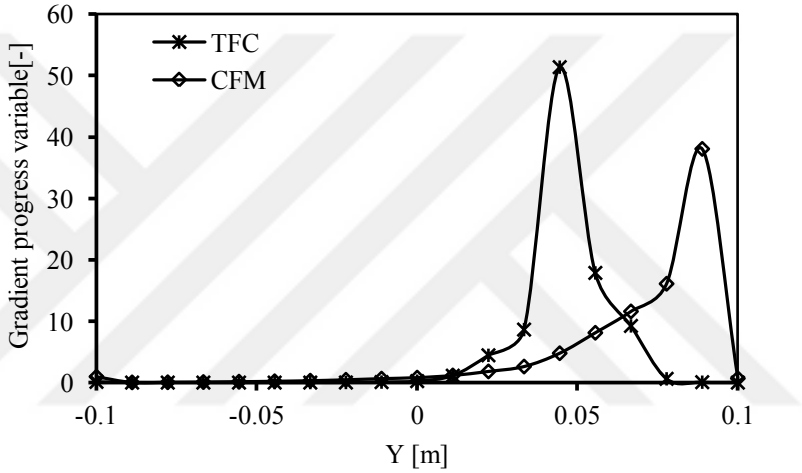

Figure 4.29 Gradient progress variable distribution of TFC and CFM models at Re_λ =110 of 9 kW.

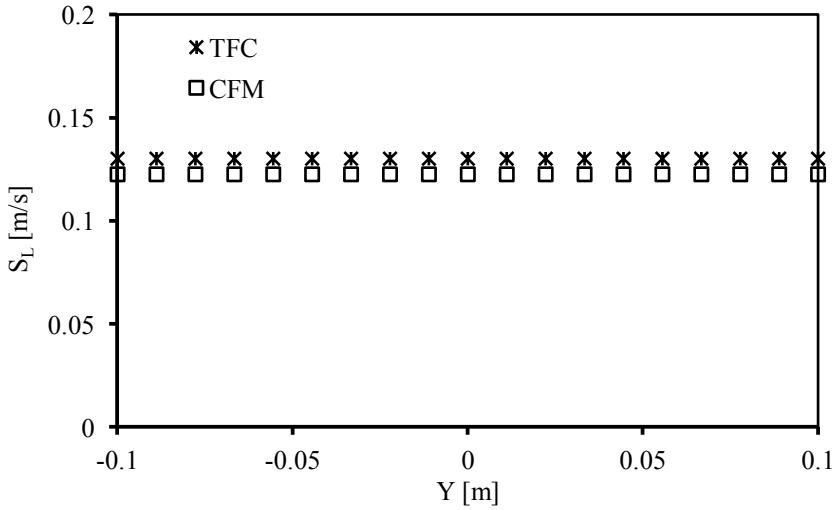

Figure 4.30 Laminar flame speed S_L distribution of CFM and TFC models at Re_λ =110 of 9 kW.

Mass fraction	TFC	CFM
Y_{C3H8}	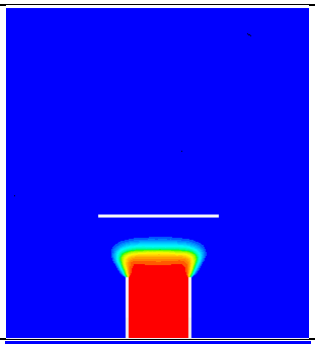	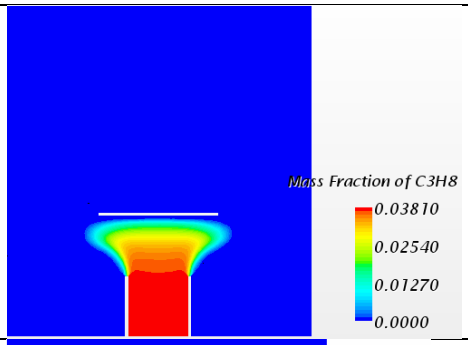
Y_{O2}	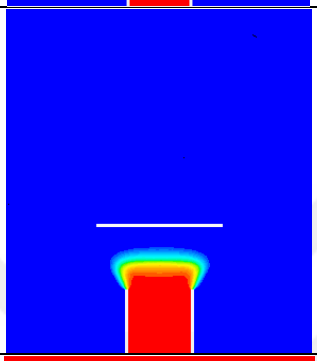	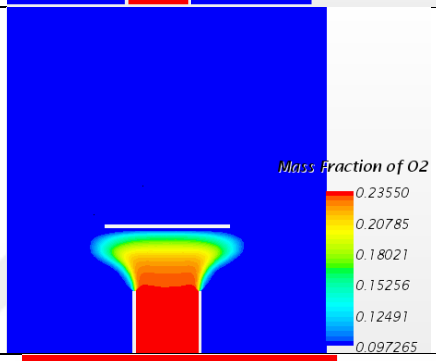
Y_{H2O}	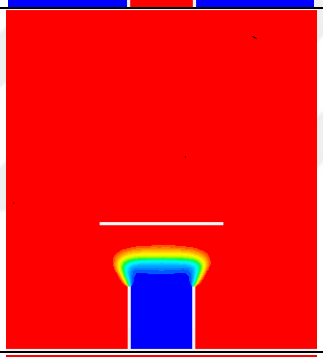	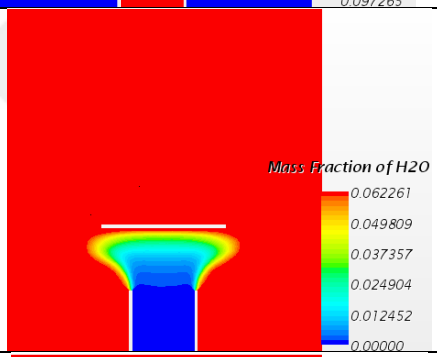
Y_{CO2}	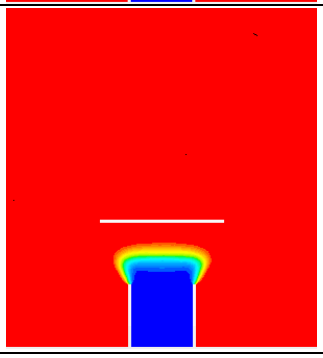	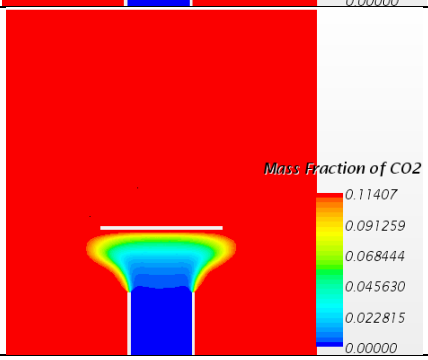

Figure 4.31 Species mass fraction of CFM and TFC models at Re_{λ} =110 of 9 kW.

The distribution of fuel mass fraction is depicted in Figure (4.32) at Re_{λ}=110 of 9 kW. The fresh fuel that enters the combustor generates 0.0381 mass fuel fractions for both models. The mass fraction of the TFC model dropped lower than that of CFM in the reaction region after combustion due to high reaction rate as shown in Figure (4.27). We obtain a different position in the centerline of the combustor for the same value of fuel mass fraction in the reaction region of the CFM and TFC models.

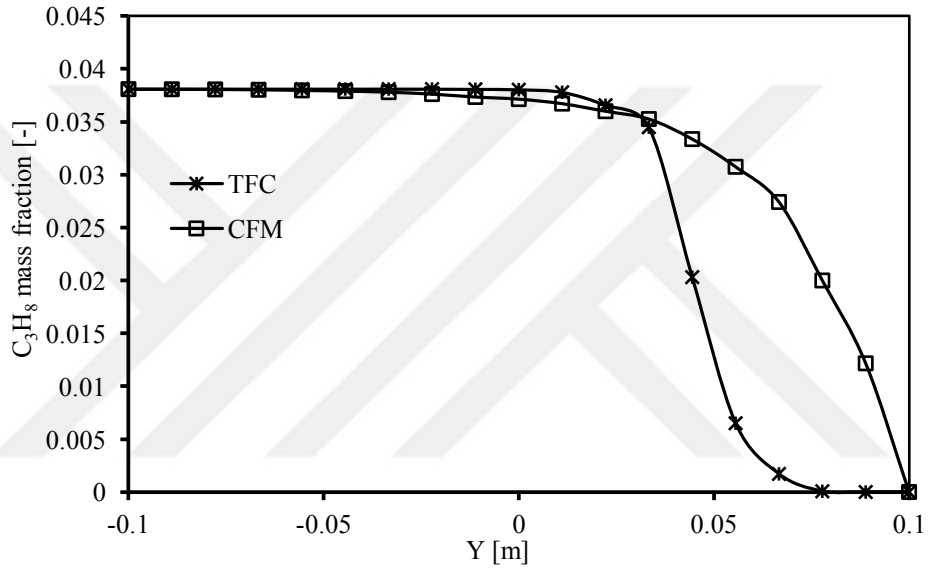

Figure 4.32 C_3H_8 mass fraction distribution of CFM and TFC models at Re_{λ} =110 of 9 kW.

The flame area density (FAD) of the CFM model at different turbulent level is depicted in Figure (4.33). We can determine the location of the flame front on the basis of FAD parameter. FAD is represented as a function of turbulence level. The maximum value of FAD increases by increasing Re_{λ}. Heat release and flame location move to the inlet region. The combustion temperature of the CFM and TFC models, which are calculated along the centerline of the combustor, is plotted in Figure (4.34). The temperature of the TFC model increased sharply to 1500 K after combustion. By

contrast, gradual increases in CFM cause more diffusion flame above the burner exit region.

Figure (4.35) shows the flame location of the CFM and TFC models, which decreases gradually with increased Re_λ [106]. The flame gradually moves upstream to the flame front toward the burner exit with increasing Re_λ at 9 kW, as shown in Figures (3.3) and (3.4). The flame in the TFC model moves downwards toward the inlet region to a degree higher than that in CFM. Moreover, flame shape changes in the CFM and TFC model with the change in flame location as depicted in Figures (4.26) and (4.30).

The flame shape of the CFM and TFC models differ in the reaction regions as shown in Figures (4.11) and (4.21). Understanding the behaviour of flame location and topology in the jet flow combustor with various Re_λ values at a constant thermal load is important in controlling flame location. Heat release contour visualizes flame topology. Flame location is assumed to be located in the midpoint of the bright region [21]. We calculated flame location on the basis of this assumption. The flame shape of CFM resembles a mushroom and is located far from the burner exit. The flame in the TFC model is symmetrical and is located near the burner exit. Flame location was calculated on the basis of maximum heat release from the reaction as in Equations 2.56 and 2.57. Turbulent flame speed was calculated using Equation 2.34, which depends only on Re_λ as shown in Figure (4.20). Maximum *HR* changes, but flame topology and flame location did not change after increasing k at constant Re_λ. This result satisfies U_t in Equation 2.34.

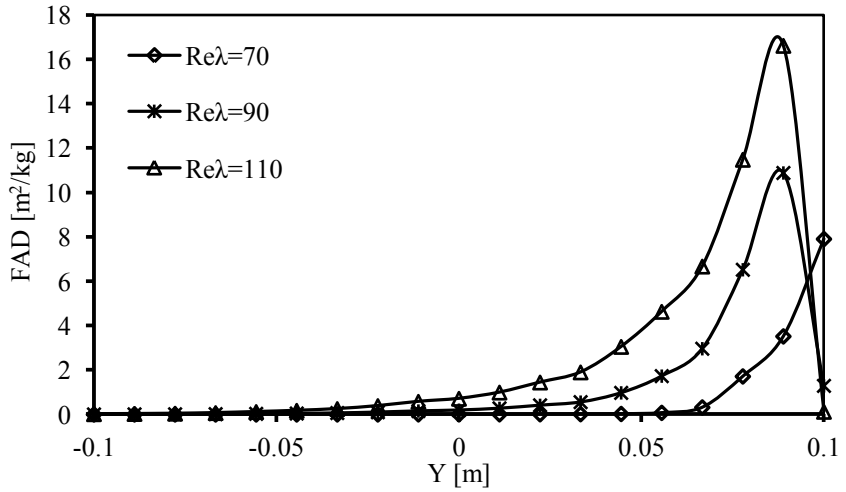

Figure 4.33 Flame area density (FAD) distribution of CFM model at different Re_λ of 9 kW.

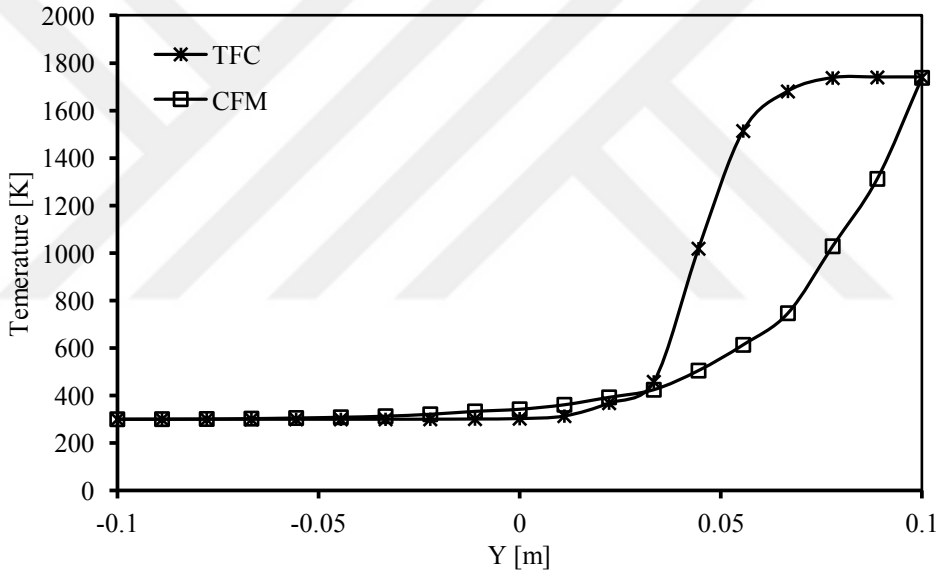

Figure 4.34 Temperature distribution of CFM and TFC models at Re_λ =110 of 9 kW.

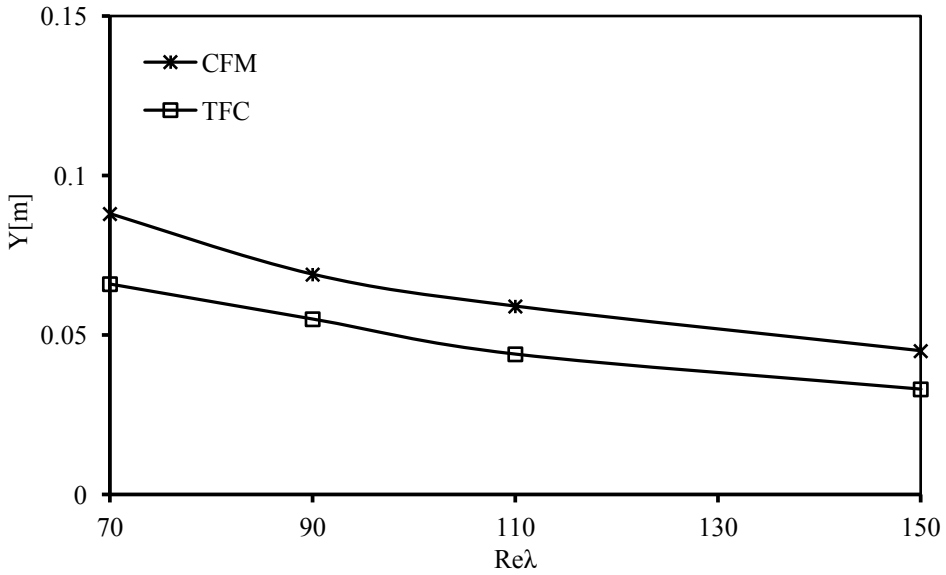

Figure 4.35 Flame location of the CFM and TFC models at different Re_λ and thermal load 9 kW.

4.5 LES Results

In the steady reacting flow, the turbulence parameters provide reasonable predictions on the behaviour of flame location, but in an unsteady reacting flow, the matter is more complicated. In the LES model, turbulence is achieved by setting the characteristics of the sinusoidal wave in the inlet region and the ratio of the mass flow rate of the mixture from each inlet. The sinusoidal wave in the two-inlet region is used to generate turbulence. The flame topology and flame location are sensitive to the variations of the characteristics of the sinusoidal wave. The characteristics of this wave are the amplitude of pulsation A_o, which represents the fluctuation in the inlet velocity, and the frequency of the sine inlet velocity calculated by Equation (2.47). As mentioned, we considered a two-inlet region, and the characteristic parameters were set for these inlets. In general, air–fuel mixture with a constant mass flow rate of 5.086 g/s enters the combustor at an equivalence ratio of 0.588. The behaviour of flame topology and that of flame location were investigated by varying one parameter and fixing the others. The stagnation temperature of the air entering the combustor is 300 K, and therefore, the existing of the ignitor or hot surface flame holder is essential to ignite the fuel.

4.5.1 Effect of the Frequency

The effects of turbulence parameters, which include frequency, pulsation amplitude and mass flow rate ratio, on the flame topology and flame location were studied here by fixing two parameters and varying the third, as shown in Table (4.5). This procedure was used for all test cases. Figure (4.36) shows the flame location along the centerline of the jet flow combustor at different frequencies f. The flame location was calculated from the maximum value of the mean heat release rate along the

centerline of the combustor. Because of the unsteady reacting flow, the heat release fluctuation is dominant in all numerical simulations related to the LES method. Clearly, increasing the frequency of the sinusoidal wave from 150 Hz to 500 Hz at constant amplitude of pulsation of 0.3 m/s and 30% mass flow rate ratio in inlet 1 ($MFRR1$) induces the flame location to move downstream in the jet pipe flow region.

Table 4.5 Turbulence parameters for LES and flame location from mean heat release at time of 4 s.

Mass flow rate ratio in inlet1 MFRR1 [%]	Frequency f [1/s]	Amplitude of oscillation in inlet 2 A_o[m/s]	Reynolds number Inlet 1 [-]	Reynolds number Inlet 2 [-]	Flame location [m]
30	150	0.3	1505	6195	-0.06
	200		1505	6195	-0.05
	250		1505	6195	-0.03
	300		1505	6195	-0.03
	500		1505	6195	-0.01
30	200	0.1	1505	6195	-0.03
		0.15	1505	6195	0.0
		0.2	1505	6195	-0.03
		0.3	1505	6195	-0.05
		0.4	1505	6195	-0.03
10	200	0.1	502	7964	0.02
15			752	7522	0.06
20			1003	7080	0.06
25			1254	6637	-0.01
30			1505	6195	-0.03

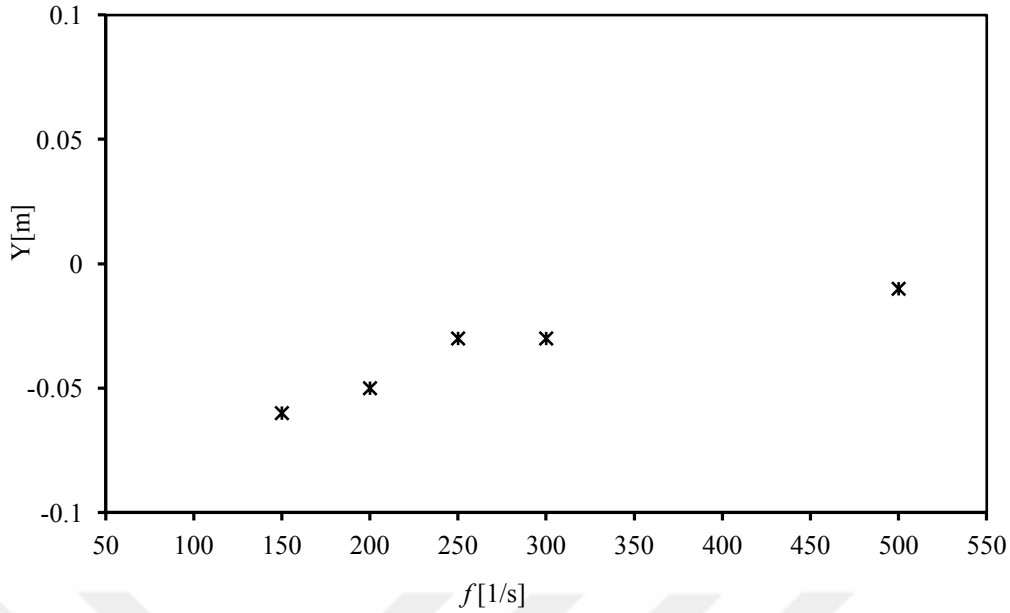

Figure 4.36 Flame location at different frequency and 30% mass flow rate ratio in inlet 1 at maximum values of mean heat release and amplitude=0.3 m/s at t=4 s.

Figure (4.37) shows the contours of the mean of the heat release rate (left) and the heat release rate (right) from the combustion over time (i.e. 4 s) at different frequencies (i.e. 150, 200, 250 and 300 Hz), a constant $MFRR1$ of 30% whilst passing through inlet 1 and an amplitude of pulsation of 0.3 m/s. In this study, the initial static temperature of the flame holder is set to 1700 K. The combustion starts by self - ignition, when the air–fuel mixture reaches the combustion region of the flame holder. The dynamics of the reaction along the centerline of the combustor start in a region below the flame holder; the flame moves downwards and meets with the fresh mixture, which continuously enters the combustion region, and the fresh mixture pushes the flame outside. As a result, a V-shaped flame is formed. Given that the combustion is lean, not all the oxygen entering the combustor can participate in the reaction. In addition, owing to the turbulent effect, the flame is spread far away from the combustor centerline, and flame wings are formed. Similarly, Figure (4.38) shows the flow field, that is, the line integral convolution of the velocity streamlines at different turbulence parameters and the contours of the temperature and turbulent kinetic energy. Clearly,

the flame is sucked from the centerline of the combustor and escapes far away from the region below the flame holder inside the combustion domain. The corrugated flame is observed at a low frequency in the temperature contour. The fresh mixture needs 0.34 s, i.e. 1135 from time step or 5675 iteration, to reach flame holder region and after that the combustion is occur. At a 0.6 s, i.e. 2000 from time step or 10000, iteration the corrugated flame is formed in the combustion region at different aspects until reach final form as in Figure (4.38) right top row. As demonstrated in the velocity streamline configuration, vortices are formed in the inlet region and then decay inside the jet pipe flow region towards the burner exit until they reach the reaction region. Taken together, Figures (4.37) and (4.38) show that the vortex induces the corrugated flame more than increasing the pulsation frequency does and the numerical simulation tool has an acceptable level of performance when used for investigating the flame topology and flame location under the influence of turbulence.

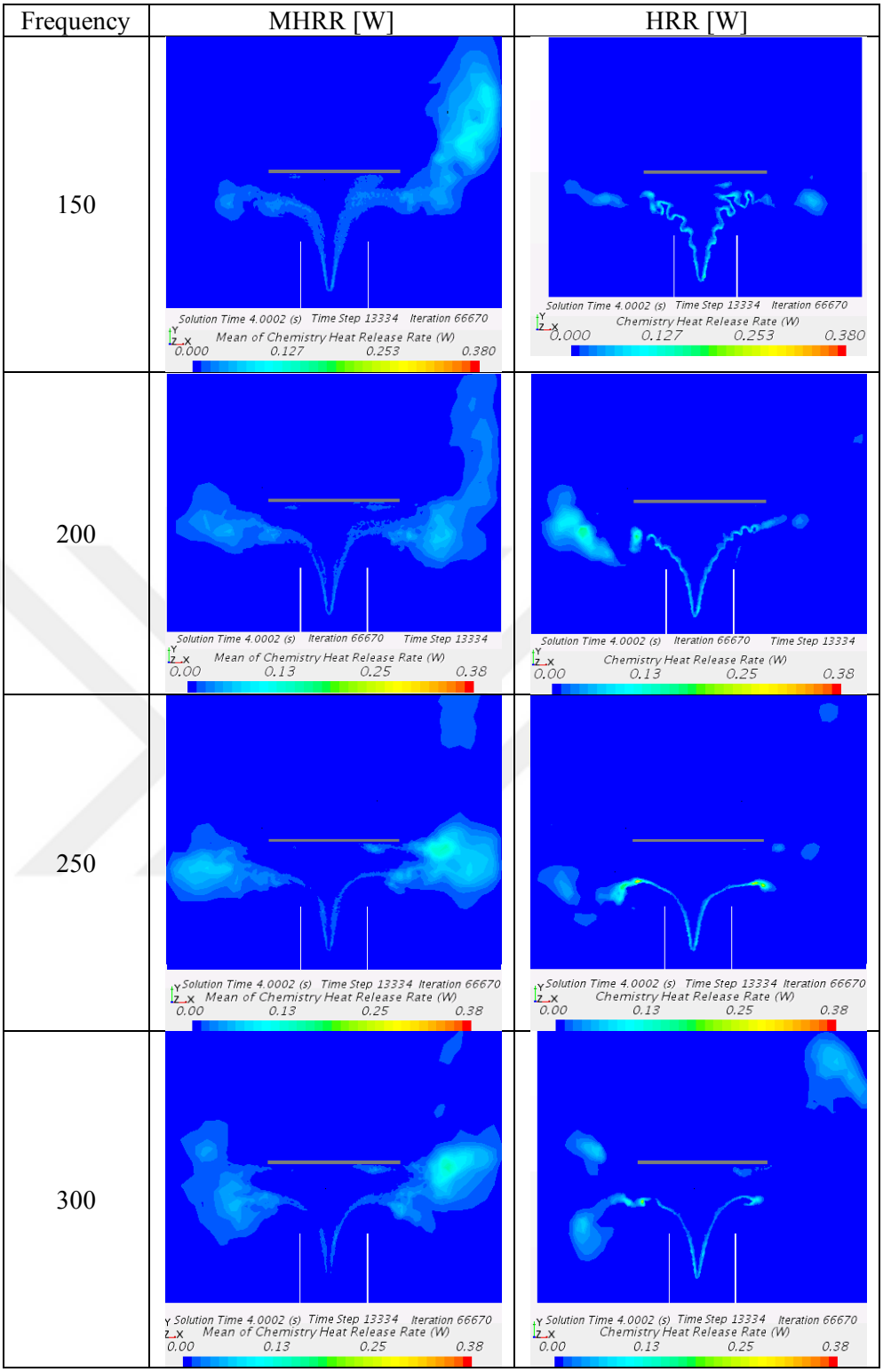

Figure 4.37 Contours of mean of heat release rate (MHRR) and heat release rate (HRR) from the combustion over time 4s at different frequency of 150, 200, 250 and 300 Hz and constant mass flow rate ratio passing through inlet 1 is 30%, and amplitude of pulsation of 0.3 m/s.

f [Hz]	Temperature [K]	Velocity streamline [m/s]	k [m^2/s^2]
150	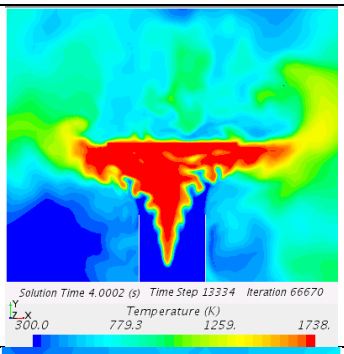	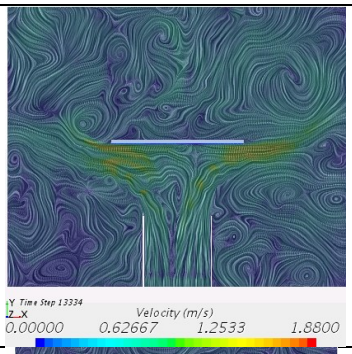	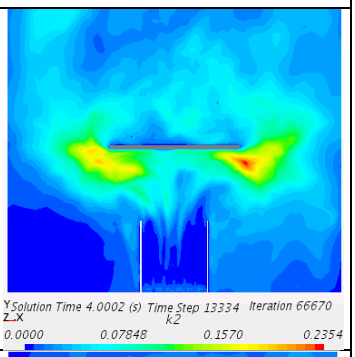
200	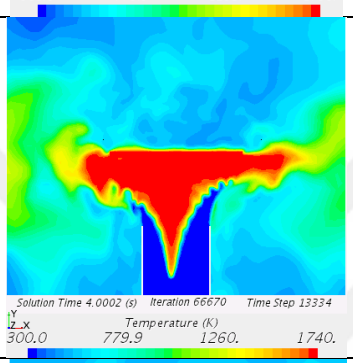	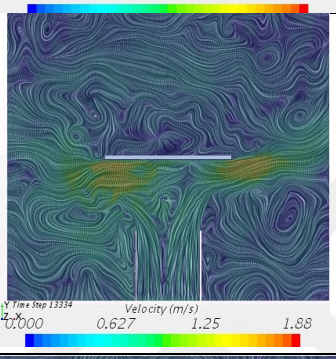	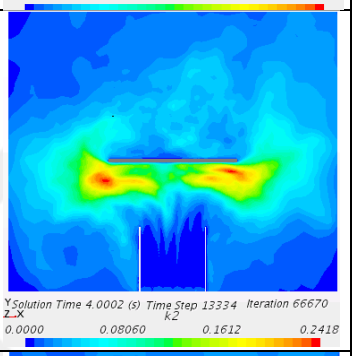
250	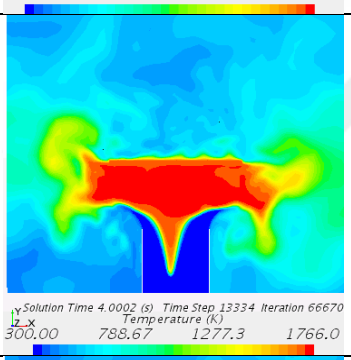	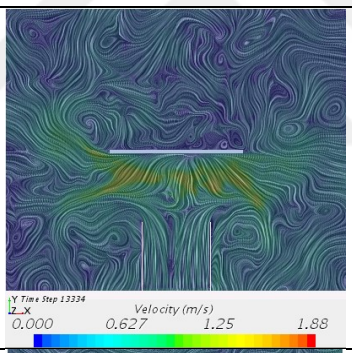	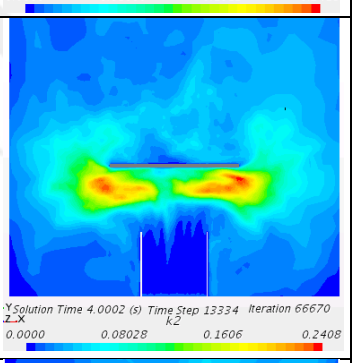
300	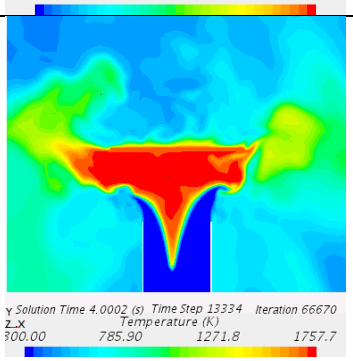	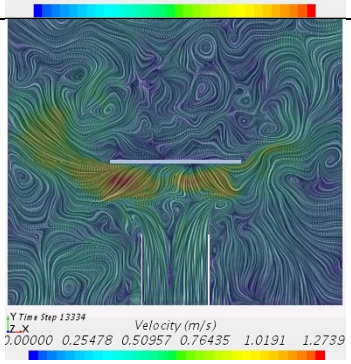	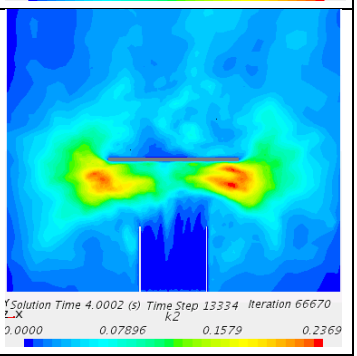

Figure 4.38 Contour of the temperature, line integral convolution of velocity stream line and turbulent kinetic energy at different frequency of 150, 200, 250 and 300 Hz and mass flow rate ratio passing in inlet 1 is 30%, and amplitude is 0.3 m/s and t=4 s.

4.5.2 Effect of the Amplitude of Pulsation

Another parameter of sinusoidal wave that affects both flame topology and flame location is the amplitude of pulsation of the sine wave. Figure (4.39) shows the effect of the amplitude of pulsation on the flame location at a frequency of 200 Hz and 30% mass flow rate ratio passing through inlet 1. The fluctuation in heat release is dominant in the combustion regime due to the unsteady reacting flow. The flame location calculated from the maximum value of the mean heat release along the centerline of the jet flow combustor generally shows a small variation when the amplitude of pulsation is increased, whereas the flame topology variation is evident. Figure (4.40) shows the contours of the MHRR and HRR from the combustion. While Figure (4.41) shows the streamline velocities and temperature contours and turbulent kinetic energy at solution time 4 s at different amplitudes of pulsation (i.e. 0.1, 0.15, 0.2 and 0.3 m/s), 30% mass flow rate ratio passing through inlet 1, and frequency of 200 Hz. In addition, the V- shaped flame is formed at different amplitudes of pulsation, and the flame becomes more corrugated by increasing the amplitude of pulsation, especially at A_O=0.3 m/s. The pulsation effect induces the corrugated flame more than the vortex flow effect does.

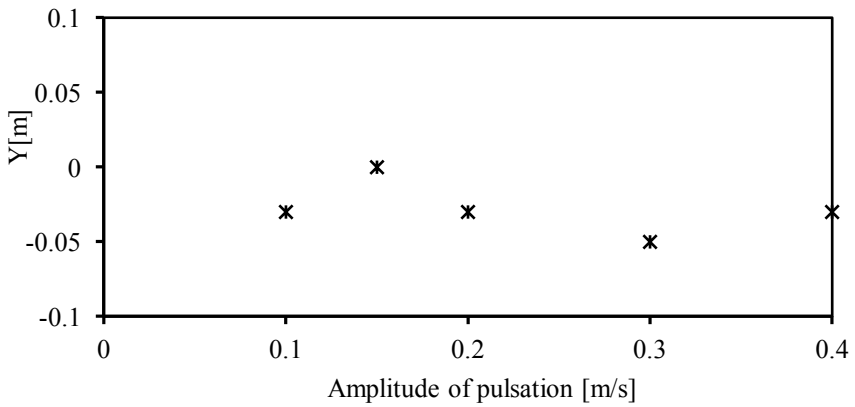

Figure 4.39 Flame location at different amplitude of pulsation and 30% mass flow rate ratio in inlet 1 at maximum values of mean heat release and frequency of 200 Hz.

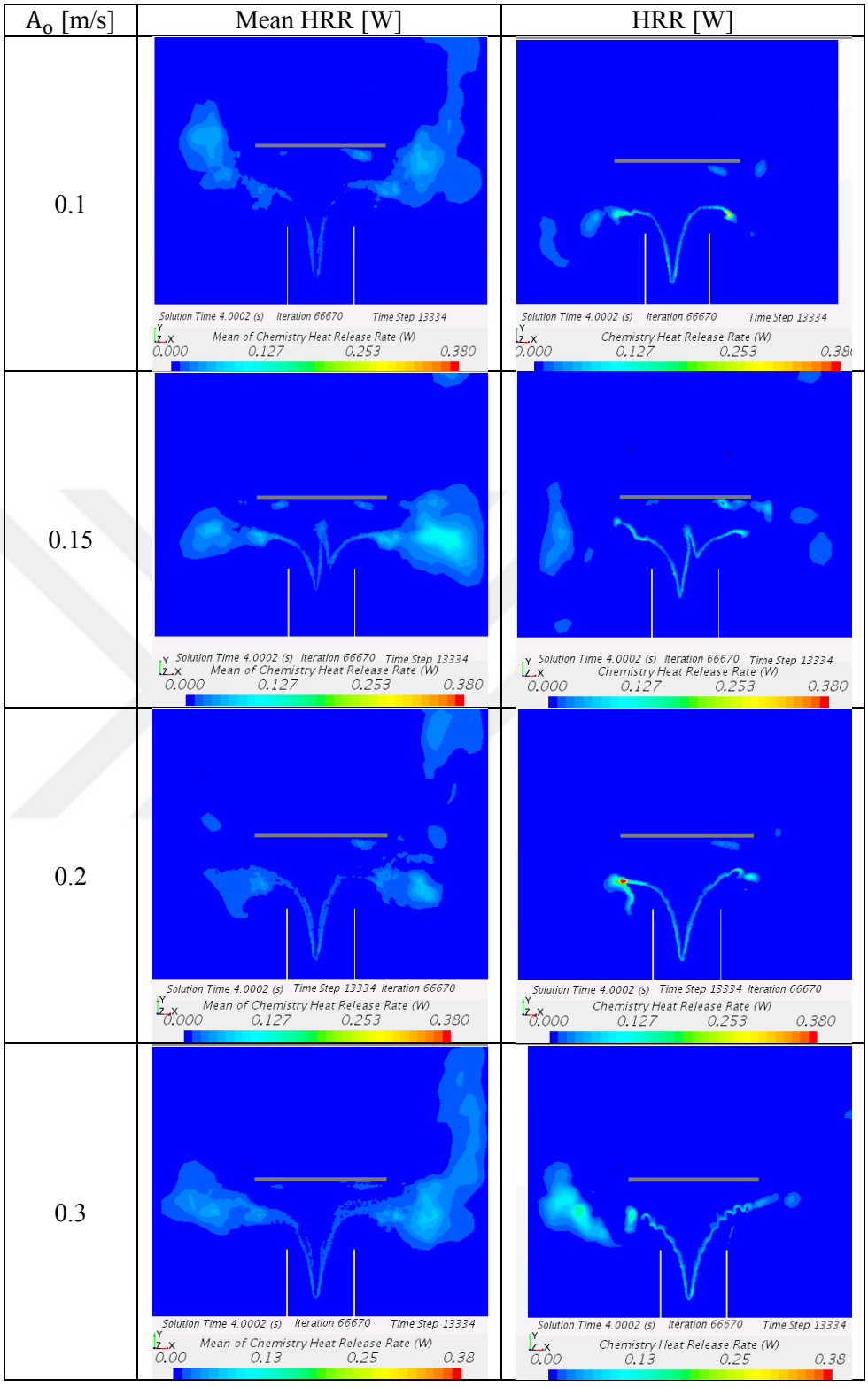

Figure 4.40 Contours of mean of heat release rate (left) and heat release rate (right) from the combustion over time 4s at different amplitude of oscillation of 0.1, 0.15, 0.2 and 0.3 m/s and mass flow rate ratio passing in inlet 1 is 30%, and frequency of 200 Hz.

Ao [m/s]	Temperature [K]	Velocity streamline [m/s]	k [m^2/s^2]
0.1	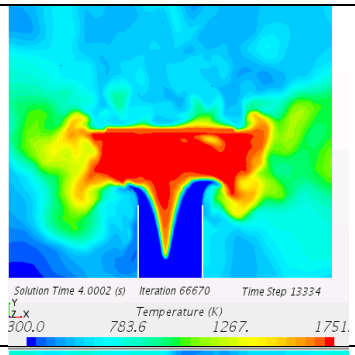	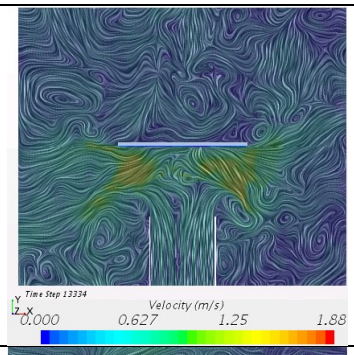	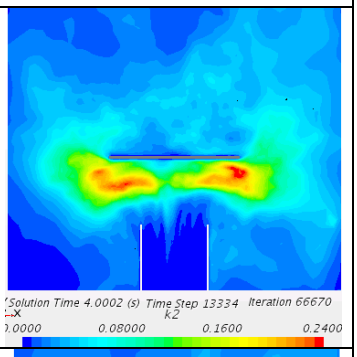
0.15	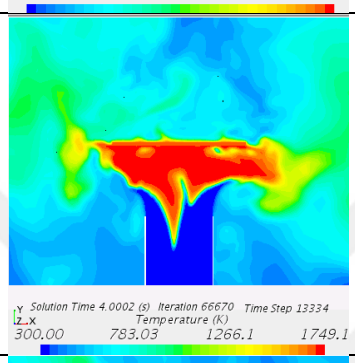	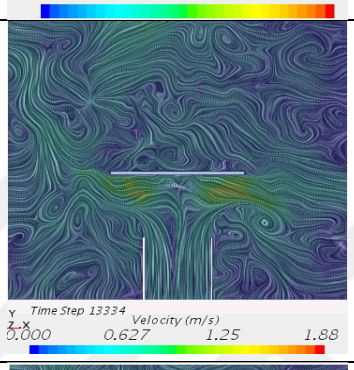	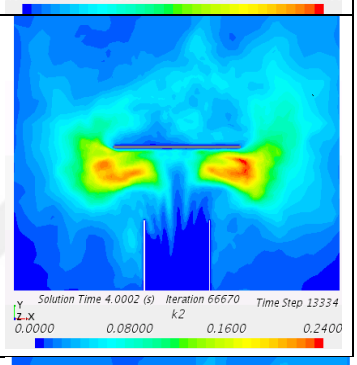
0.2	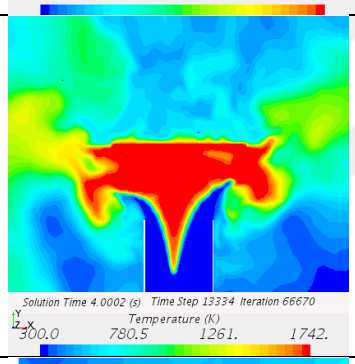	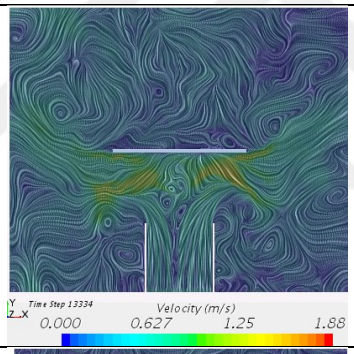	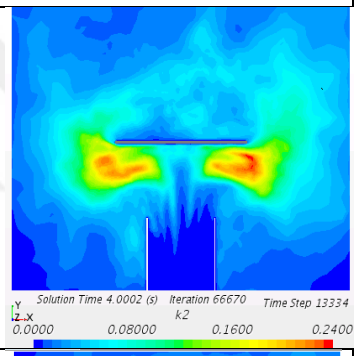
0.3	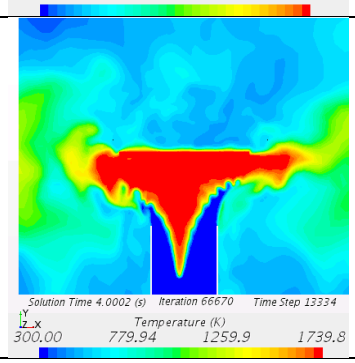	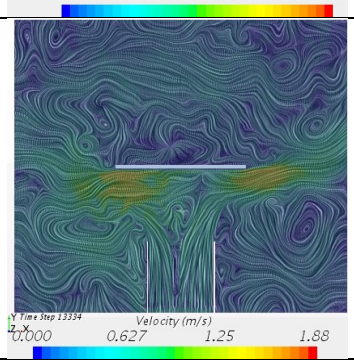	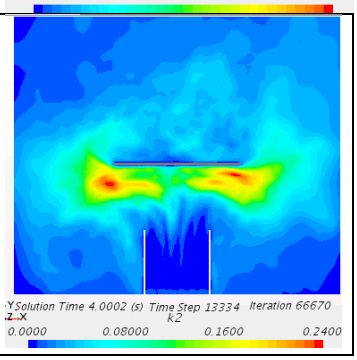

Figure 4.41 Contour of the temperature and line integral convolution of velocity stream line and turbulent kinetic energy at different amplitude of oscillation of 0.1, 0.15 ,0.2 and 0.3 m/s and mass flow rate ratio passing in inlet 1 is 30%, and frequency of 200 Hz and t = 4 s.

4.5.3 Distribution of Mass Flow Rate among Different Inlet

The effect of the ratio of the mass flow rate of the mixture on the flame location is shown in Figure (4.42). The mass flow rate ratios passing through inlet 1 $\dot{m}_1$ are 10%, 15%, 20%, 25% and 30%. The constant frequency is 200 Hz, and the amplitude of pulsation is 0.1 m/s. The flame location is calculated from the maximum value of the mean heat release along the centerline of the combustor. The flame location moves upwards with increasing mass flow ratio until 20%, then moves downwards because of the decrease in the flow velocity at inlet 2. The flame topology configuration is clear in Figures (4.43) and (4.44). The vortex effect induces the corrugated flame more than increasing the MFRR1. The contours of the mean heat release from the combustion at solution time 4 s; different mass flow rate ratios passing through inlet 1 of 10%, 20%, 25%, and 30%; f of 200 Hz; and amplitude of 0.1 m/s are depicted in both figures. The flame is very corrugated at a low mass flow rate ratio through inlet 1 (i.e. high mass flow rate ratio through inlet 2) because the total mass flow rate ratios passing through inlet 1 and inlet 2 are unity, as mentioned in Chapter 2. Given that the flame is corrugated the flame surface density is increased. Consequently, the heat release rate increases. This observation about the flame shape is consistent with the experimental results.

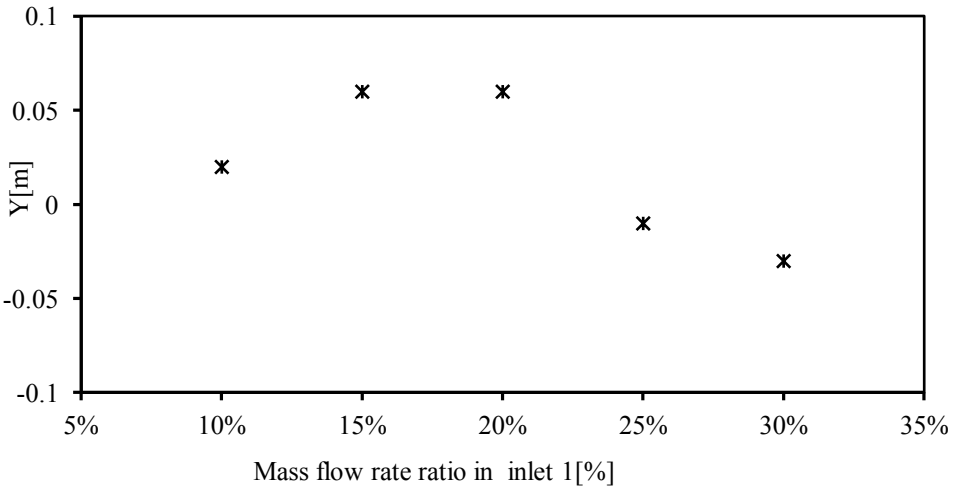

Figure 4.42 Flame location at different mass flow rate ratio in inlet 1at maximum values of mean heat release and frequency of 200 Hz, amplitude=0.1 m/s.

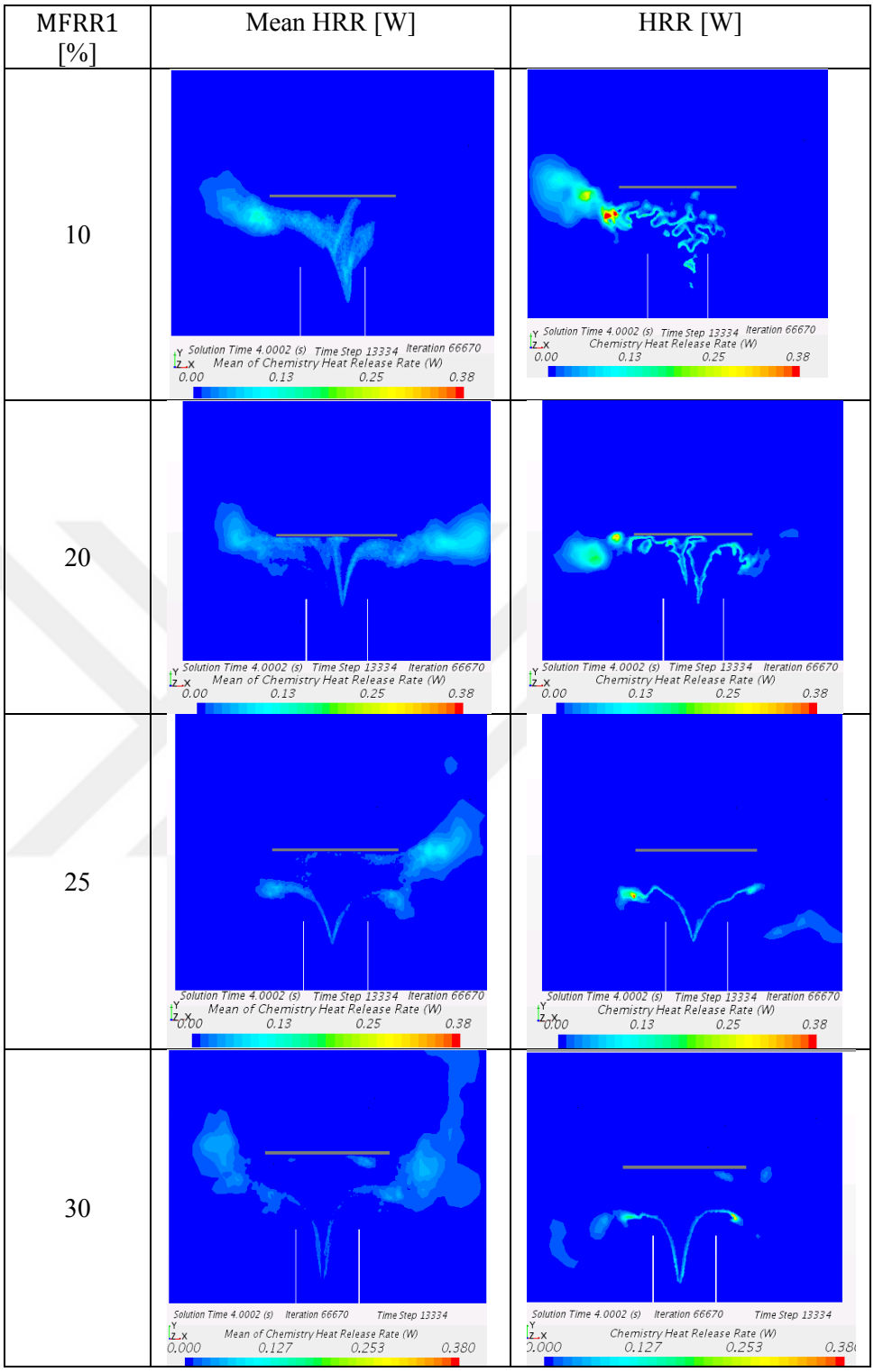

Figure 4.43 Contours of mean of heat release rate (left) and heat release rate (right) from the combustion over time 4s at different mass flow rate ratio passing in inlet 1 of 10%, 20%, 25% and 30%, at amplitude of 0.1 m/s and frequency of 200 Hz.

MFRR1 [%]	Temperature [K]	Velocity streamline [m/s]	k [m^2/s^2]
10	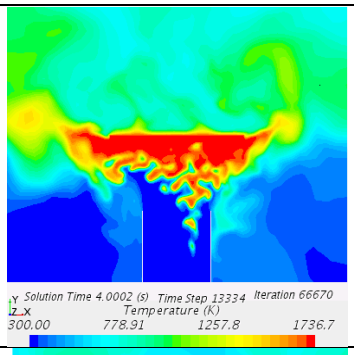	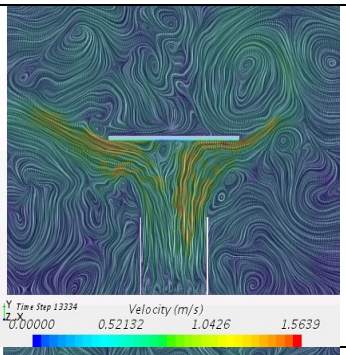	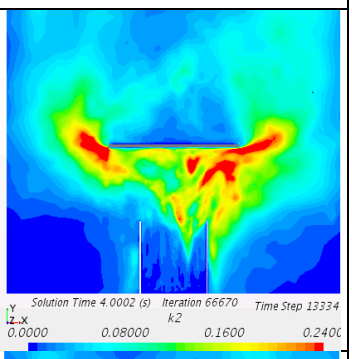
20	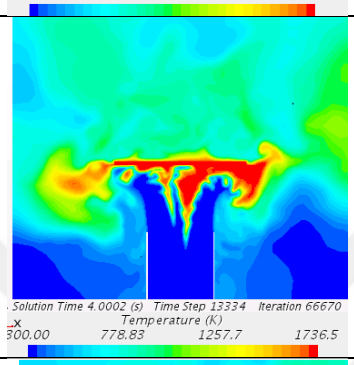	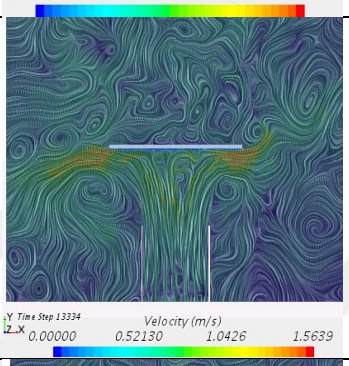	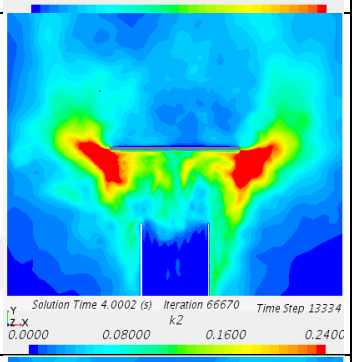
25	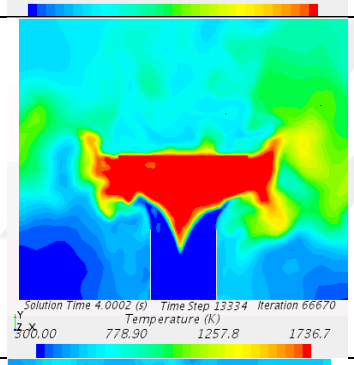	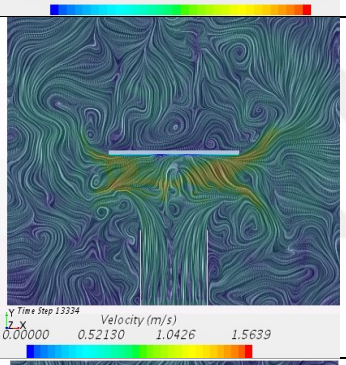	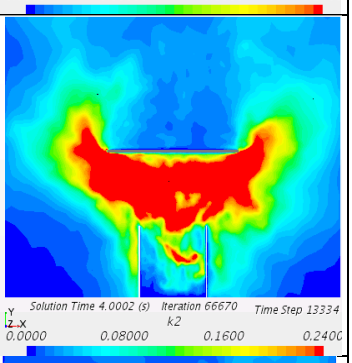
30	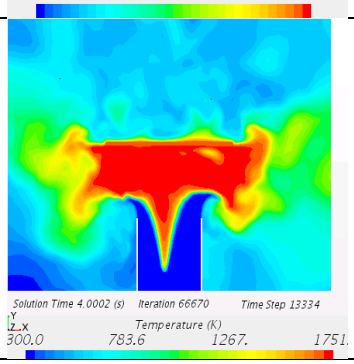	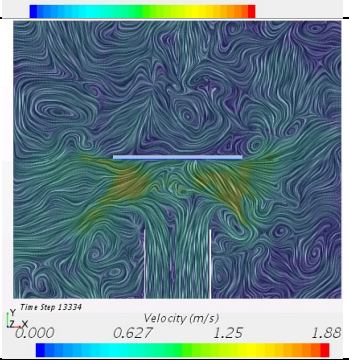	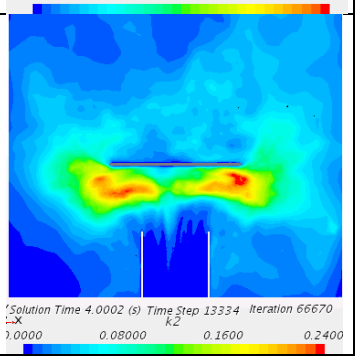

Figure 4.44 Contour of the temperature (left) and line integral convolution of velocity streamline (right) at different mass flow rate ratio passing in inlet 1 of 10%, 20%, 25% and 30% at amplitude of 0.1 m/s and frequency of 200 Hz and t = 4 s.

CHAPTER V

CONCLUSIONS AND RECOMMENDATIONS FOR FUTURE RESEARCH

This study on turbulent flow of lean premixed combustion was motivated by previous studies on propane–air mixture in steady and unsteady-state flow systems. Lean premixed combustion under the influence of active-grid turbulence was computationally investigated, and the results were compared with the experimental data. The experiments and numerical simulations were performed to generate a premixed flame at thermal loads of 3, 5 and 9 kW from a jet flow combustor with a constant-velocity inlet. The turbulent combustion models, namely the CFM and TFC model for steady-state conditions and the LES model for unsteady state flow conditions were established and used in simulations performed under different turbulent flow conditions. The turbulence parameters in the TFC and CFM models include the Reynolds number based on the Taylor microscale (Re_λ), the dissipation rate of turbulence (ε) and turbulent kinetic energy (k). In the LES model, the turbulence was generated by setting the characteristics of the sinusoidal wave, namely $A_o$and f in the inlet region, and the ratio of the mass flow rate of the mixture ($\dot{m}$). The three models were utilised to predict the flame topology and the flame location under turbulent conditions. All of these models yielded three different sets of results, which were compared with the experimental data. Furthermore, heat release, species mass fraction and temperature distribution along the centerline of the combustor were investigated.

5.1 Conclusions

After the computational efforts in generating turbulence in the three different models, especially in the LES model, have been resolved and tested against the experimental data, turbulent flows were generated in terms of Re_λ, $\mathrm{A_o}$ and f. The important conclusions for each model are summarised in the following subsections.

5.1.1 TFC Model

In the initial stage of this study, special attention was paid to the selection of the turbulent combustion model in the STAR-CCM+ software on the basis of the available experimental data obtained by Ertunc in 2007. The calibration of the model's constant A was performed comprehensively in terms of fuel mass fraction at different turbulence intensities (Ti) and turbulent length scale (l_t) in view of the lack of consensus in the literature regarding the most suitable value of A for jet flow combustors. Different flame characteristics in various turbulent conditions were implemented to investigate the flame topology and the flame location along the centerline of the jet flow combustor. The following conclusions were drawn.

1. The best value of constant A of the TFC model that matches the experimental data is A= 0.37 for a one-inlet jet flow combustor and not 0.5, as previously suggested by Zimont. In addition, the TFC and CFM models were run in STAR CCM+ v10.02 software.
2. A new formula for turbulent flame speed U_t was derived from the Zimont formula and used in all simulations related to the TFC model with varying Re_λ. The results showed that the flame location and the flame topology were influenced solely by Re_λ, as suggested by the derived equation for U_t.

3. The simulations were performed at 3, 5 and 9 kW under the same turbulent conditions. The results showed that the flame topology and the flame location were remarkably modified by changing the constant A within the range 0.1<A < 0.5, turbulence intensity within the range 0.1 < Ti < 0.25, and Re_λ within the range 5 < Re_λ < 150.
4. The results showed that the combustion occurs in the wrinkled and corrugated flamelet regions on the Borghi diagram. Moreover, at a low Re_λ value, the flame topology was wrinkled and symmetric with respect to the vertical axis of the combustor, whereas at medium and high Re_λ values, the flame topology exhibited cusps.
5. Along the centerline of the jet flow combustor, calculated from the maximum heat released, the flame location decreases gradually towards the inlet region with an increase in Re_λ. This behaviour of the flame indicated the increase in the reaction rate due to an increase in the mixing process. This observation on the flame location is compatible with the experimental results.
6. The TKE initially decays from turbulence dynamics as expected in the inlet region. At a low turbulence level, the effect of TKE diminishes whilst $Re_\lambda >$ 40, and the effect of TKE is very noticeable in the hot flow region.

5.1.2 Conclusion about the CFM Used

The second turbulent flow model selected was CFM model. The turbulent conditions were achieved by setting Re_λ, k and ϵ in the inlet region to calculate the flame characteristics and the flame topology. The results were then compared with those from experiments. The results showed that.

1. The flame topology generated from this model resembles a mushroom. The behaviour of the flame inside the entire domain of the combustor is not constant at different Re_λ values; therefore, the readings were taken from four different line probe positions in the combustor, and the maximum heat release value was monitored. In addition, the models were performed at 3, 5 and 9 kW thermal loads.
2. The flame topology and the flame location are highly modified by increasing Re_λ and the flame moves towards the inlet region at the three thermal loads of 3, 5 and 9 kW.
3. The diffusion of the flame towards the inlet region was examined when Re_λ is increased. The results showed that the flame in CFM diffused more into the inlet region than that in the TFC model when Re_λ is increased. This observation verifies the experimental results on transport small turbulent eddies, that is, combustion can be enhanced by increasing the flame area.
4. The flame location and the flame topology did not show any dependence on turbulent kinetic energy at a constant Re_λ.

5.1.3 Conclusion about LES Model Used

The flame topology and the flame location of the lean, turbulent premixed V-shaped flames in the jet flow combustor were computationally investigated and compared with the experimental data. The experiments and simulations were performed at constant thermal loads (i.e. a constant inlet velocity of 0.52 m/s and a constant equivalence ratio of 0.588). Numerical simulations were conducted using the LES model. Turbulence was generated using sinusoidal waves in two different inlets in the simulations, whereas turbulence was generated with active grids in the experiments. The turbulence parameters are more complicated to obtain in an unsteady reacting flow than in a steady one because of the long convergence time during simulations. Furthermore, the turbulence parameters obtained by the latter provides reasonable prediction for the behavior of flame topology and flame location, as found in our previous work [106]. Nevertheless, in this study, the turbulence was realized by setting the characteristics of the sinusoidal wave in the inlet region. These characteristics include the amplitude of pulsation A_o, the frequency f and the ratio of the mass flow rate of the mixture through inlet 1($MFRR1$). The main outcomes from this work are as follows:

1. The simulations were performed within certain ranges of the characteristics of the sinusoidal wave, that is, the pulsation amplitude range in inlet 2 is $0.1<A_o<0.4$, the frequency range is $100 < f < 500$, and the mass flow rate ratio range is $10\% < MFRR1 < 30\%$. Both flame topology and flame location are sensitive to the variations of these characteristics.
2. The flame V- shape is formed and the flame wings are corrugated by velocity fluctuations.

3. When the frequency is increased, the flame location moves downstream in the jet pipe flow region. Moreover, the corrugated flame is very noticeable at a low frequency due to the vortex effect.
4. The flame location shows a small variation by increasing the amplitude of pulsation at a constant frequency and a constant mass flow rate of the mixture. By contrast, the flame topology variation is apparent from the mean heat release rate, temperature and streamline flow contours. Increasing amplitude of pulsation enhances the corrugation of the flame.
5. The flame location moves upwards when the mass flow ratio through inlet 1 is increased until 20% at a constant frequency and constant amplitude of pulsation. The flame is very corrugated at a low mass flow rate ratio through inlet 1 due to the vortex effect. This observation on the flame shape is consistent with the experimental results. Thus, the numerical simulation tool has an acceptable level of performance when investigating flame topology and flame location.

5.2 Recommendations for Future Research

The TFC, CFM and LES models based on a transported equation could be provide favorable approximation in the simulations of lean, turbulent premixed combustion. However, further research is required to improve the applicability of these models to other practical combustor configurations. Future studies may consider the following details:

1. Additional practical experiments may be conducted, and the results thereof should be compared with the numerical simulation results of TFC, CFM and LES to ensure the reliability of the results on flame topology and flame location depending on their turbulent conditions.
2. The TFC and CFM models do not appear to provide accurate prediction of flame topology when $Re_\lambda < 40$. Having a complete grasp of the limitation of the TFC and CFM models in relation to flame topology is necessary before searching for a sensible treatment. Specifically, some of the insufficiencies could be corrected as regards the turbulent conditions of turbulent kinetic energy and dissipation rate of turbulent kinetic energy in the inlet region.
3. All numerical simulations were performed to generate turbulence in the inlet region and then progressed to the entire combustion domain at a constant inlet velocity, equivalence ratio and thermal loads without changing the diameter of the burner. Future research may consider changing one or more of these factors to generate turbulence and study their effects on flame topology and flame location.
4. This study provides explanations for three-dimensional flames of a single-step reaction. Future studies should cover multistep reactions.

5. In LES model simulation, the amplitude of the pulsation and frequency can be modulated to simulate oscillatory conditions of gas turbine burners and turbulent combustion.

APPENDIX A

1. Algebraic Model

In this model, turbulent mixing controls the reaction rate. The first model was put forward by Spalding and Mason in 1973, on the basis of this relationship. It is known as the premixed eddy break-up (PEBU) model [107]:

$$\frac{\partial \rho c}{\partial t} + \nabla.(\rho u c) - \nabla.(\Gamma_c \nabla c) = W_{pebu} \quad \text{(A-1)}$$

where the reaction rate is defined as

$$W_{pebu} = -\rho.a.b(1-b)\frac{(Y_{ft}-Y_{res})}{\tau_t} \quad \text{(A-2)}$$

where a, b, Y_{ft} and Y_{res} are the model coefficient, the regress variable, the mass fraction of the mixture and the quantity of fuel that is left at the end of combustion respectively.

In addition, the regress variable can defined as

$$b = \frac{(c - Y_{res})}{(Y_{ft}-Y_{res})} \quad \text{(A-3)}$$

Afterwards, this model was improved by Hjertager and Magnussen [108] and Bray [30] and became known in multidimensional numerical simulation and widely applied in industrial applications.

2. Presumed PDF Model

In this model the reaction rate can be determined by using the presumed probability density function P(x, t, c) from the following equation [28]:

$$\overline{W}(x,t) = \int_0^1 W(c)P(x,t,c) \quad \text{(A-4)}$$

Accordingly, the problem of modelling the influence of turbulence on combustion can be solved by guessing the general shape of P(c) and then assuming the PDF of the mixture fraction (f), which depends on the second moment gf [107]:

$$P(f) = \frac{f^{k-1}(1-f)^{m-1}}{\int_0^1 f^{k-1}(1-f)^{m-1}df}, \quad \text{(A-5)}$$

where k, m and g_f are

$$k = \frac{\bar{f}}{g_f}\left[\bar{f}\left(1-\bar{f}\right) - g_f\right] \quad \text{(A-6)}$$

$$m = \frac{(1-\bar{f})}{\bar{f}}k, \quad \text{(A-7)}$$

$$g_f = \overline{\left(f-\bar{f}\right)^2} \quad \text{(A-8)}$$

3. Self-Similarly Developing, Premixed, Turbulent Flame Model

In this model, which is also known as the Zimont model or turbulent flame speed closure (TFC) model, the balance equation for the Favre-averaged premixed combustion progress variable is written as [28]

$$\frac{\partial}{\partial t}(\bar{\rho}\tilde{c}) + \frac{\partial}{\partial x_j}\left(\bar{\rho}\tilde{u}_j\tilde{c}\right) = \frac{\partial}{\partial x_j}(\bar{\rho}D_t\frac{\partial\tilde{c}}{\partial x_j}) + \rho U_t|\nabla\tilde{c}| \quad \text{(A-9)}$$

The analytical solution of Equation (A-9) is

$$\bar{c} = \frac{1}{\sqrt{\pi}}\int_{\xi\sqrt{\pi}}^{\infty} e^{-\xi^2}\,d\xi \quad \text{(A-10)}$$

where ξ is the normalised distance defined as

$$\xi = \frac{x-x_f(t)}{\delta_t(t)} \quad \text{(A-11)}$$

In Equation (A-11), $x_f(t)$ is the mean flame coordinate expressed as

$$x_f(t) = x_f(t=0) + \int_0^t U_t d\theta, \text{ and} \quad \text{(A-12)}$$

$$\delta_t^2 = 4\pi \int_0^t D_t d\theta \quad \text{(A-13)}$$

where $\theta = \frac{\Omega_t}{\tau_\eta}$ is the time scale.

The reaction rate can be written as

$$\overline{W} = \frac{\rho_u \Omega}{\tau_f} \quad \text{(A-14)}$$

where

$$\Omega = -B_1 \frac{dc}{d\xi} - B_2 \frac{D_t \tau_f}{\delta_t^2} \frac{d}{d\xi}\left(\frac{\bar{\rho}}{\rho_u}\frac{d\tilde{c}}{d\xi}\right) \quad \text{(A-15)}$$

where Ω is an arbitrary time-dependent function, and B_1 and B_2 are model constants.

4. Flame Surface Density and Scalar Dissipation Rate Models

The flame surface density model is sometimes called the coherent flame model (CFM). It assumes that the effect of turbulent eddies on the local combustion rate within instantaneous flame fronts will separate from the effect of turbulent eddies. The flame surface density is defined mathematically as [28]

$$\Sigma = |\nabla c| \quad \text{(A-16)}$$

For this model, the reaction rate is [13]

$$\overline{W} = \rho_u S_L G \Sigma \quad \text{(A-17)}$$

where G is the flame stretch factor. Furthermore, the reaction rate is obtained from a balance equation for the mean scalar dissipation rate ($\bar{\chi}_c$), which was posited by Borghi in 1990:

$$\bar{W} \approx \frac{\bar{\chi}_c}{(2c_m - 1)} \tag{A-18}$$

where

$$c_m = \frac{\int_0^1 cWP_f dc}{\bar{W}} \tag{A-19}$$

APPENDIX B

In this study, the Reynolds number based on the Taylor microscale is a fundamental factor used in CFM and TFC models and can be derived from the Taylor and Kolmogorov scales. The turbulent length scale of a large eddy is defined from turbulent kinetic energy and dissipation rate of the turbulent kinetic energy:

$$L_t = \frac{k^{1.5}}{\epsilon} \tag{B-1}$$

The turbulent Reynolds number can be defined as

$$Re_t = \frac{k^{0.5} L_t}{\nu} = \frac{k^2}{\epsilon \upsilon} \tag{B-2}$$

The transverse Taylor microscale, which represents the diameter of the smallest eddy, which is responsible for the dissipation of energy:

$$\frac{\lambda_g}{L_t} = 3.163 {Re_t}^{-0.5} \tag{B-3}$$

For a large eddy, the Kolmogorov scale is used:

$$\frac{\eta}{L_t} = Re^{-0.75} \tag{B-4}$$

When the size of the intermediate eddy is between the Kolmogorov scale and Taylor scale, the Reynolds number based on the Taylor microscale is used. The Taylor microscale describes the grid turbulence at a high Reynolds number and is defined as

$$Re_\lambda = \frac{\acute{u}\lambda_g}{\nu} \tag{B-5}$$

where $\acute{u} = \bar{U}T_i = \sqrt{\frac{2}{3}k}$

The parameters $\acute{u}$ and $\bar{U}$ are the fluctuation and the mean velocity respectively.

Equations (B-1) and (B-3) yield

$$\lambda_g = 3.163 L_t Re_t^{-0.5}$$

or

$$\lambda_g = 3.163 \eta^{0.667} L_t^{0.334} \quad \text{(B-6)}$$

Finally, the Reynolds number based on the Taylor microscale can be written as

$$Re_\lambda = 2.582 k (\nu\epsilon)^{-0.5} \quad \text{(B-7)}$$

REFERENCES

[1] N. Swaminathan and K. Bray, "*Turbulent Premixed Flames,* " First Edition. Cambridge University Press,UK, 2011.

[2] I. Glassman and R. Yetter, "*Combustion,* "Fourth Edition. Elsevier Inc Press, 2008.

[3] W. Lin, "Large Eddy Simulation of Premixed Turbulent Combustion Using Flame Surface Density Approach by," *Ph.D thesis, University of Toronto*, 2010.

[4] T. Sponfeldner, N. Soulopoulos, F. Beyrau, Y. Hardalupas, A. Taylor, and J. Vassilicos, "The Structure of Turbulent Flames in Fractal- and Regular-Grid-Generated Turbulence," *Combust. Flame*, Vol. 162, No. 9, pp. 3379–3393, 2015.

[5] L. Mydlarski and Z. Warhaft, "On The Onset of High-Reynolds-Number Grid-Generated Wind Tunnel Turbulence," *J. Fluid Mech*., Vol. 320, No. 1, 1996.

[6] N. Mazellier, L. Danaila, and B. Renou, "Multi-Scale Energy Injection: A New Tool to Generate Intense Homogeneous and Isotropic Turbulence For Premixed Combustion," *J. Turbul*., Vol. 11, No. 2, N43, 2010.

[7] N. Soulopoulos, J Kerl, T Sponfeldner, F Beyrau, Y Hardalupas, A. Taylor and J. Vassilicos "Turbulent Premixed Flames on Fractal-Grid-Generated Turbulence," *Fluid Dyn. Res*., Vol. 45, No. 6, p. 061404, 2013.

[8] K. Goh,P. Geipel, and R. P. Lindstedt "Lean Premixed Opposed Jet Flames in Fractal Grid Generated Multiscale Turbulence," *Combust. Flame*, Vol. 161, No. 9, pp. 2419–2434, 2014.

[9] G. Cafiero, S Discetti, and T. Astarita, "Heat Transfer Enhancement of Impinging Jets With Fractal-Generated Turbulence," *Int. J. Heat Mass Transf*., Vol. 75, pp. 173–183, 2014.

[10] H. Kido,M. Nakahara,K. Nakashima,J. Hashimoto, "An Experimental Study on The Local Configuration of Premixed Turbulent Flame," *JSME International Journal*, Vol. 46, No. 1. p. 92, 2003.

[11] Ö. Gülder and F. Yuen, "Turbulent Premixed Flame Front Dynamics and Implications For Limits of Flamelet Hypothesis," *Proc. Combust. Inst*., Vol. 34, pp. 1393–1400, 2013.

[12] B. Yilmaz, S. Özdoğan and I. Gökalp "Numerical Study of Turbulent Lean Premixed Methane-Air Flames," *Fuels Combust. Eng. J*., pp. 26–33, 2015.

[13] S. Muppala, B. Manickam and F. Dinkelacker, "A Comparative Study of The Different Reaction Models For Turbulent Methane-Hydrogen-Air," *J. Therm. Eng*., Vol. 1, No. 1, pp. 367–380, 2015.

[14] V. Moreau, " A Self-Similar Premixed Turbulent Flame Model,"*Appl. Math. Model*., Vol. 33, No. 2, pp. 835–851, 2009.

[15] M. Barbato, M. Talice, V.L. Zimont "Numerical Simulation of Premixed Combustion Flows : a Comparative Study." *Journal of Thermal Engineering Yildiz Technical University Press,* Istanbul, Turkey Vol. 1, Special Issue 1, pp. 367-380, February, 2015.

[16] I. Nazzal And Ö. Ertunc, "Effects of Turbulence Intensity and Length Scale on The Flame Location of Premixed Turbulent Combustion in a Diffuser Combustor," *J. Therm. Sci. Technol*., Vol. 12, No. 2, pp. JTST0029-JTST0029, 2017.

[17] U. Ahmed and R. Prosser, "Modelling Flame Turbulence Interaction in RANS Simulation of Premixed Turbulent Combustion," *Combust. Theory Model*., Vol. 20, No. 1, pp. 34–57, 2015.

[18] S. Pope, "*Turbulent Flows*,"First Edition, Cambridge Univ. Press, UK, 2000.

[19] A. N. Lipatnikov, " *Fundamentals of Premixed Turbulent Combustion*, " First edition. CRC Press, 2012.

[20] Zeinab and Pouransari, "Fundamental Studies of nonpremixed Combustion in Turbulent Wall Jets Using Direct Numerical Simulation, " *R. Inst. Technol*., No. September, 2011.

[21] O.K. Law, "*Combustion Physics*.,"First edition, Cambridge University Press,UK, 2006.

[22] P. Belardini, C. Bertoli, S. Corsaro, and P. D'Ambra, "Introducing Combustion-Turbulence Interaction in Parallel Simulation of Diesel Engines, " High Performance Computing and Communications , pp. 1–10, 2006.

[23] A. Steinberg, J. F. Driscoll, and S. Ceccio, "Turbulence Flame Interactions The Mechanisms of Flame Strain and Wrinkling," *AIAA Pap*., No. July 2008, pp. 1–13, 2008.

[24] T. Echekki and E. Mastorakos, "*Turbulent Combustion Modeling, Advances, New Trends and Perspectives* " Springer Press, p 513, 2011.

[25] T. Poinsot and D. Veynante, "*Theoretical and Numerical Combustion*, "Second Edition. R. T. Edwards, Philadelphia, USA, 2005.

[26] I. Zaidi, "Reliability of CFD for Buoyancy Driven Flows in Industrial Applications, " *Ph.D thesis*, *Manchester University, UK*: 2013.

[27] C.Wagner, T. Hüttl, and P. Sagaut, "Large-Eddy Simulation for Acoustics," *Large-Eddy Simul. Acoust.,* Vol. 9780521871, pp. 1–441, 2007.

[28] P. Sagaut, "*Large Eddy Simulation for Incompressible Flows*. " 3rd Edition, Springer-Verlag Berlin Heidelberg Press, 2002.

[29] E. Yasari, S. Verma, and A. N. Lipatnikov, "RANS Simulations of Statistically Stationary Premixed Turbulent Combustion Using Flame Speed Closure Model," *Flow, Turbul. Combust*., Vol. 94, No. 2, pp. 381–414, 2015.

[30] V. Sabelnikov and A. Lipatnikov, "Towards an Extension of TFC Model of Premixed Turbulent Combustion,"*Flow, Turbul. Combust*., Vol. 90, No. 2, pp. 387–400, 2013.

[31] F. Dinkelacker and S. Hölzler, "Investigation of a Turbulent Flame Speed Closure Approach for Premixed Flame Calculations," Combust. Sci. Technol., Vol. 158, No. September, pp. 321–340, 2000.

[32] A. Lipatnikov and J. Chomiak, “A simple Model of Unsteady Turbulent Flame Propagation, ” *J. Engines, SAE Transactions*, 106 ,SAE paper 972993, 1997.

[33] B. Manickam, S. Muppala, J. Franke, and F. Dinkelacker, “ Numerical Simulation of Rod Stabilized Flames,” V Eur. Conf. Comput. Fluid Dyn. ECCOMAS CFD, No. June, pp. 14–17, 2010.

[34] P. Flohr and H. Pitsch, “A Turbulent Flame Speed Closure Model for LES of Industrial Burner Flows,” Proc. Summer Progr., pp. 169–179, 2000.

[35] V. L. Zimont and A.N. Lipatnikov, “To Computations of the Heat Release Rate in Turbulent Flames, ” *Dok l. Phys. Chem. 1* (Russian original 1993, translated 1994) 332, 592.

[36] M. Amico “CFD Simulation of a Burner for Syngas Characterization: Preliminary Results and Experimental Validation,” 18th Eur. Biomass Conf. Exhib., Vol. 3000, No. May, pp. 3–7, 2010.

[37] Kanniche and Zurbach, “Coherent Flame Model for Turbulent Combustion Operatıng with Both Premixed and Non-Premixed Flames,”ASME Paper, No. 95-GT-168, pp. V003T06A034; 1995.

[38] S. Candel, D. Veynante, F. Lacas, E. Maistret, N. Darabiha, T. Poinsot, “ Coherent Flame Model: Applications and Recent Extensions, ”*Advances in Combustion Modeling*, World Scientific, Singapore, pp. 19–64, 1990.

[39] P. Belardini, C.Bertoli, S.Corsaro and P.Anbra “ Introducing combustion-turbulence interaction in parallel simulation of diesel engines,” *High Perform,* pp. 1–10, 2006.

[40] T. Mastorakos, “Turbulent Combustion Modeling,” *Fluid Mech. Appl*., Vol. 95, pp. 119–142, 2011.

[41] T. Poinsot and D. Veynante, “*Theoretical and Numerical Combustion*, ” Second Edition, Cambridge Univ. Press, p. 522, 2005.

[42] G.Hartung, J.Hult, C.Kaminski, J.Rogerson, N.Swaminathan “Effect of Heat Release on Turbulence and Scalar-turbulence Interaction in Premixed Combustion” Phys. Fluids, 20(2008),3, pp. 1–17.

[43] H. Schmid, P. Habisreuther, and W. Leuckel, “A Model for Calculating Heat Release in Premixed Turbulent Flames,” Combust. And Flame, Vol. 113, No. 97, pp. 79–91, 1998.

[44] Z. M. Nikolaou and N. Swaminathan, “Heat Release Rate Markers for Premixed Combustion,” *Combust. Flame*, Vol. 161, No. 12, pp. 3073–3084, 2014.

[45] S. Möller, E. Lundgren, and C. Fureby, “Large Eddy Simulation of Unsteady Combustion,” *Symp. Combust*., Vol. 26, No. 1, pp. 241–248, 1996.

[46] P. Pavael and S.Pope, “Large Eddy Simulation/Probability Density Function Simulations of Bluff Body Stabilized Flames,” *Combust. Flame*, Vol. 161, No. 12, pp. 3100–3133, 2014.

[47] V. Battaglia and V. Zimont, “Joint RANS / LES Modeling of Flameless Combustion,” *Energy Power Eng*., Vol. 3, No. 5, pp. 616–624, 2011.

[48] M.Wu, S.KW on, J.Driscoll, G.Faeth, “Preferential Diffusion Effects on The Surface Structure of Turbulent Premixed Hydrogen / Air Flames” *Combust. Sci.*

Technol. ,78, February, pp. 69–96, 1991.

[49] P.Tamadonfar, ,Ö. L Gülder,. "Effects of Mixture Composition and Turbulence Intensity on Flame Front Structure and Burning Velocities of Premixed Turbulent Hydrocarbon / Air Bunsen Flames" *Combust. Flame*, 162,12, pp. 4417–4441, 2015.

[50] P.Coelho, "Numerical Simulation of the Interaction Between Turbulence and Radiation in Reactive Flows " Progress in Energy and Combustion Science 33, pp 311–383, 2007.

[51] J. Li and M. Modest "Importance of Turbulence-Radiation Interactions in Turbulent Diffusion Jet Flames" *Journal of Heat Transfer ASME* , Vol. 125 /831, 2003.

[52] V. Zimont, W. Polifke, M. Bettelini and W. Weisenstein, "An Efficient Computational Model for Premixed Turbulent Combustion at High Reynolds Numbers Based on a Turbulent Flame Speed Closure," *J. Eng. Gas Turbines Power*, Vol. 120, No. 3, p. 526, 1998.

[53] CD-AdapcoTM, " STAR-CCM +v 10_ User Guide," 2015.

[54] L.Wang, "Detailed Chemistry, Soot, and Radiation Calculations in Turbulent Reacting Flows," Ph.D Thesis, The Pennsylvania State University, USA, 2004.

[55] K. Bray, M. Championt , P. Libby, "The Interaction Between Turbulence and Chemistry in Premixed Turbulent Flames," *Turbulent Reactive Flow*s, Vol. 9, No. 5, p. 247, 1980.

[56] U. Ahmed, "Flame Turbulence Interaction in Premixed Turbulent Combustion," *Ph.D Thesis, Manchester University*, 2013.

[57] K. Bray, "The Interaction BetweenTurbulence and Combustion," *Symp. Combust*., Vol. 17, No. 1, pp. 223–233, 1979.

[58] A. Steinberg, J. F. Driscoll, and S. Ceccio, "Turbulence Flame Interactions The Mechanisms of Flame Strain and Wrinkling," *AIAA Pap*., No. July 2008, pp. 1–13, 2008.

[59] N. Swaminathan and R. W. Grout, "Intergaction of Turbulence and Scalar Fields in Premixed Flames," *Phys. Fluids*, Vol. 18, No. 4, pp. 1–10, 2006.

[60] V. Zimont, V. Moreu and Modi, "RANS and LES Modelling of The GE10 Combuster.," *Energy Power Eng*., Vol. 3, No. November, pp. 607–615, 2011.

[61] A. N. Lipatnikov and J. Chomiak, "Developing Premixed Turbulent Flames : Part I . A Self- Similar Regime of Flame Propagation," *Journal Combustion Science and Technology,* Vol 161, 2001.

[62] B. Özdemir, "Simulation Of Turbulent Combustion in a Self-Aerated Domestic Gas Oven," *Appl. Therm. Eng*., Vol. 113, pp. 160–169, 2017.

[63] T. Frank and Ö. L. Gülder, "Investigation of Dynamics of Lean Turbulent Premixed Flames by Rayleigh Scattering," *AIAA J.*, Vol. 47, No. 12, pp. 2964–2973, 2009.

[64] L.Chris and R. W. Schefer, "Scaling of Premixed Turbulent Flames in The Corrugated Regime," *Combust. Flame*, Vol. Volume 146, pp. 180-199, 2006.

[65] F. Ghirelli, “Turbulent Premixed Flame Model Based on a Recent Dispersion Model,” *Comput. Fluids*, Vol. 44, No. 1, pp. 369–376, 2011.

[66] W. Polifke, M. Bettelini, W. Geng, U. Müller, W. Weisenstein, and P. Jansohn, “A Comparison of Combustion Models for Industrial Applications,” *Eccomas* 98, No. November, pp. 1–6, 1998.

[67] A. N. Lipatnikov and J. Chomiak, “Turbulent Flame Speed and Thickness: Phenomenology, Evaluation, and Application in Multi-Dimensional Simulations,” *Prog. Energy Combust.* Sci., Vol. 28, No. 1, pp. 1–74, 2002.

[68] C. Meneveau and T. Poinsot, “Stretching and Quenching of Flamelets in Turbulent Premixed Combustion,” *Combust. Flame*, Vol. 86, pp. 311–332, 1991.

[69] M. Hideharu, “ Realization of a Large-Scale Turbulence Field in a Small Wind Tunnel,” *Fluid Dyn. Res*., Vol. 8, No. 1, pp. 53–64, 1991.

[70] S. Kheirkhah and Ö .L. Gülder, “Topology and Brush Thickness of Turbulent Premixed V-Shaped Flames,” *Flow, Turbul. Combust.*, Vol. 93, No. 3, pp. 439–459, 2014.

[71] Ö. L. Gülder. and G. J. Smallwood, “Flame Surface Densities in Premixed Combustion At Medium To High turbulence Intensities,” *Combust. Sci. Technol.*, Vol. 179, No. 1, pp. 191–206, 2007.

[72] J. Yuan, Y. Ju, and C. Law, “Effects of Turbulence and Flame Instability on Flame Front Evolution,” *Phys. Fluids*, Vol. 18, No. 10, 2006.

[73] P. Clavin and G. Joulin, “Premixed Flames in Large Scale and High Intensity Turbulent Flow,” *J. Phys. Lettres*, Vol. 44, pp. 1-12, 1983.

[74] R. C. Aldredge and F. A. Williams, “Influence of Wrinkled Premixed-Flame Dynamics on Large-Scale, Low-Intensity Turbulent Flow,” *J. Fluid Mech*., Vol. 228, No. July, pp. 487–511, 1991.

[75] A. Bagdanavicius, P. J. Bowen, D. Bradley, M. Lawes, and M. S. Mansour, “Stretch Rate Effects and Flame Surface Densities in Premixed Turbulent Combustion up to 1.25 Mpa,” *Combust. Flame*, Vol. 162, No. 11, pp. 4158–4166, 2015.

[76] G. Fru, D. Thévenin, and G. Janiga, “ Impact of Turbulence Intensity and Equivalence Ratio on The Burning Rate of Premixed Methane-Air Flames,” *Energies,* Vol. 4, No. 6, pp. 878–893, 2011.

[77] M. Alhumairi and Ö. Ertunc, “The Calibration of Turbulent Flame Speed Closure Model to Predict the Premixed Combustion Flame Under The Influence of Weak to Strong Turbulence,” Int. Conf. Energy Therm. Eng. Yildiz Tech. Univ. Istanbul, Turkey, No. 25-28 April 2017. PP. 1–7, 2017.

[78] N. Peters, “*Turbulent Combustion*. ” First Edition, Cambridge University Press ,2004.

[79] V. L. Zimont, “Theory Of Turbulent Combustion of a Homogenous Fuel Mixture at High Reynolds Number,” *Combust. Explos. Shock Waves,* Vol. 15, No. 3, pp. 305-311, 1979.

[80] S. Pope, “Turbulent Premixed Flame,” *Ann. Rev. Fluid Mech*, Vol.19, pp.237-

270, 1987.

[81] N. Peters, "*Combustion Theory*," First Edition, RWTH Aachen University Press, 2010.

[82] N. Peters, "Turbulent Combustion : The, State of The Art.Lecture 10,"pp.1-107, 2010.

[83] P. Tamadonfar and Ö. L. Gülder, "Experimental Investigation of The Inner Structure of Premixed Turbulent Methane/Air Flames in The Thin Reaction Zones Regime," *Combust. Flame*, Vol. 162, No. 1, pp. 115–128, 2015.

[84] P. Siewert, "Flame Front Characteristics of Turbulent Lean Premixed Methane / Air Flames at High-Pressure." *Swiss Federal Institute of Technology Zurich*,NR.16369 2006.

[85] L.Gicquel, G.Staffelbach and T.Poinsot "Large Eddy Simulations of Gaseous Flames in Gas Turbine Combustion Chambers," *Prog. Energy Combust. Sci.*, Vol. 33, No. 1, 2012.

[86] D. Poitou, M. El Hafi, and B. Cuenot, "Analysis of Radiation Modeling for Turbulent Combustion: Development of a Methodology to Couple Turbulent Combustion and Radiative Heat Transfer in LES," *J. Heat Transfer*, Vol. 133, No. 6, p. 062701, 2011.

[87] R. Gonzalez, "Evaluation of a Detailed Reaction Mechanism for Partial and Total Oxidation of C 1 - C 4 Alkanes," DOI. 10.11588/heidok.00008338, 2007.

[88] *P.* Koutmos, G. Giannakis and P. Marazioti, "A Global Oxidation Scheme for Propane-Air Combustion Suitable for Use Into Complex Reacting Flow Computations," *Eng. Trans.*, Vol. 55, No. 4, pp. 293–316, 2007.

[89] M Amico, U. Desideri and F Fantozzi. "CFD Simulation of a Burner for Syngas Characterization: Preliminary Results and Experimental Validation," *18th Eur. Biomass Conf. Exhib.*, Vol. 3000, No. May, pp. 3–7, 2010.

[90] W. Tsang, "Chemical Kinetic Data Base for Combustion Chemistry. Part 3. Propane," *J. Phys. Chem. Ref. Data*, Vol. 17, No. 2. pp. 887–952, 1988.

[91] V. Brinzea, M. Mitu, D. Razus And D. Oancea, "Overall Activation Parameters of Propane Oxidation in Flames From Normal Burning Velocities," *Academia Romania*, Vol. 55, No. 1, Pp. 55–61, 2010.

[92] C. Rosado-Reyes and J. Francisco, "Atmospheric Oxidation Pathways of Propane and Its By-Products: Acetone, Acetaldehyde, and Propionaldehyde," *J. Geophys. Res. Atmos.*, Vol. 112, No. 14, 2007.

[93] K. Kuo and R. Acharya, "*Fundamentals of Turbulent and Multi-Phase Combustion*, " First eddition , John Wiley and Sons, Inc Press, USA, 2012.

[94] V. Robin, A. Mura, M. Champion, O. Degardin, B. Renou, and M. Boukhalfa, "Experimental and Numerical Analysis of Stratified Turbulent V-Shaped Flames," *Combust. Flame*, Vol. 153, No. 1–2, pp. 288–315, 2008.

[95] D. Veynante, J. Piana, J. M. Duclos, and C. Martel, "Experimental Analysis of Flame Surface Density Models for Premixed Turbulent Combustion," *Symp. Combust.*, Vol. 26, No. 1, pp. 413–420, 1996.

[96] R. Riazi and M. Farshchi, “Laminar Premixed V-Shaped Flame Response to Velocity and Equivalence Ratio Perturbations: Investigation on Kinematic Response of Flame,” *Sci. Iran.*, Vol. 18, No. 4 B, pp. 913–922, 2011.

[97] R. K. Cheng, B. Bédat, and L. W. Kostiuk, “Effects of Buoyancy on Lean Premixed V-Flames Part I: Laminar and Turbulent Flame Structures,” *Combust. Flame*, Vol. 116, No. 3, pp. 360–375, 1999.

[98] Ö. Ertunç, “Individual Experimental Work Unpublished Study” 2007.

[99] H. S. Kang, S. Chester, and C. Meneveau, “Decaying Turbulence in an Active-Grid-Generated Flow and Comparisons With Large-Eddy Simulation,” *J. Fluid Mech.*, Vol. 480, No. 2003, pp. 129–160, 2003.

[100] V. L. Zimont and F. Biagioli, “Modelling Turbulent Premixed Combustion in The Intermediate Steady Propagation Regime,” *Prog. Comput. Fluid Dyn. An Int. J.*, Vol. 1, No. 1, pp. 14–28, 2001.

[101] J. a. M. Withag, J. B. W. Kok, and K. Syed, “ Transient Combustion Modeling of an Oscillating Lean Premixed Methane/Air Flame,” *Vol. 3 Combust. Fuels Emiss. Parts A B*, pp. 823–832, 2008.

[102] J. Wen., V.Rao and V. Tam, “Numerical Study of Hydrogen Explosions in a Vehicle Refill Environment and in a Model StorageRoom,” *International Journal of Hydrogen Energy*, Volume 35, Issue 1, pp. 385-394 ,2010.

[103] V. Moreau, “ Progress in the Self-Similar Turbulent Flame Premixed Combustion Model,” *Appl. Math. Model.*, Vol. 34, No. 12, pp. 4074–4088, 2010.

[104] S. D. Salusbury, “Experiments in Laminar and Turbulent Premixed Counter-Flow Flames at Variable Lewis Number,” No. April 2014, 2014.

[105] J. Bendat, and A. piersol, “ *Random Data Analysis and Measurement Procedures*,” second edition, John Wily Sons Inc, 1986.

[106] M. Alhumairi and Ö. Ertunç, “Active-Grid Turbulence Effect on The Topology and The Flame Location of a Lean Premixed Combustion,” *Therm. Sci. Int. Sci. J. Serbia*, Thermal Science, Vol. 22, No. 6A, pp. 1-14, 2018.

.

CURRICULUM VITAE

Mohammed Alhumairi was born in Iraq. He enrolled in the Al-Rasheed College of Engineering and Science of the University of Technology, Iraq in 1989. He received his BS degree in Mechanical Engineering in 1993. He has worked as an aeronautical and mechanical engineer for many companies. In 2004, he earned his MSc degree in mechanical engineering from the same university. Subsequently, he pursued his PhD degree in the Mechanical Engineering Department of the Graduate School of Engineering and Science of Ozyegin University, Istanbul, Turkey, under Assistant Professor Ozgur Ertunc, and received his PhD degree in Mechanical Engineering in October 2018. After completion of his Ph.D. studies, he will work at Diyala University, Iraq.

His previous research interests included performance of wind turbines and heat transfer in spark-ignition engines. His current research interests include turbulent flow in turbulent premixed combustion. He published many papers and conferences in Iraq and Turkey.

.